JOINT TRANSPORTATION RESEARCH PROGRAM

FHWA/IN/JTRP-2006/38

Final Report

MECHANICALLY STABILIZED EARTH WALL ABUTMENTS FOR BRIDGE SUPPORT

Ioannis Zevgolis
Philippe Bourdeau

April 2007

INDOT Research

TECHNICAL *Summary*

Technology Transfer and Project Implementation Information

TRB Subject Code: 62-6 Soil Compaction and Stabilization *April 2007*
Publication No.FHWA/IN/JTRP-2006/38, SPR-2855 *Final Report*

Mechanically Stabilized Earth Wall Abutments for Bridge Support

Introduction

Using MSE structures as direct bridge abutments would be a significant simplification in the design and construction of current bridge abutment systems and would lead to faster construction of highway bridge infrastructures. Additionally, it would result in construction cost savings due to elimination of deep foundations. This solution would also contribute to better compatibility of deformation between the components of bridge abutment systems, thus minimize the effects of differential settlements and the undesirable "bump" at bridge / embankment transitions. Cost savings in maintenance and retrofitting would also result. The objective of this study was to investigate on the possible use of MSE bridge abutments as direct support of bridges on Indiana highways and to lead to drafting guidelines for INDOT engineers to decide in which cases such a solution would be applicable. The study was composed of two major parts. First, analysis was performed based on conventional methods of design in order to assess the performance of MSE bridge abutments with respect to external and internal stability. Consequently, based on the obtained results, finite element analysis was performed in order to investigate deformation issues.

Findings

MSE walls have been successfully used as direct bridge abutments for more than thirty years. Numerous such structures exist in the USA and around the world. Design methods are readily available through AASHTO and FHWA guidelines. In principle, these methods are similar with the design methods for conventional MSE walls. These are the result of soil classical plasticity theories (i.e. Coulomb's and Rankine's) combined with empirical knowledge. The methods are based on limit equilibrium principles and address ultimate limits of resistance with respect to external and internal stability. In terms of external stability, safety must be verified with respect to overturning around the toe, sliding on the base, and bearing capacity of the foundation soil. In terms of internal stability, safety must be verified with respect to tensile and pull out failure of the reinforcement elements. The bridge concentrated loads naturally increase the magnitude and location of tensile stresses within the MSE mass. The primary advantage of MSE walls compared to conventional reinforced concrete walls is their ability to withstand differential settlements without structural distress. Nevertheless, in case of MSE bridge abutments, settlements have to be examined carefully on a case by case basis, in order to determine their effect on the superstructure. Uniform settlements are usually of little concern (unless they are excessively large), but differential settlements can cause serious problems, even in small amounts. Therefore, AASHTO provides criteria for allowable differential settlements with respect to longitudinal angular distortion, i.e. the ratio of differential settlements over the bridge span length. Another advantage of abutments directly founded on MSE walls, is that differential movements between the bridge deck and the approach embankment are not expected to be significant, because the deck is practically supported by the embankment itself.

The performance of MSE bridge abutments based on conventional design methods was

investigated, in order to identify cases where the criteria for ultimate limits of resistance with respect to external and internal stability are satisfied. The program *MSEW v.2.0* was used for the analysis of twenty-seven case examples, based on variation of loading, geometric, and foundation soil conditions. The analysis was performed for single span bridges, with span length between 18 and 30 m (60 and 100 ft), and visible height of MSE abutment walls between 5 and 7 m (16 and 23 ft).

The results indicate that MSE structures shall not be used as direct bridge abutments when soft soil layers, such as normally consolidated clays, are present near the surface. In such occasions, a design configuration including piles shall be used. In more competent foundation profiles, MSE walls can be used as direct support of bridge abutments. In these cases, the application of bridge loads on top of MSE walls has an impact on the design width of the wall, i.e. the required design of reinforcement elements. For the case examples analyzed in this study, the ratio of width over total height of the wall had to be taken equal to 1 – 1.15 (which comes in agreement with FHWA recommendations). For the conditions assumed in the study, bearing capacity controlled the design. Specifically, in 8 out of 27 case examples, bearing capacity safety factor was (slightly) below 2.5, which is the recommended minimum value by AASHTO. On the other hand, safety factors against sliding and overturning were in all cases well above the minimum recommendations, and therefore these two modes of failure do not cause serious concerns. So, overall, the decisive factor is the bearing capacity, which as expected is significantly affected by foundation soil conditions. When these conditions are marginal, loading and geometric characteristics can play an important role, too. Sensitivity analyses with respect to shear strength properties of the foundation soil were performed and a chart in terms of bearing capacity safety factors was produced. Given the conditions assumed in this study, this chart may be used as preliminary decision tools regarding whether or not piles can be eliminated. In terms of internal stability, the presence of bridge loads on top of MSE walls increases the required density of reinforcement elements, i.e. decreases the vertical and horizontal distance of the steel strips. However, an appropriate internal design based on AASHTO and FHWA reveals the exact density requirements, and as long as this is performed, tensile and pull out failure modes are not expected to cause serious problems.

In summary, the results of the analysis with respect to the ultimate limit states of external and internal stability, confirm the recommendations already provided in the AASHTO and FHWA guidelines. The currently available methods of design take into consideration the impact of bridge loads, when these are present, and therefore provide the necessary means to decide whether or not an MSE wall used as direct bridge abutment can be designed with safety. When this is the case, the recommendations also provide the means in order to perform an accurate design with respect to external and internal stability based on the project's site conditions. However, using MSE walls as direct bridge abutments also requires their high performance, over the long term, with respect to deformations. In this context, an aspect that needed investigation was the analysis of stresses and strains under service loads. This type of analysis was performed using the finite element method.

*F*inite element analysis was performed in plane strain (2-D) conditions using Plaxis v. 8.2. Soil was modeled with 15-node triangular elements using two constitutive models. Mohr-Coulomb was used for the reinforced backfill, the approach embankment, and part of the foundation soil. The Plaxis "Hardening Soil" model was used to model an impermeable compressible layer. This advanced model takes into consideration the effects of confinement and stress history on the soil moduli. Simulations were performed for five case examples that, based on the results of conventional design methods, were identified as more interesting (FS_{BC} = 2.5). Two types of analysis were performed for each example. First, foundation soil was assumed fully permeable, so the resulting vertical displacements correspond to immediate settlements of the system due to MSE wall self-weight and bridge loads. Second, a layer of non-permeable compressible soil was introduced in the foundation profile. Magnitudes and time rates of consolidation settlements were investigated in this second type of analysis. In all cases, the construction sequence of MSE structures followed in practice was taken into consideration in the numerical simulations.

In total, four different foundation profiles were analyzed for each of the examined examples: three profiles included a homogeneous permeable material with Young moduli varying between 100,000, 50,000 and 25,000 kPa (14,500, 7,250 and 3625 psi), while the fourth profile introduced a non-permeable compressible layer

with compression index equal to 0.250. The resulting maximum settlements along the top of the MSE structure were 6, 9.5, 16.5, and 24 cm (2.35, 3.75, 6.5 and 9.5 in), respectively. These values refer to settlements due to both MSE self-weight and bridge loads. The fraction of settlements that are caused due to the bridge loads is small with respect to settlements caused by the MSE self-weight. For instance, for the examples that involved a 3-m thick compressible layer as part of the foundation profile (those were the examples with the larger total settlements, i.e. up to 24 cm), the application of bridge loads increased the settlements by 5 to 14 % near the facing of the wall and by 2 to 8 % at the back of the wall. This means that proper adjustments during the construction process and before the application of the bridge loads, can compensate for elevation losses due to settlements caused by the self-weight of the MSE wall. If such adjustments are assumed, then final settlements just below the bridge seat range between 0.5 and 2.5 cm (0.2 and 1.0 in).

In addition to foundation soil compressibility, settlements depend on the height of the structure, as well. Larger settlements appear in the taller walls, although these were subjected to smaller bridge loads compared to the short walls. The impact of wall's height was found to increase with increasing compressibility of the foundation soil. Finally, settlements were found to depend on the magnitude of bridge loads. However, for the case examples analyzed in this study, varying the bridge loads had a smaller impact than varying foundation soil compressibility or height of the structure. Overall, the resulting settlements are relatively uniform and that transitions between approach embankment / reinforced fill and reinforced fill / bridge deck are smooth. In other words, the so-called "bump" that often appears at these transitions when the bridge seat is founded on piles, seems to be eliminated in the configuration under study.

Dissipation of excess pore pressures depends on the coefficient of consolidation c_v of the clay layer and the length of the drainage path. This study was based on the assumption of double drained 3-m thick clay layers. For such layers, the results indicate that for coefficients of consolidation larger than approximately 10^{-3} cm^2/s (10^{-6} ft^2/s) a great fraction of excess pore pressures has already dissipated by the time that bridge loads are applied. Specifically, by the end of construction consolidation settlements were completed by 87 to 92 %. This means that no waiting periods for consolidation to occur need to be accounted in the construction process, since only a small fraction of settlement has not occurred by the end of construction. In terms of absolute values, the maximum remaining settlement after the end of construction was found to be approximately 2 cm (0.8 in). When coefficients of consolidation were decreased by one order of magnitude ($c_v = 10^{-4}$ cm^2/s), only 50 % of consolidation settlement had occurred by the end of construction. In that case, the time required for complete consolidation to occur was almost one year after the end of construction. So, in such cases the construction sequence needs to be modified in order to take into account consolidation settlements.

Implementation

On the basis of this study, it appears that use of MSE walls as direct bridge abutments would be reliable under certain conditions. Conclusions and recommendations are based on case examples that reflect relatively typical situations. However, several assumptions and simplifications were made in the course of the study. Therefore, the implementation of the work reported herein, requires in practice a case by case rigorous analysis that will take into account the project characteristics. The following are suggested as implementation items:

1. Selection of future projects in Indiana that fall within the range of geometric and loading conditions examined in this study. As a first step, selected projects shall satisfy the least adverse loading and geometric conditions (i.e. 18 m length spans on 5 m visible height MSE abutments).
2. Selection of the one (or more) from the above, on which foundation soil conditions are favorable and meet the criteria of this study. A careful site investigation that will provide reliable information regarding the foundation soil profile is necessary during this step.
3. Design and construction of the MSE bridge abutment with strict adherence to the appropriate AASHTO and FHWA guidelines. For issues not mentioned in the guidelines, such as deformations, verification should be made that they do not exceed the appropriate limits.

Based on the performance of the pilot project, and as confidence on the proposed configuration builds up, more projects that meet the criteria of

this study may be selected in the future. Ideally, the pilot project would be instrumented so that monitoring verifies the conclusions of this study. In such eventuality, the acquired capability to numerically model MSE structures would provide the analytical framework for the preparation of the pilot project and would be extremely helpful during its design phase and for planning its instrumentation.

Contacts

For more information:

Prof. Philippe Bourdeau
Principal Investigator
School of Civil Engineering
Purdue University
West Lafayette IN 47907
Phone: (765) 494-5031
Fax: (765) 496-1364
E-mail: bourdeai@ecn.purdue.edu

Indiana Department of Transportation
Office of Research & Development
1205 Montgomery Street
P.O. Box 2279
West Lafayette, IN 47906
Phone: (765) 463-1521
Fax: (765) 497-1665

Purdue University
Joint Transportation Research Program
School of Civil Engineering
West Lafayette, IN 47907-1284
Phone: (765) 494-9310
Fax: (765) 496-7996
E-mail: jtrp@ecn.purdue.edu
http://www.purdue.edu/jtrp

Final Report

FHWA/IN/JTRP-2006/38

MECHANICALLY STABILIZED EARTH WALL ABUTMENTS FOR BRIDGE SUPPORT

by

Ioannis Zevgolis
Graduate Research Assistant

and

Philippe L. Bourdeau
Professor

School of Civil Engineering
Purdue University

Joint Transportation Research Project
Project No. C-36-50Z
File No. 6-19-25
SPR-2855

Conducted in Cooperation with the
Indiana Department of Transportation
and the
U.S. Department
Federal Highway Administration

Purdue University
West Lafayette, IN 47907
April 2007

ACKNOWLEDGMENTS

The investigators are grateful to the SAC members:

- Som Hiremath (INDOT)
- Daehyeon Kim (INDOT)
- Tony Uremovich (INDOT)
- Steve Morris (INDOT)
- Keith Hoernschemeyer (FHWA)

for their continuing support and collaboration throughout the study.

TABLE OF CONTENTS

Page

LIST OF TABLES

Table Page

LIST OF FIGURES

Figure Page

CHAPTER 1. INTRODUCTION

1.1. Background and Problem Statement

Mechanically Stabilized Earth (MSE) walls are a technically and economically attractive alternative to traditional reinforced concrete earth retaining structures. The MSE technology has been increasingly used by INDOT as the solution of choice for lateral support of embankment fills or access ramps, and for bridge abutment retaining walls. In the later case, current practice in Indiana highway projects is to support independently the bridge on piles, as shown conceptually in Figure 1.1. Because it requires the piles to cross the reinforced soil fill, this type of design is a source of considerable complication in the construction process. Another shortcoming is that, in this case the bridge support is rigid in comparison to the surrounding MSE. This difference of rigidity may generate detrimental differential movements between the bridge structure, the MSE wall and the approach embankment, and contribute in particular to creating a “bump” at the bridge/embankment transition.

In a number of cases, these problems could be avoided or minimized if the MSE abutment was designed not only to retain the approach embankment but also to support the bridge structure. In practice, this means the bridge seat would consist of a reinforced concrete footing built on top of the MSE fill, as illustrated in Figure 1.2. Such a configuration is acknowledged in FHWA’s and AASHTO’s guidelines on reinforced soil structures, and design methods are available for cases where MSE walls are subjected to combination of lateral earth pressure from a retained backfill and concentrated surface applied loads. Examples can be found in Europe and North America where these principles were applied to building MSE bridge abutments.

There is need for an investigation on the possible use of MSE bridge abutments as direct support of bridge structures for Indiana highways, in order to avoid unnecessary construction cost and complication, and the possible detrimental effects of independent pile foundations crossing the reinforced soil fill. The investigation would lead to drafting guidelines for INDOT engineers to decide in which cases such a solution would be applicable, and related design and construction specifications.

1.2. Scope of Research and Objectives

The type of application envisioned herein for MSE bridge supporting abutment requires high performance of reinforced soil over the long term. This means that, not only internal resistance and external stability with respect to ultimate states of loading must be adequate, but also that excessive deformation will not accumulate over time under service load. The later consideration suggest geogrid reinforcement made of plastic polymer not be considered in the present study, because this type of soil reinforcement undergoes significant creep deformation under sustained load. Therefore, only MSE abutments with metallic reinforcement (galvanized steel strips) are considered. Another limitation of the study is with respect to seismic response. Available data on MSE performance in seismic conditions is still very limited and the application of MSE technology for bridge abutments in earthquake prone areas is beyond the scope of this project.

The research study starts with a review, based on published literature and other accessible sources, of current design methods and construction practices in North America and other parts of the world where MSE bridge abutments have been constructed. The synthesis of this information is then used to perform preliminary designs in case examples of interest to INDOT. These examples are classified in terms of bridge geometry, loading, and foundation soil conditions. Results are obtained in terms of ultimate limit states. i.e. the external and internal stability of the MSE wall, according to AASHTO’s and FHWA’s guidelines.

For those cases whose ultimate resistance criteria are met, numerical modeling using the finite element method is performed in order to assess the anticipated performance in terms of serviceability limit states (deformations). This is so because the designer's decision will depend not only on consideration of external and internal stability criteria, but also on total and relative deformation of the system's components (i.e. structure, MSE abutment wall, approach embankment and foundation soil) during and after construction. A software environment, PLAXIS, has been selected for performing this task.

The results of conventional design and numerical modeling serve as a basis for drafting guidelines and recommendations. The role played in the applicability of the technology by such characteristics as the compressibility of the foundation soil, height of embankment, magnitude and orientation of applied loads, is given particular attention.

The ultimate goal of the research is to formulate recommendations that will result in more effective design and improved economy of highway bridge abutments by using MSE technology whenever it is the best solution. It is expected that the results of the study will contribute to new or improvement INDOT's guidelines and specifications in this particular area.

1.3. Organization of Contents

In Chapter 1, the background and problem statement of this project is briefly introduced, followed by the study scope and objectives.

Chapter 2 provides a literature review of topics including the design principles of MSE bridge abutments and the impact of bridge loads on their internal and external stability, and the performance of such structures with respect to ultimate and serviceability limit states.

Chapter 3 discusses details of the analyzed case examples and provides results, in terms of external and internal stability, based on conventional design methods.

Chapter 4 introduces the finite element method and the program Plaxis that was used in the current study in order to assess the performance of MSE bridge abutments in terms of deformations.

Chapter 5 presents the results of finite elements analysis with respect to immediate and consolidation settlements. Both magnitude and time rate of consolidation issues are addressed.

Finally, Chapter 6 summarizes the findings of this project and provide recommendations regarding the use of MSE structures as direct bridge abutments.

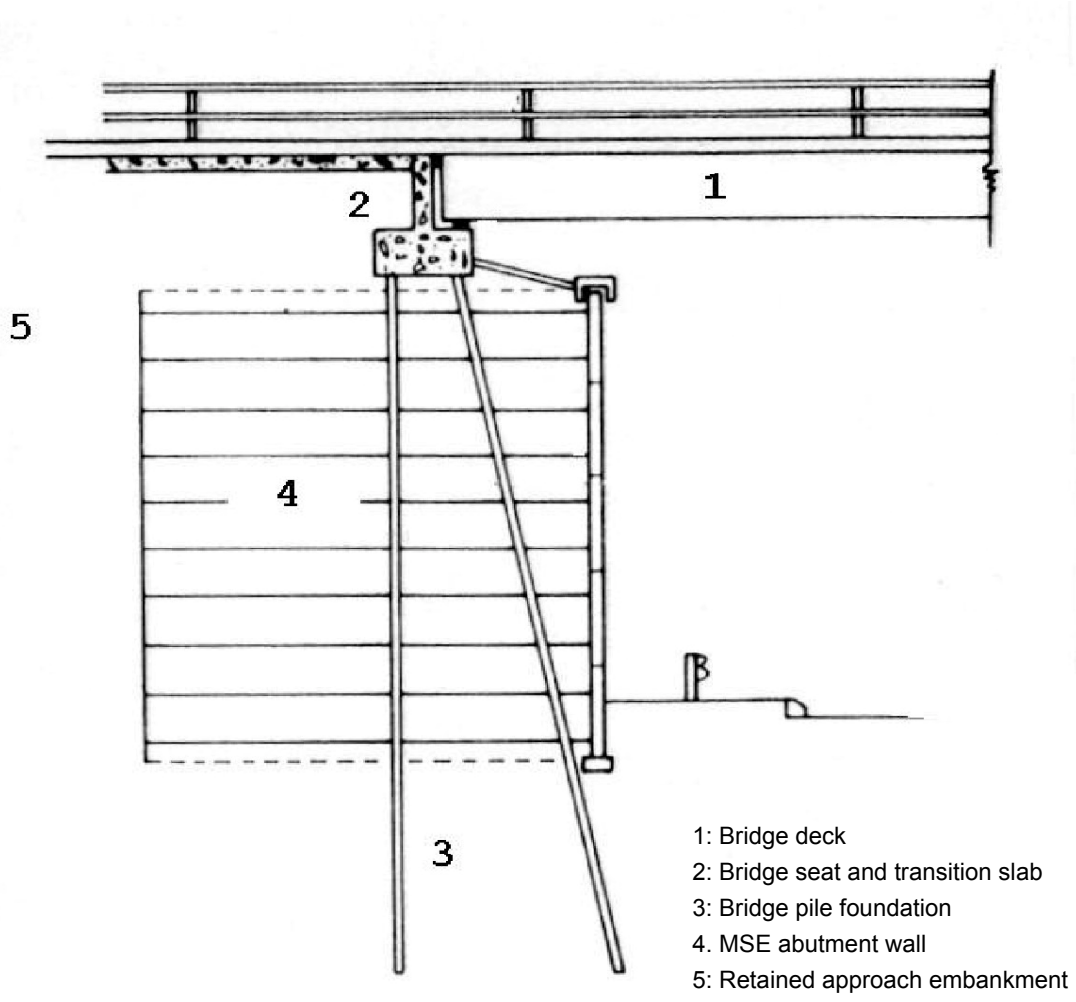

Figure 1.1 Conventional design of MSE abutment wall (from Jones, 1996)

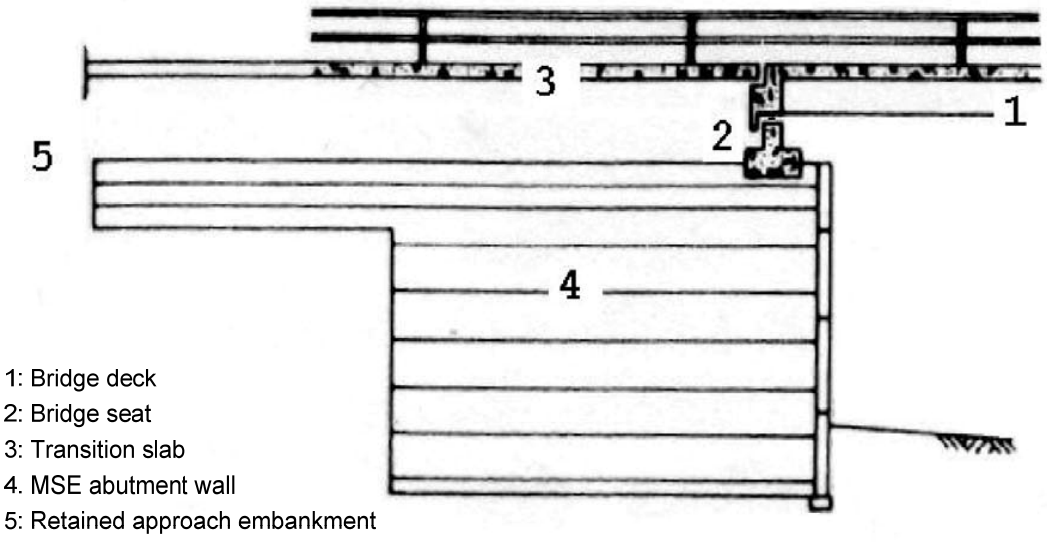

Figure 1.2 MSE abutment used as bridge support (from Jones, 1996)

CHAPTER 2. LITERATURE REVIEW

2.1. Introduction

Mechanically stabilized earth (MSE) walls, also known as reinforced soil walls, are a special type of earth retaining structures, composed primarily of the following three elements: the earth fill, which is typically made of granular soil, reinforcements that can be made of metallic or geosynthetic material, and facing units. In principle, reinforced soil retaining walls can be considered as composite structures where the earth fill stability and capacity to retain backfill are improved by the reinforcements (Vidal, 1969; Schlosser and Vidal, 1969; Lee et al, 1973; Ingold, 1982). Tensile – resistant inclusions provide the strength and internal confinement that are naturally lacking in granular earth fill. Depending on the type of reinforcement, stresses are transferred between fill and reinforcement through interface friction, passive resistance of interface particle, or a combination of both (Schlosser and Elias, 1979; Schlosser and Guilloux, 1981; Schlosser and Bastick, 1991). Figure 2.1 shows the stress transfer mechanisms for typical ribbed steel strips. More than thirty years after their introduction in civil engineering, MSE structures have become an attractive alternative to traditional reinforced concrete retaining walls. They have a broad range of applications such as retaining walls, bridge abutments, sea walls, industrial storage walls, and others. In comparison to traditional walls, they offer two major advantages: they are often more economical and, due to their inherent flexibility, they can tolerate relatively large differential settlements without excessive structural distress (Mitchell and Christopher, 1990; Schlosser, 1990; Jones, 1996).

MSE walls have been extensively used as lateral support of highway embankment fills or access ramps, and as bridge abutment retaining walls. There

are two types of bridge abutments that incorporate reinforced soil walls (Jones 1996; Anderson and Brabant, 2005). The first one, often called mixed or false MSE abutment, is a pile-supported abutment where the reinforced soil wall provides only lateral support to the approach embankment. The piles are installed first, then the MSE structure is constructed. This type of design has shortcomings: construction process is complicated, cost is increased by the use of deep foundations up to 25 % (Brabant, 2001), and different stiffnesses induce differential movements between the bridge structure, the reinforced soil wall and the approach embankment. In a number of cases, these problems can be avoided or minimized if the reinforced soil structure is designed not only to retain the approach embankment, but also to support the bridge. In this second type of design the bridge seat lays on a strip footing that is directly built on the reinforced soil mass. This means that the reinforced soil structure, in this case often called true MSE abutment, must be designed in order to sustain not only the approach embankment earth pressure, but also the loads induced by the superstructure.

Currently, design analyses for MSE structures in practice are the result of soil classical plasticity theories (i.e. Coulomb's and Rankine's), combined with empirical knowledge accumulated over the past three decades from experiences on small-scale models or instrumented full-scale prototypes. Design methods are based on limit equilibrium analysis and address ultimate limits of resistance with respect to external and internal stability following a semi-empirical approach. More recently, numerical models have allowed to develop more generic methods than the earlier proprietary methods.

Design methods for MSE abutments follow the same principles as these for conventional MSE structures. The difference between the two is the presence of heavy concentrated loads due to the bridge superstructure. This means that MSE abutments serve not only as retaining structures, but as load bearing structures too. The analysis of these two functions is based on the principle of superposition: the forces or displacements produced at any point of the wall by the combined and simultaneous effect of the dual function can be evaluated by

adding (superimposing) the forces or displacements produced by each function individually. The principle of superposition holds true for linearly elastic solids. However, based on laboratory experiments, full scale models, and theoretical analyses mainly using the finite element method, the applicability in the case of MSE abutments seems to be fairly reasonable.

2.2. Impact of superstructure loads

The vertical and horizontal concentrated loads applied by the superstructure on the MSE wall increase the magnitude of tensile stresses and influence the locus of points of maximum tensile stresses within the reinforced soil.

2.2.1. Magnitude of tensile forces

The concentrated loads dissipate throughout the soil mass with depth, following approximately a Boussinesq distribution (Juran et al, 1979; Bastick, 1985). For design purposes, the simple and more conservative 2V:1H distribution has been adapted (AASHTO, 2002). For a strip footing, the increment of vertical stress due to the loads for any given depth, is given by:

$$\Delta\sigma_v = \frac{P_v}{D}$$

with

$$D = \begin{cases} B' + z & \text{for } z \leq z_o \\ \frac{B' + z}{2} + d & \text{for } z \geq z_o \end{cases}$$

where $\Delta\sigma_v$ is the increment of vertical stress, P_v is the concentrated vertical load per linear meter of strip footing, D is the effective width of applied load at any depth, B' is the effective width of footing (equal to the nominal width reduced by two times the eccentricity, i.e. B' = B – 2e), z_o is the depth where D intersects the facing of the wall, d is the distance between the centerline of the footing and the facing of the wall, and z is the depth on which tensile forces are calculated ($0 \leq z \leq H$). Figure 2.2 shows a schematic representation of the 2V:1H distribution.

The dissipation of the horizontal loads is approximated by a Rankine plane, as shown on Figure 2.3. The maximum increment of horizontal stresses due to these loads is given by:

$$\Delta\sigma_{h,max} = \frac{2F}{l}$$

with

$$F = P_h + F_1 + F_2$$

and

$$l = \left(c + B'\right) \tan\left(45^o + \frac{\varphi}{2}\right)$$

where $\Delta\sigma_{h,max}$ is the maximum increment of horizontal stresses, P_h is the concentrated horizontal load per linear meter of strip footing, F_1 is the lateral force due to earth pressure, F_2 is the lateral force due to traffic surcharge, c is the distance between the facing and the front edge of the footing, l is the depth of complete dissipation of horizontal load, and φ is the friction angle of reinforced soil.

2.2.2. Locus of maximum tensile forces

Early research has indicated that the failure surface that develops in the MSE structures defines two zones within the reinforced soil mass: the active zone, on which the shear stresses are directed outwards and lead to a decrease in the tensile forces, and the resistant zone, on which the shear stresses are directed inwards, preventing the sliding of the reinforcement elements. The locus of points of maximum tensile stresses is assumed to coincide with this failure surface. On conventional MSE walls, the locus depends primarily on the type of reinforcement that is used. In the case of inextensible reinforcements, which is the focus of the current research, the locus is assumed to be bilinear and varies with depth. In the case of MSE abutments though, it has been observed that the locus may change depending mainly on the geometry of the footing (Schlosser and Bastick, 1991). As shown in Figure 2.4, the locus of maximum tension points swifts in order to intersect the back of the bridge seat.

2.3. Design of External Stability

In terms of external stability, MSE abutments are analyzed similarly to conventional MSE walls and other types of gravity walls, i.e. the reinforced fill is assumed to behave as a rigid body for the purpose of limit equilibrium considerations. Major forces taken into account are the active earth thrust from the approach embankment, self weight of the reinforced soil mass including the fill located behind the bridge seat, vertical and horizontal loads transferred through the bridge seat, and traffic surcharges (Figure 2.5). Stability must be verified with respect to overturning around the toe, sliding on the base, and bearing capacity of the foundation soil (Schlosser and Bastick, 1991; Elias et al., 2001). Design manuals, such as AASHTO (2002), provide details regarding the use of the involved forces in the stability calculations for each mode. Safety factors (FSs) should be at least FS_{OT} = 2.0 for overturning, FS_{SL} = 1.5 for sliding, and FS_{BC} = 2.5 for bearing capacity. The flexibility of the reinforced soil structure has a favorable effect on the bearing capacity of the foundation soil. Therefore

FS_{BC} can be smaller than in the case of rigid reinforced concrete walls for which usually $FS_{BC} > 3$ is required.

2.4. Design of Internal Stability

The internal stability of an MSE structure relates to the tensile and pull out failure of the reinforcement elements. Both modes of failure may lead to large movements and possible collapse of the structure. The minimum recommended safety factors for the two failure modes are (Elias et al., 2001; AASHTO 2002): $FS_{PO} = 1.5$ for pull out failure, and $FS_{TF} = 1.8$ for tensile failure of steel strips.

Tensile failure occurs when the tensile forces in the reinforcement elements become larger than their tensile strength, so that they elongate excessively or break. The maximum tensile force in each reinforcement layer per unit length of wall is given by:

$$T_{max} = \sigma_h \, S_v$$

where σ_h is the horizontal stress at the depth on which the tensile forces are calculated, and S_v is the vertical spacing of the reinforcement layers. The horizontal stress is given by:

$$\sigma_h = K_r \left(\sigma_v + \Delta\sigma_v + q \right) + \Delta\sigma_h$$

where σ_v is the vertical stress due to self weight at a given depth, $\Delta\sigma_v$ is the increment of vertical stress due to the vertical concentrated loads from the bridge, q is the uniform surcharge load (if any), $\Delta\sigma_h$ is the increment of horizontal stress due to possible horizontal concentrated loads, and K_r is a coefficient of lateral earth pressure that for steel strips reinforcement is given by:

$$K_r = \begin{cases} K_a\left(1.7 - \dfrac{z}{12}\right) & \text{for } 0 \le z \le 6\,\text{m} \\ 1.2 & \text{for } z \ge 6\,\text{m} \end{cases}$$

where K_a is the coefficient of active earth pressure based on Coulomb's theory.

The pull out failure mode occurs when the tensile forces become larger than the force required pulling the reinforcement elements out of the soil mass (pull out resistance). For steel strip reinforcement, the pull out resistance of a single strip is given by:

$$P_R = 2\,b\left(\sigma_v + \Delta\sigma_v\right) f^* L_a$$

where b is the gross width of the strip, f^* is the coefficient of apparent friction, and L_a is the length of reinforcement within the resistant area. The coefficient of apparent friction is given by:

$$f^* = \begin{cases} \left(1.2 + \log C_u\right) - \dfrac{\left(1.2 + \log C_u\right) - \tan\varphi}{6} z & \text{for } 0 \le z \le 6\,\text{m} \\ \tan\varphi & \text{for } z \ge 6\,\text{m} \end{cases}$$

where C_u and φ are the coefficient of uniformity and the friction angle, respectively, of the reinforced soil. Note that f^* shall be equal to or smaller than 2.

2.5. Bridge seat stability

The proportioning of the bridge seat on the top of the MSE mass depends on a series of factors, such as the deck and the girders of the bridge, the loading conditions, the overall geometry of the structure, and others. Overall, the bridge seat has to meet the typical criteria for a strip footing, against sliding and overturning failure modes. Furthermore, the bearing pressure applied on the

underlying soil shall be limited to 200 kPa (4 ksf) taking into account the effective width of the footing (B´). AASHTO (2002) also recommends that the distance between the center line of the footing and the outer edge of the facing is at least 1 m (3.5´), while the distance between the inner edge of the facing and the front edge of the footing should be at least 150 mm (6´´). In cases where frost penetration is expected, the footing should be place on a bed of approximately 1 m thick (3´) compacted aggregate.

2.6. Overall (slope) stability

Overall stability of MSE walls (and MSE abutments) is typically performed using slope stability analysis methods, like rotational or wedge analysis. Such an analysis is recommended when the MSE wall is located on a slope, or when the foundation conditions are weak.

Figure 2.6 presents an overview of the stability controls, i.e. the ultimate limit states, of an MSE abutment.

2.7. Settlement Criteria

The extent of concerns that an abutment's settlement causes to the superstructure depends not only on the magnitude of the settlement (total or differential), but also on the type of the superstructure, the number and length of spans, the girder stiffness, and other characteristics of the bridge. Total settlements of equal magnitude throughout the structure are of little consequence to the structural integrity (Egan, 1984). Of course, excessive total settlements may cause practical problems, such as bridge beam encroaching on the required clearances. On the other hand, even small amounts of differential settlements can cause serious problems. In fact, based on extensive field data from bridges whose foundations had experienced movements, Moulton and Kula (1980) noticed that damages requiring costly maintenance occurred more frequently as the longitudinal angular distortion, i.e. the ratio of differential settlements over the

span length, increased. Although some of the occurring problems were jeopardizing the structural integrity of the superstructure, most of the times the problems were related to issues such as poor riding quality, deck and/or pavement cracking, and other kind of functional distresses (GangaRao and Moulton, 1981). Moulton et al. (1985) noted that for single span steel bridges, 97.2 % of the angular distortions less than 0.005 were considered tolerable. On the other hand, for continuous span steel bridges, 93.7 % of the angular distortions less than 0.004 were considered tolerable. Moulton et al. performed further statistical analysis including concrete bridges, and they finally recommended that the limits for angular distortions be set to 0.005 and 0.004 for single and continuous span bridges, respectively. Based on this recommendation, AASHTO (2002) states that abutments shall not be constructed on MSE walls, if the anticipated angular distortion is greater than one half (50%) of the values recommended by Moulton et al. (Figure 2.7). It is worth mentioning that other design manuals, that refer to proprietary type of MSE structures, suggest the limit of allowable angular distortion to be 0.01 (RECO, 2000).

As it will be explained in CHAPTER 3, the current research study investigates the performance of MSE abutments for single span bridges with span length ranging between 18 m and 30 m (60 ft and 100 ft). Based on the AASHTO recommendations, the allowable differential settlements for this type and length of span are provided in Table 2.1.

2.7.1. Bridge approach

Specifically about the settlement of the approaching embankment and the resulting “bump” at the end of the bridge, a common practice in conventional type of abutments is the use of an approach or transition slab behind the abutment. The main purpose of the slab is to provide a gradual transition between the superstructure and the settling embankment. Without an approach slab, the transition at the end of the bridge becomes much more abrupt (Hoppe, 1999). Several researchers have suggested criteria of maximum allowable change in

slope between the abutment pavement and the embankment pavement. Briaud et al. (1997) recommends a maximum value of 1/200. Long et al. (1988) suggest the same value for rider comfort and a value between 1/100 and 1/125 for initiating remedial measures. Briaud et al. also suggested a formula for determining the minimum length of the approach slab (L_{SLAB}) in relation to the total fill settlement (W_{FILL}) and the abutment settlement (W_{ABUT}). This formula is given by:

$$L_{SLAB} \geq 200 \times \left(W_{FILL} - W_{ABUT} \right)$$

The above recommendations for use of approach slabs refer mainly to abutments that are rigidly founded on piles, conventional reinforced concrete walls, and so on. When it comes specifically to abutments placed directly on top of MSE walls, the situation may be different. In principle, there is no differential settlement between the bridge deck and the approaching embankment, because the deck is supported by the embankment itself. Therefore, an approach slab should not be necessary, or it should be very small (Group TAI, undated).

2.8. Performance

Not late after the introduction of MSE technology in the late 1960s, it was found that this technology could be easily adapted to the construction of abutments for the direct support of bridge superstructures (Juran et al, 1979). From 1969 to 1977, a series of structures, either experimental prototypes or in-service abutments, were constructed primarily in France and provided the opportunity to investigate the effect of concentrated loads on a mechanically stabilized earth structure. Those structures were the industrial abutment at Strasburg (1969), the double-sided wall at Dunkirk (1970), the in-service abutment on Thionville (1972),

the experimental physical-scale model in Lille (1973-74), the abutments in Triel (1975) and in Angers (1977).

In the United States, the concept and principles of MSE technology were introduced in 1969 (Vidal, 1969). In 1970, FHWA initiated a series of experimental projects in order to evaluate this new type of earth structures (Demonstration Project 18: Reinforced Earth Construction). By 1979, dozens of MSE walls had already been constructed throughout the country (Goughnour and DiMaggio, 1979). Among these walls, many served as bridge abutments. The very first ones were constructed in 1974 in Lovelock, Nevada to support a precast bridge span of 21 m (70 ft) (Hanna, 1977). The soil profile on site consisted of silts, clays, and sands in the upper 30 m (100 ft); however serious concerns were raised regarding 60 m (200 ft) of highly compressible organic and inorganic clays and silts that existed exactly below the above stratum. Pile foundations and conventional reinforced concrete retaining walls were rejected due to concerns for extensive settlements and structural damage, and MSE technology was chosen as the best solution. Instrumentation of the abutments showed satisfactory performance and the project was considered successful by the Nevada Department of Transportation. By the end of 1977, twenty two MSE abutments and wing walls were constructed in several states in the US (McKittrick 1979).

So, MSE walls have been successfully used as direct bridge abutments for more than thirty years. Current design methods, described earlier, address ultimate states of resistance with respect to external and internal stability following a semi-empirical approach. The performance of MSE abutments in terms of these states of resistance has been very good and no special problems have been particularly reported (collapses, etc).

2.8.1. Serviceability limit states

MSE walls are an appropriate solution for retaining purposes, especially in cases where significant total and differential settlements are anticipated (AASHTO

2002). This is so because, due to their inherent flexibility, they can tolerate higher magnitude settlements compared for example to rigid or semi-rigid walls. As stated by Elias et al. (2001), MSE walls demonstrate a significant tolerance in deformations and poor foundation conditions is not usually a dissuasive factor into a decision for constructing them. According to the same authors, a limiting value of differential settlements, above which special precautions need to be taken, is 1/100. When the wall though serves a more complicated purpose, then special attention must be paid. For instance, in the case of a bridge abutment, it is clear that even though the wall itself may tolerate extensive settlements, this may have significant effects on the bridge superstructure, most of them associated with serviceability issues. Therefore, the issue of settlements needs to be studies thoroughly before a decision for construction of an abutment is made. Based on experience of in-service MSE abutments, a general guideline is to move towards their construction when the anticipated settlement is rapid or small, or practically completed before the erection of the bridge superstructure (Elias et al, 2001). If the above criteria are not met, then either long waiting periods for the settlement to be completed have to be established, or special techniques of settlement acceleration (i.e. preloading) must be employed.

Table 2.1. Allowable differential settlements between abutments.

Span length (m)	Allowable differential settlement (cm)
18	4.5
24	6.0
30	7.5

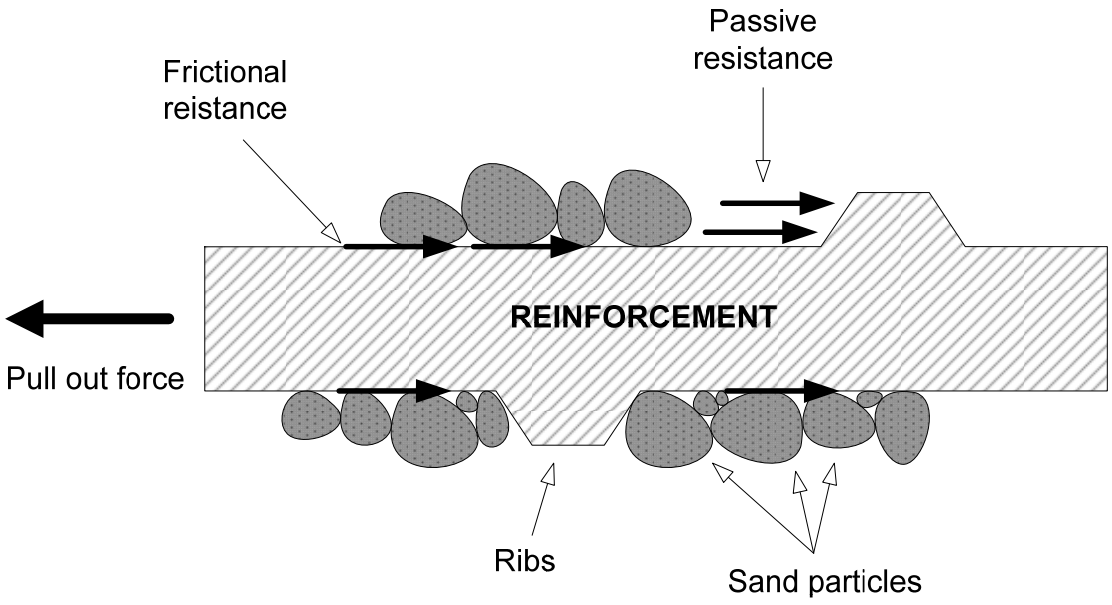

Figure 2.1 Stress transfer mechanisms on ribbed strips

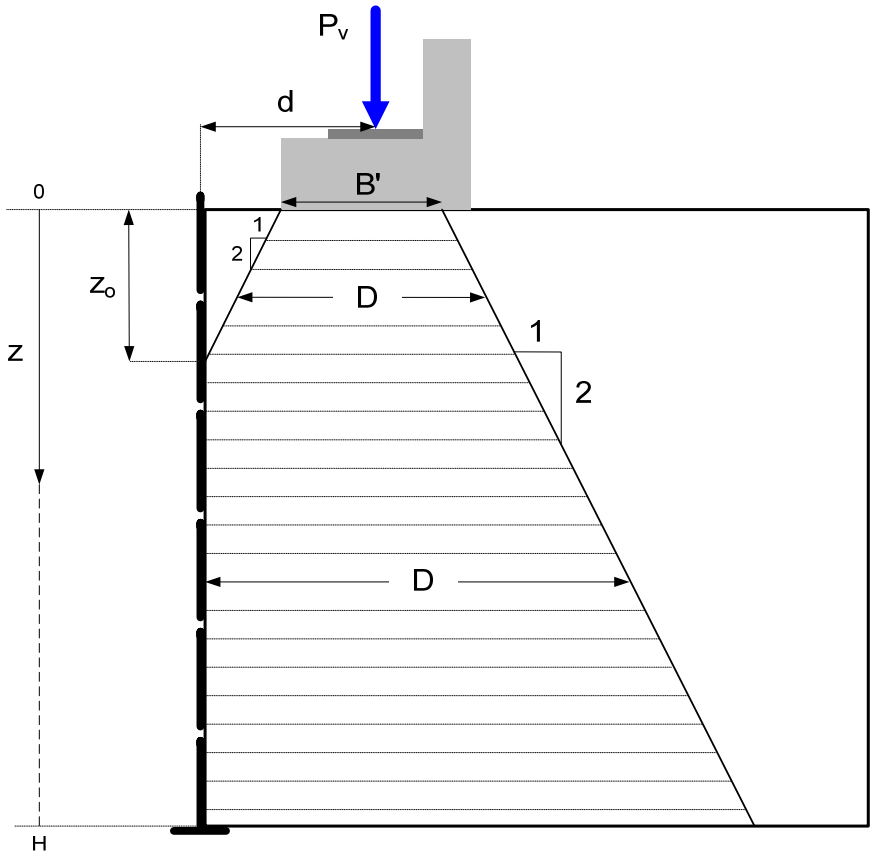

Figure 2.2 Distribution of vertical concentrated loads

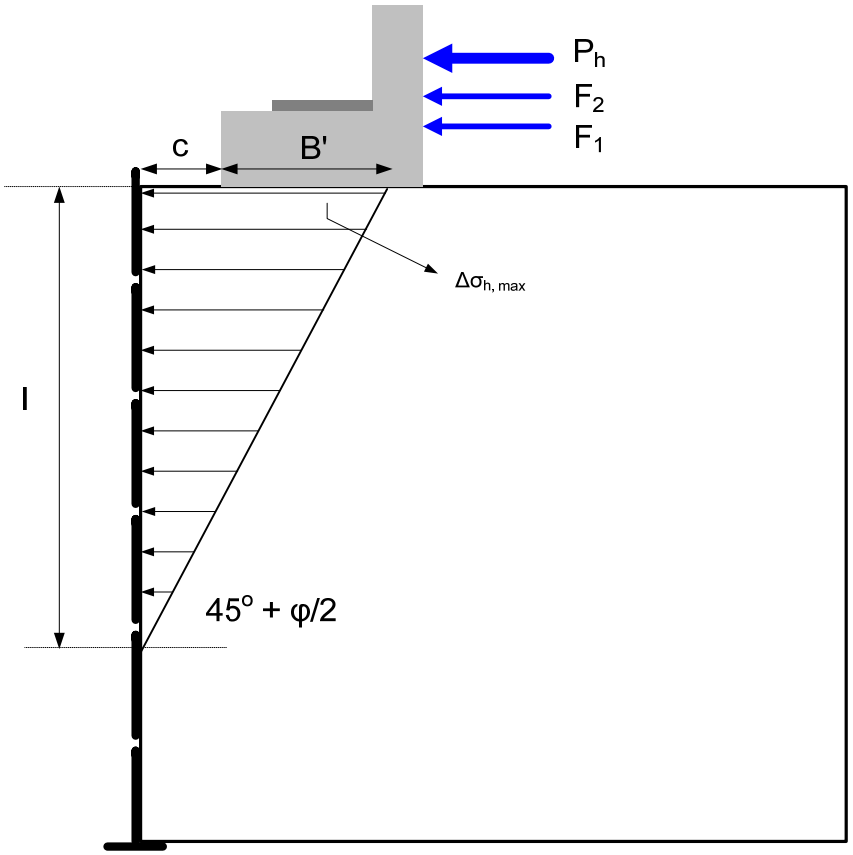

Figure 2.3 Distribution of horizontal concentrated loads

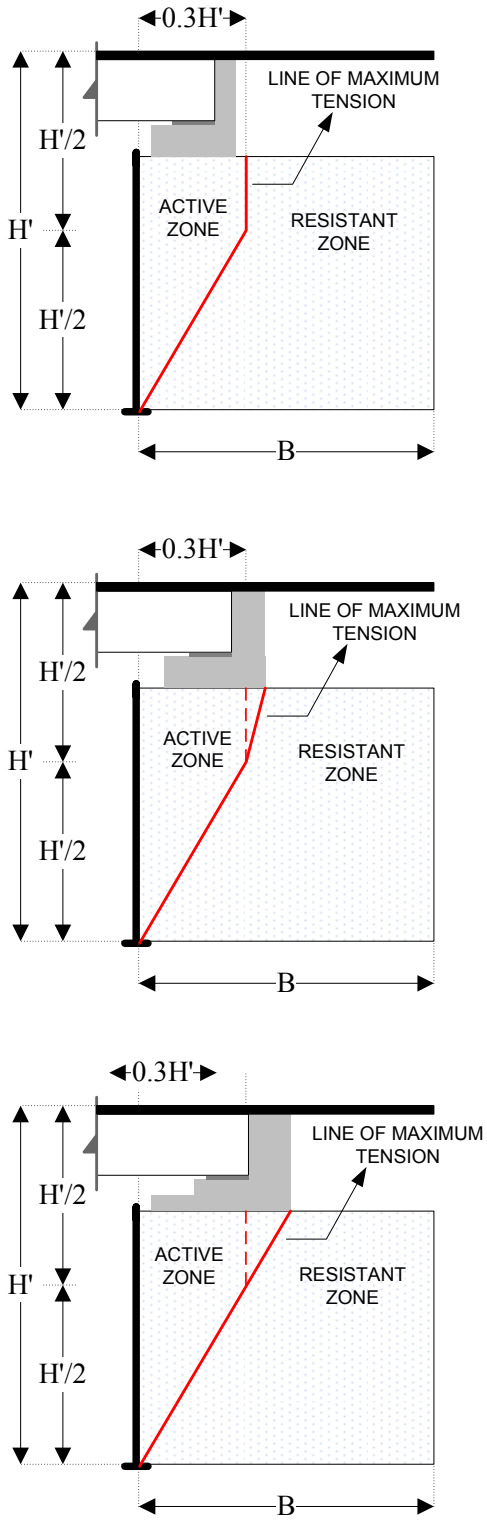

Figure 2.4 Locus of points of maximum tension for different bridge seats geometry (based on Brabant, 2001)

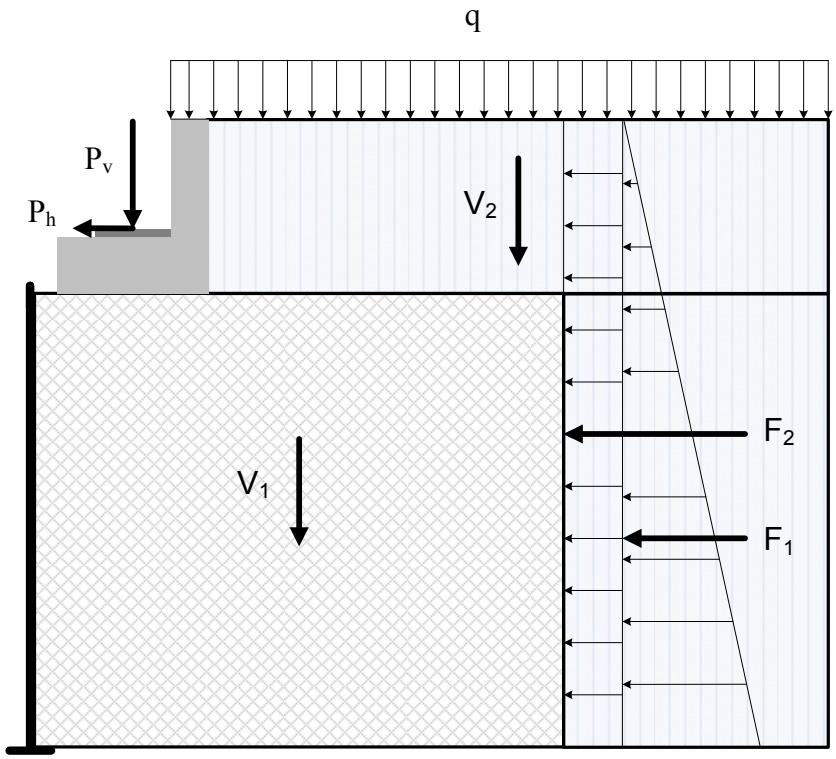

V_1	Self weight of reinforced soil mass
V_2	Weight of fill behind bridge seat
F_1	Active earth thrust from the retained soil
F_2	Active earth thrust due to traffic surcharge
P_v	Vertical concentrated loads (dead and live)
P_h	Horizontal concentrated loads
q	Traffic surcharge

Figure 2.5 Major forces involved in the design of MSE abutments

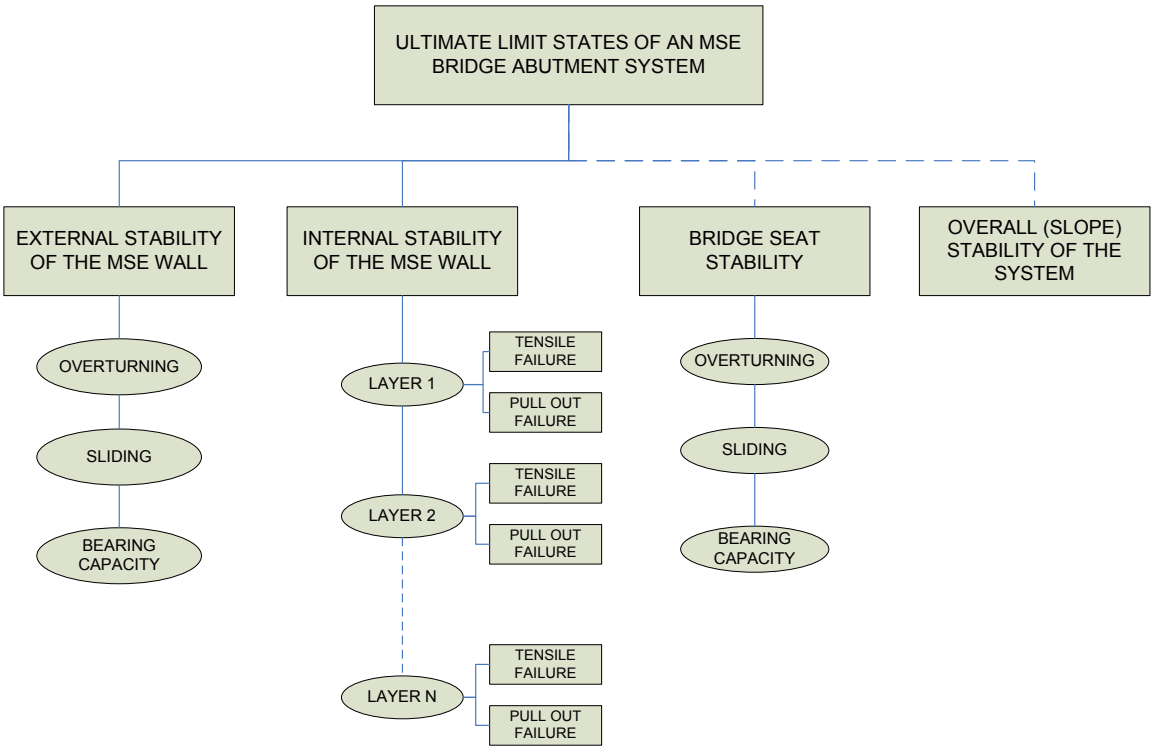

Figure 2.6 Overview of stability controls for MSE abutments

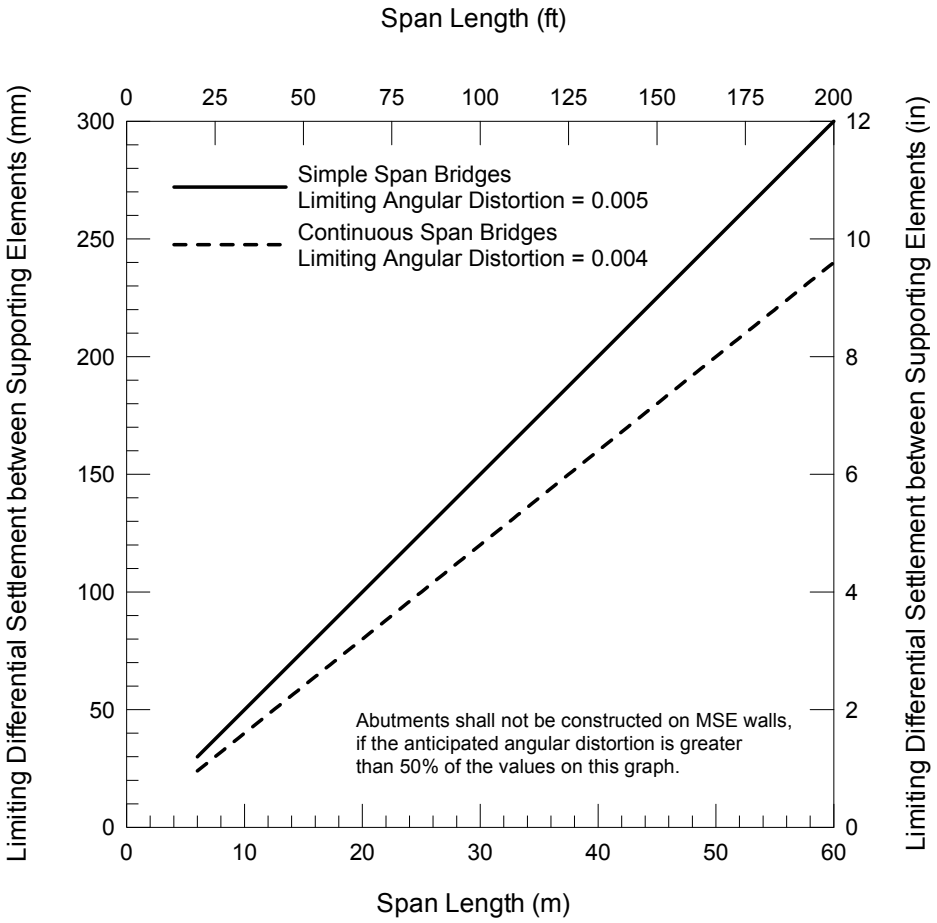

Figure 2.7. Limiting values of differential settlements between abutments (single span) or between abutments and piers (continuous span) (after AASHTO, 2002)

CHAPTER 3. LIMIT EQUILIBRIUM ANALYSIS

3.1. Analysis

The purpose of this part of the study was to identify cases on which the performance of reinforced soil walls used as abutments, with respect to ultimate limit states is satisfactory. Bearing this in mind, the approach that was followed was to examine cases for different loading, geometric, and foundation soil conditions. A detailed description of these conditions follows in the next paragraphs. The program MSEW (v.2.0) was used for the analysis (Adama Engineering Inc., 2004). This is an interactive program for the design and analysis of reinforced soil walls (Figure 3.1), and it follows the FHWA design guidelines. In fact, the first version of the program (v.1.0) was developed for FHWA and it is designed exclusively for use by Federal and State Highway Agencies. Although the program generally follows the guidelines of established design procedures, it also gives the possibility to the user to explore design options and concepts beyond the formal guidelines.

3.1.1. Loading and geometric conditions

Single span bridges with span length (L) ranging from 18 to 30 m were of interest in the current study. The dead and live vertical concentrated loads transmitted from the bridges to the reinforced soil walls were calculated according to the AASHTO LRFD Bridge Design Specifications (AASHTO, 2004). In total, 16 cases with different span lengths, beam types, spacing of beams, and other factors, were analyzed in order to obtain representative values for these loads. An in-depth analysis of reinforced soil abutments for three different loading conditions, corresponding to span lengths of 18, 24, and 30 m, was performed. The average

loads for these three conditions, hereinafter referred to as L_1, L_2, and L_3, are provided in Table 3.1.

In addition to the vertical concentrated loads, the issues of the horizontal (longitudinal) loads and the uniformly distributed loads were addressed. Regarding the first ones, their determination requires a detailed structural analysis on a case by case basis. Among other things, these loads depend on the exact geometry of the abutment, while in case of integral abutments thermal forces may play a significant role. For preliminary purposes and for general cases, the concentrated horizontal loads are usually taken equal to 5 % of the vertical live load. For simplicity, the concentrated horizontal loads were taken equal to 8 kN per linear meter for all three cases (L_1, L_2, and L_3) based on Table 3.1. Finally, the uniformly distributed loads are typically considered equivalent to a uniform load applied by 0.5 m of earth similar to the retained soil, placed on the top of the reinforced soil wall. As stated on the next paragraph, the unit weight of the retained soil in the current study was taken equal to 19 kN/m^3, therefore the equivalent load is equal to 9.5 kPa.

Based on commonly required vertical clearances, three different cases of visible heights of the abutment walls (H) were analyzed: 5, 6, and 7 m, hereinafter referred to as H_1, H_2, and H_3, respectively. Finally, the embedment depth of the walls was taken equal to 1 m for all examined cases, based on code recommendations and current practice. So, the overall heights, H´, of the walls under examination were 6, 7 and 8 m, respectively. Note that the contribution of the reinforced soil wall embedment to the bearing capacity calculations is usually neglected.

3.1.2. Soil profiles

Three different soil profiles, hereinafter referred to as S_1, S_2, and S_3, were examined. These profiles were chosen in accordance with typical profiles found in Indiana. On the other hand, the properties of the soil composing the reinforced backfill are standardized. The minimum requirements regarding the

physicochemical, electrochemical, and engineering properties of the reinforced backfill are stated in the FHWA guidelines (Elias et al., 2001). Regarding the engineering behavior of the material, the major requirement is that it has to be granular and prone to good drainage, with an amount of fines (i.e. material passing the 0.075 mm / No. 200 sieve) less than 15 %. The retained backfill, that is the fill material located between the reinforced soil mass and the natural soil, may be either coarse or fine grained soil. In order though to avoid possible drainage problems behind the reinforced mass, it is recommended to use coarse grained (granular) material. The coefficient of uniformity, C_u, of the reinforced backfill was taken equal to 7 for all cases, corresponding to a pull out resistance factor f^* equal to 2 at the top of the structure. Table 3.2 summarizes the values of the shear strength parameters and the unit weights that were used in the current study, for the reinforced and retained backfill, as well as the three different foundation soil profiles.

3.1.3. Spread footing

The strip footing seating on top of the reinforced soil wall must be designed in accordance to all design aspects of a typical footing founded on a granular soil (structural design and check against overturning, sliding, and bearing capacity). One important aspect in the case of reinforced soil walls used as abutments is that the bearing pressure at the bottom of the footing shall not exceed 200 kPa. Preliminary designs of footings capable to accommodate the loading conditions corresponding to L_1, L_2, and L_3 were performed. Several widths were analyzed and based on the results of these analyses the footings were designed with widths 2, 2.25, and 2.5 m (corresponding to bearing pressures of 168, 174, and 188 kPa, respectively).

3.1.4. Reinforcement characteristics

Although the last few years there has been research related to the use of geosynthetics on reinforced soil bridge abutments (Lee and Wu, 2004; Skinner and Rowe, 2005), most of the existing cases around the world use inextensible reinforcement elements, i.e. steel strips or steel grids (Elias et al., 2001). Ribbed steel strips with a yield strength 450 MPa, 4 mm thickness, and 50 mm gross width were used in this study. The cross sectional area of the strips corrected for corrosion loss throughout a 75 years service life was calculated equal to 129 mm^2. The horizontal and vertical spacing of the reinforcement layers was set at 0.50 m, with the first layer being placed 0.30 m above the leveling pad of the wall.

For conventional reinforced soil walls the minimum reinforcement length is recommended to be 70 % of the total height of the wall. However, for special geometric configurations, external surcharge loadings, or soft foundation soil conditions, the minimum reinforcement length shall be increased. Elias et al., (2001) mention that the reinforcement length in such cases can be from 80 up to 110% of the wall height. Different strip lengths varying between the above ranges were examined during the study. The results presented in this study refer to strip lengths equal to 7, 7.5, and 8 m, corresponding to total wall heights of 6, 7, and 8 m, respectively.

3.2. Results and Discussion

As already explained, three varying parameters were chosen in order to perform the analysis. These parameters were the span length L (corresponding to specific loading conditions), the height of the reinforced soil wall H, and the foundation soil profile S. Three different cases were examined for each parameter, leading in a total of 27 analyzed cases (Table 3.3). All cases were analyzed with respect to external and internal stability criteria.

3.2.1. External stability

Table 3.4, Table 3.6, and Table 3.7 present the calculated factors of safety (FSs) against the external stability failure modes in terms of the three different soil profiles. Each column corresponds to a soil profile and it shows the resulted FSs for the 9 different combinations of superstructure loads and heights of the reinforced soil wall. Bearing in mind the recommended FSs, the conclusions that can be drawn from these tables are the following: In terms of bearing capacity, the resulted FSs are either above (19 cases), or slightly below (8 cases) the minimum recommended value of 2.5 (Table 3.4). The problematic cases refer exclusively to the soil profiles S_2 and S_3 and in conditions of long span or tall wall (Table 3.5). So, as expected, the bearing capacity failure mode is significantly affected by the soil conditions. For good soil conditions, the impact of geometry is secondary without really affecting the design. For weak (marginal) soil conditions, the geometry can be the decisive factor. Still, the decrease in FS_{BC} due to increase of wall height or span length is smaller than initially thought it would be. Comparing the impact of wall height (H) and span length (L), there seems to be a small tendency for H affecting the design more than L does. This may be due to the dissipation of the applied loads through the reinforced soil mass before reaching the bottom of the wall. In terms of sliding mode, as shown in Table 3.6, all 27 cases resulted in FSs within the range of 2.4 to 3.3, i.e. much larger than the recommended value of 1.5. For the specific foundation soil profiles that were used in the current study, sliding was not really affected by them, while it was found not to be affected by loading or geometric conditions either. Same conclusion was drawn for the overturning failure mode, for which the resulted FSs are between 4.7 and 5.4 (Table 3.7). The minimum recommended value in this case is 2.0. So, overall, it can be said that among the three modes of failure, the bearing capacity is the one that controls the design.

3.2.2. Internal stability

Figure 3.2 and Figure 3.3 show the resulted FSs against tensile failure. Figure 3.2 refers to the tallest wall (H_3 = 8 m) and the worst foundation soil profile (S_3), and it shows the variation of FSs with respect to the height above the leveling pad, for all three examined span lengths. It is noticed that the larger the span (and therefore the load from the superstructure), the lower the FSs. This is so because higher loads correspond to higher tensile stresses within the reinforced soil mass. The trend of variation in all three cases is that the FSs increase up to some depth and then they start decreasing. This is due to the fact that the tensile forces near the top of the wall are mainly affected by the high stresses due to the superstructure's loads. The impact due to the self weight of the reinforced soil mass is still low (low overburden). As we go deeper though, the stresses due to the superstructure's loads dissipate with depth, while the stresses due to the self weight increase with depth. The point where the FSs start decreasing is the point where the impact due to self weight becomes higher than that of the concentrated loads. Figure 3.3 shows the resulted FSs for the larger span (L_3 = 30 m) and the worst foundation soil profile (S_3), and it shows the variation of FSs with respect to the height above the leveling pad, for all three examined wall heights. Here we notice that, for the same depth below the top of the wall, the taller the wall the higher the FSs. This can be explained by the fact that for the same depth below the top of the wall, we have larger dissipation of the concentrated loads and therefore lower level of tensile stresses due to these loads applied on the strips. Once the impact of the self weight becomes larger than that of the externally applied loads, then the opposite trend is observed. Figure 3.4 and Figure 3.5 are the equivalents of Figure 3.2 and Figure 3.3, for the pull out mode of failure. They both demonstrate the trend for increase in FS_{PO}.

Overall, in terms of internal stability, the results indicate that as long as an appropriate density and length of reinforcement elements has been selected, none of the tensile or pull out failure mechanisms cause serious concerns. Note that the appropriate length is mainly important for the pull out mechanism. In both

mechanisms, some attention needs to be paid on the reinforcement elements located below the bridge seat. In the case of tensile failure, attention also needs to be paid on the very bottom layers. None of tensile or pull out failure is really affected by soil conditions or geometry.

3.2.3. Parametric studies

Recognizing the fact that the bearing capacity failure mode demonstrates the greatest interest among all modes of failure, parametric studies specifically addressing this mode were performed. The purpose of these studies was to investigate the performance of the reinforced soil bridge abutments for different shear strength properties of the foundation soil. Figure 3.6 shows the obtained FS_{BC} for the most adverse conditions in terms of wall height (H_3) and span length (L_3). Figure 3.7 presents the critical lines for the best (H_1-L_1) and worst (H_3-L_3) cases scenarios in terms of geometry. These lines represent the points on which $FS_{BC} = 2.5$. Any point below these lines corresponds to cases where $FS_{BC} < 2.5$ for the specific geometric conditions, while any point above correspond to $FS_{BC} > 2.5$.

3.3. Summary and Conclusions

Reinforced soil structures are a special type of earth retaining structures, on which the shear strength of an earth material is improved by the inclusion of reinforcement elements in the directions that tensile strains develop. The tensile stresses are transferred from the soil to the reinforcement elements based on a mechanism that is mobilized due to friction or passive resistance, or both. Reinforced soil structures have numerous applications in geotechnical engineering, one of which being their use as bridge abutments. In this type of application, the bridge seat may be founded either on piles that are constructed thru the reinforced soil mass, or directly on top of the reinforced soil mass without the use of deep foundations. In the latter case, the loads from the superstructure

affect both the magnitude and the locus of the tensile stresses that are developed in the reinforced soil mass.

Using current design methods, analysis of 27 cases of reinforced soil bridge abutments, without the use of piles, was performed. The purpose of the analysis was to identify cases where the stability criteria, with respect to ultimate limit states, are met. The different cases were based on variation of loading, geometric and foundation soil conditions. The major conclusions of the analysis can be summarized as following: The internal stability, that is the resistance against tensile and pull out failure of the reinforcement elements, does not create serious concerns, as long as an appropriate internal design (density and length of reinforcements) has been performed. In terms of external stability, the bearing capacity controls the design, since it is significantly affected by the soil conditions. The loading and geometric conditions may be a decisive factor on marginal soil conditions. The sliding and overturning failure mechanisms do not cause any serious concerns. Recognizing the importance of the foundation soil profile, parametric studies based on varying shear strength properties (c and φ) were performed and design charts, that under certain circumstances can be used as decision tools, were produced.

Overall, it can be said that in terms of ultimate limit states, the performance of reinforced soil bridge abutments can be satisfactory, except in poor foundation soil conditions. However, because the employment of reinforced soil walls for direct use as bridge abutments requires their high performance over the long term, one issue that needs further investigation is the analysis of stresses and strains under service loads. This type of analysis will provide a better insight regarding the magnitude of deformations' accumulation, in terms of total and differential settlements, over time and under service load conditions for these type of structures.

Table 3.1 Vertical applied loads for different span lengths

Span (m)	Dead load (kN/m)	Live load (kN/m)	Total load (kN/m)
L_1 = 18	105	160	265
L_2 = 24	160	165	325
L_3 = 30	215	170	385

Table 3.2 Shear strength properties and unit weights of soils

Soil profile	φ (^{o})	c (kN/m^2)	γ (kN/m^3)
Reinforced backfill	34	0	20
Retained backfill	30	0	19
Foundation soil, S_1	28	50	20
Foundation soil, S_2	30	5	19
Foundation soil, S_3	20	40	17

Table 3.3 Twenty seven combinations of different loading, geometric, and foundation soil conditions

	S_1	S_2	S_3
H_1 - L_1	□	□	□
H_1 - L_2	□	□	□
H_1 - L_3	□	□	□
H_2 - L_1	□	□	□
H_2 - L_2	□	□	□
H_2 - L_3	□	□	□
H_3 - L_1	□	□	□
H_3 - L_2	□	□	□
H_3 - L_3	□	□	□

Table 3.4 Results of analysis in terms of bearing capacity (min. recommendation ≥ 2.5)

	S_1	S_2	S_3
H_1 - L_1	6.8	2.8	2.7
H_1 - L_2	6.5	2.6	2.6
H_1 - L_3	6.2	2.5	2.5
H_2 - L_1	6.3	2.6	2.5
H_2 - L_2	6.1	2.5	2.4
H_2 - L_3	5.8	2.4	2.3
H_3 - L_1	5.8	2.5	2.3
H_3 - L_2	5.6	2.4	2.2
H_3 - L_3	5.4	2.3	2.1

Table 3.5 Cases where FS_{BC} < 2.5

Soil profile	S_1	0/9
	S_2	3/9
	S_3	5/9
Height of wall	H_1	0/9
	H_2	3/9
	H_3	5/9
Length of span	L_1	1/9
	L_2	3/9
	L_3	4/9

Table 3.6 Results of analysis in terms of sliding (min. recommendation ≥ 1.5)

	S_1	S_2	S_3
H_1 - L_1	3.1	2.8	2.8
H_1 - L_2	3.2	2.9	2.9
H_1 - L_3	3.3	3.0	2.9
H_2 - L_1	3.0	2.7	2.6
H_2 - L_2	3.1	2.8	2.7
H_2 - L_3	3.2	2.8	2.7
H_3 - L_1	3.0	2.6	2.4
H_3 - L_2	3.0	2.7	2.5
H_3 - L_3	3.1	2.7	2.5

Table 3.7 Results of analysis in terms of overturning (min. recommendation ≥ 2.0)

	S_1	S_2	S_3
H_1 - L_1	5.3	5.3	5.3
H_1 - L_2	5.4	5.4	5.4
H_1 - L_3	5.4	5.4	5.4
H_2 - L_1	5.0	5.0	5.0
H_2 - L_2	5.1	5.1	5.1
H_2 - L_3	5.0	5.0	5.0
H_3 - L_1	4.8	4.8	4.8
H_3 - L_2	4.8	4.8	4.8
H_3 - L_3	4.7	4.7	4.7

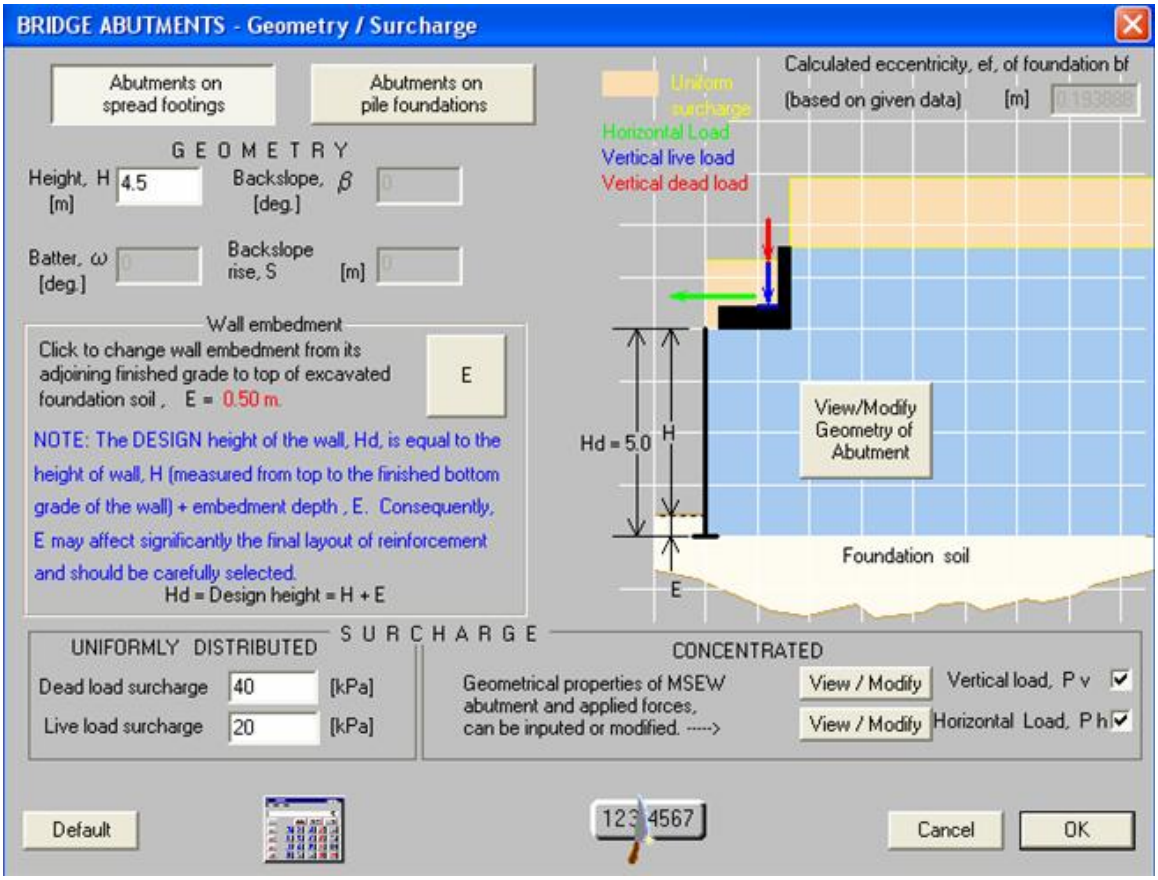

Figure 3.1 Screen view of *MSEW v. 2.0*

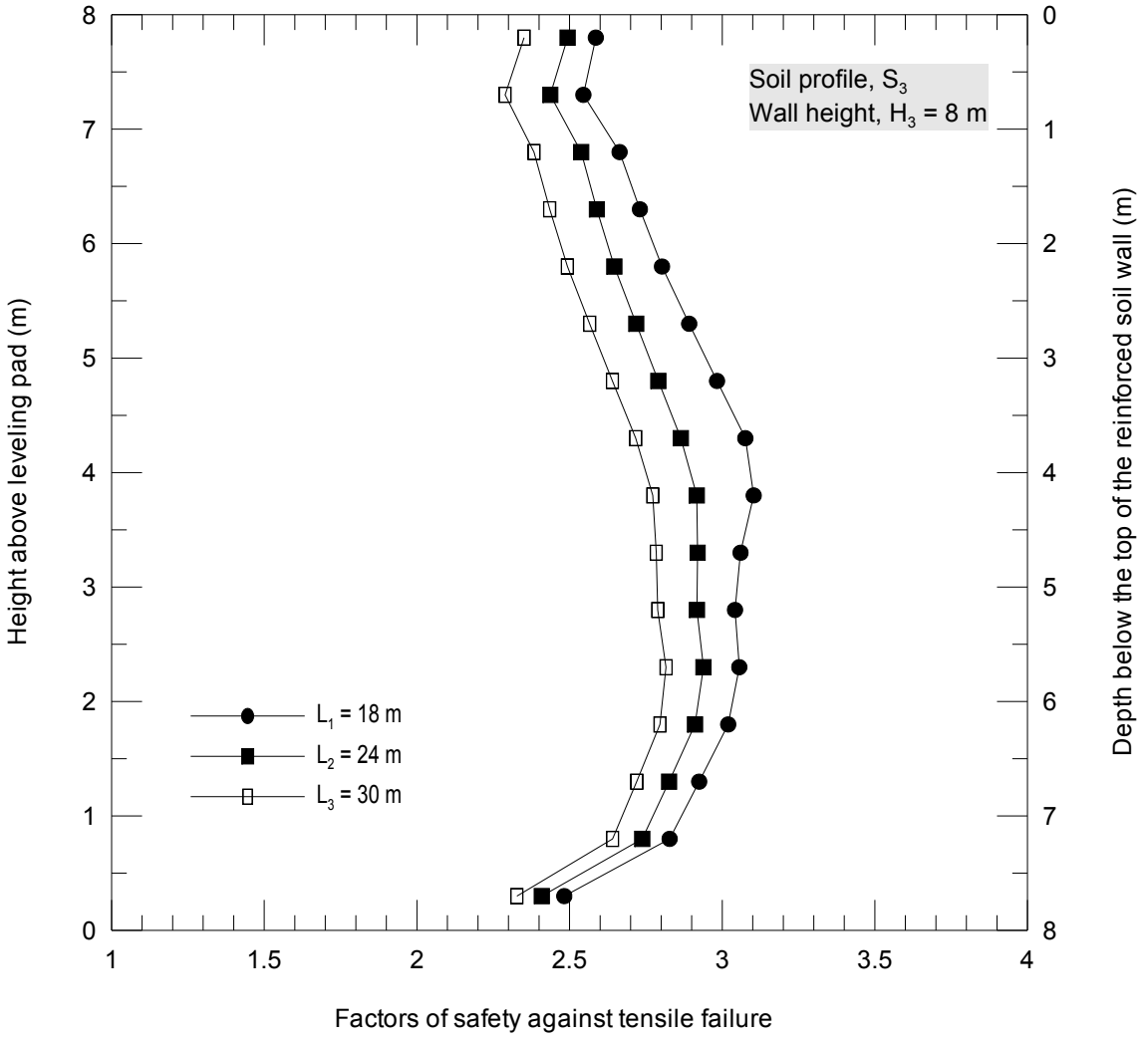

Figure 3.2 Variation of FS_{TF} with overburden, for different span lengths

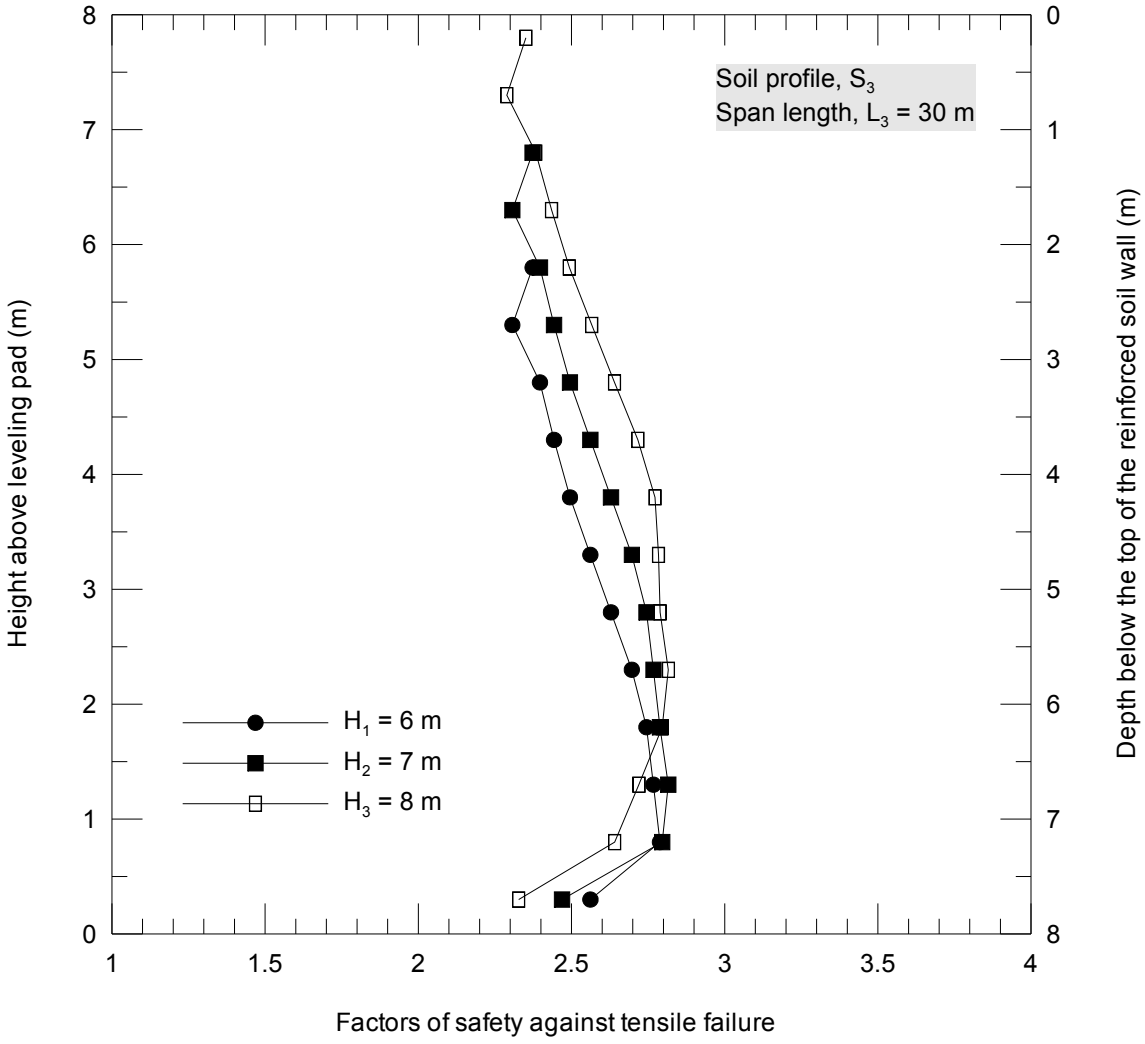

Figure 3.3 Variation of FS_{TF} with overburden, for different wall heights

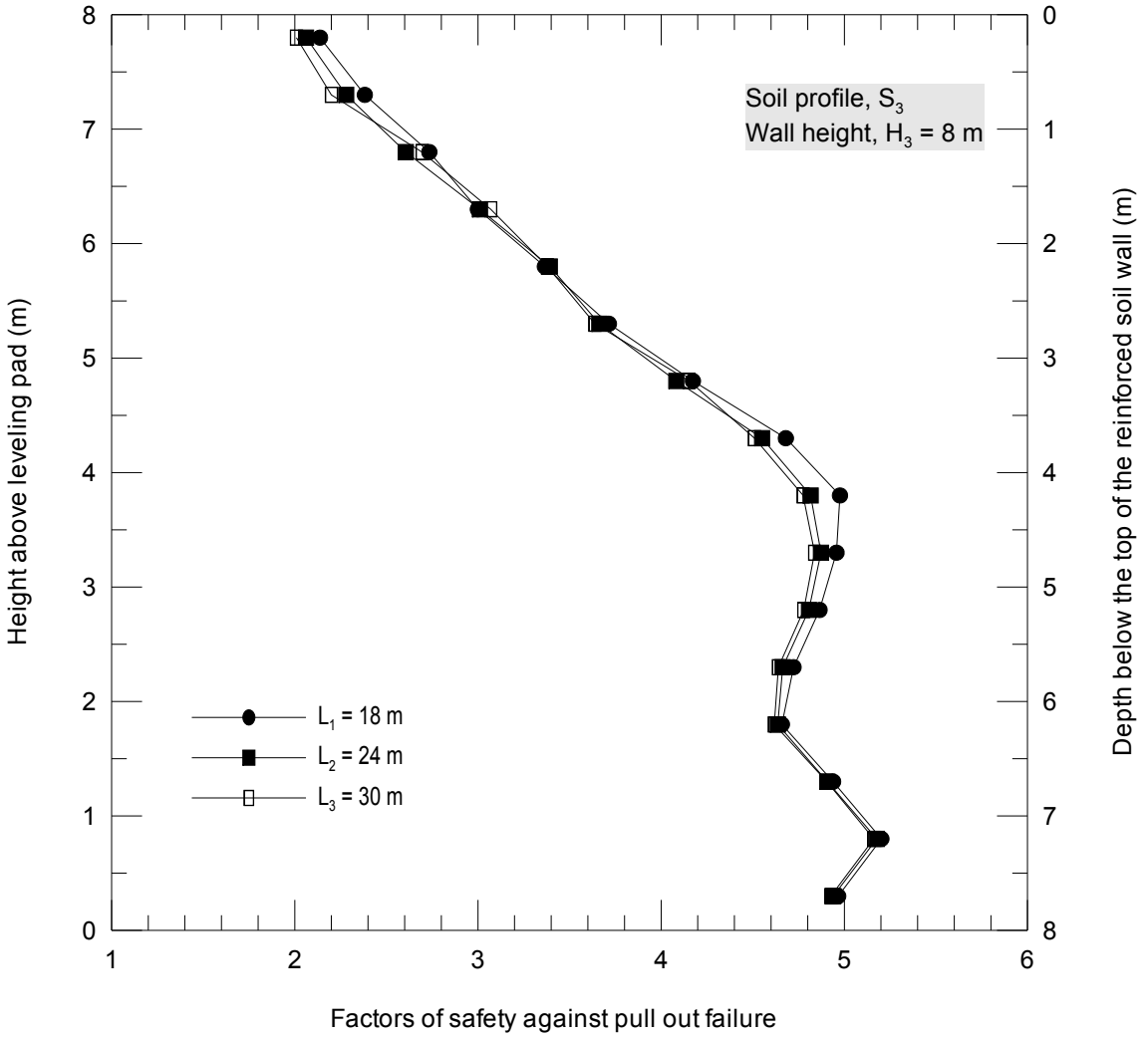

Figure 3.4 Variation of FS_{PO} with overburden, for different span lengths

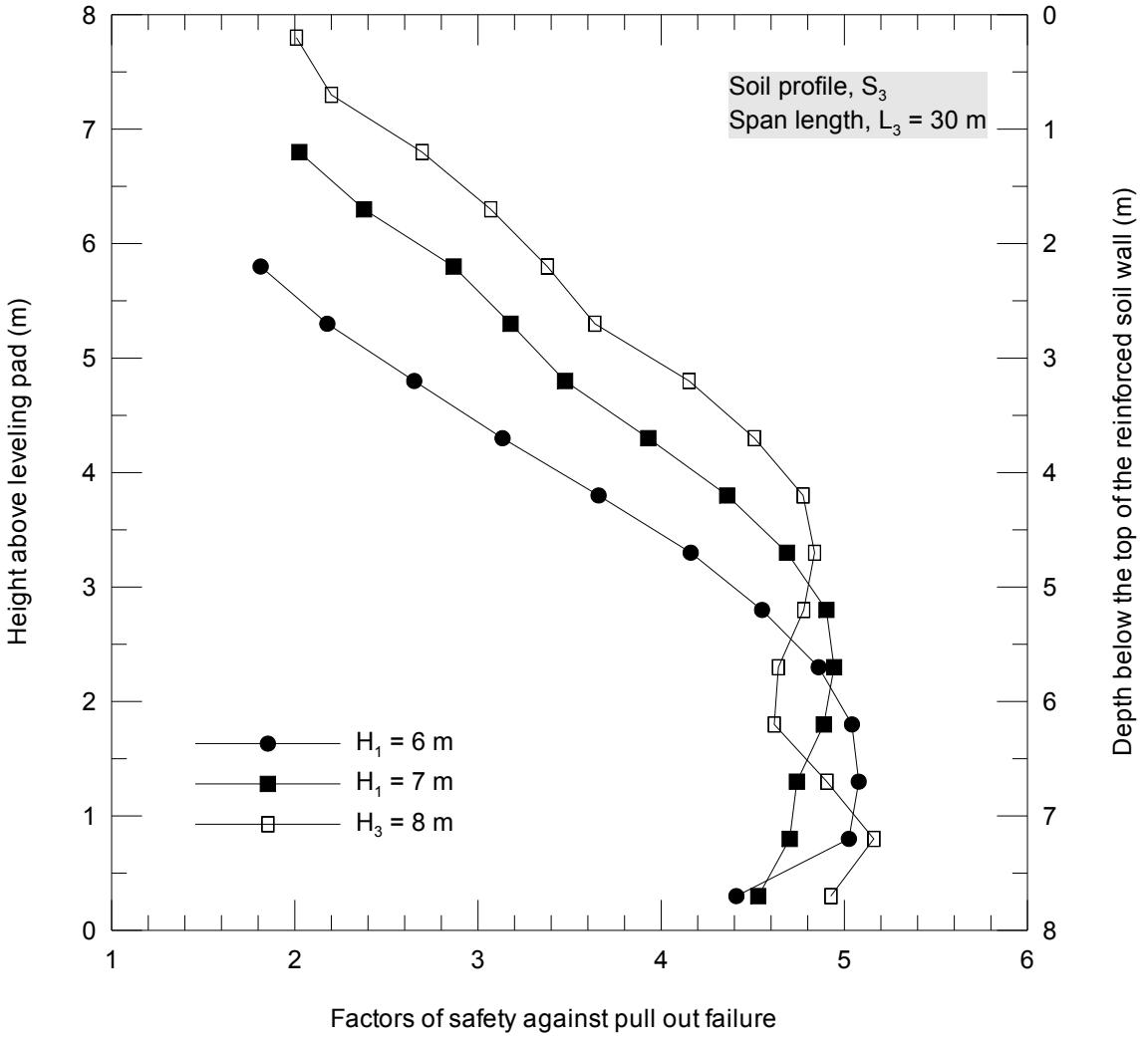

Figure 3.5 Variation of FS_{PO} with overburden, for different wall heights

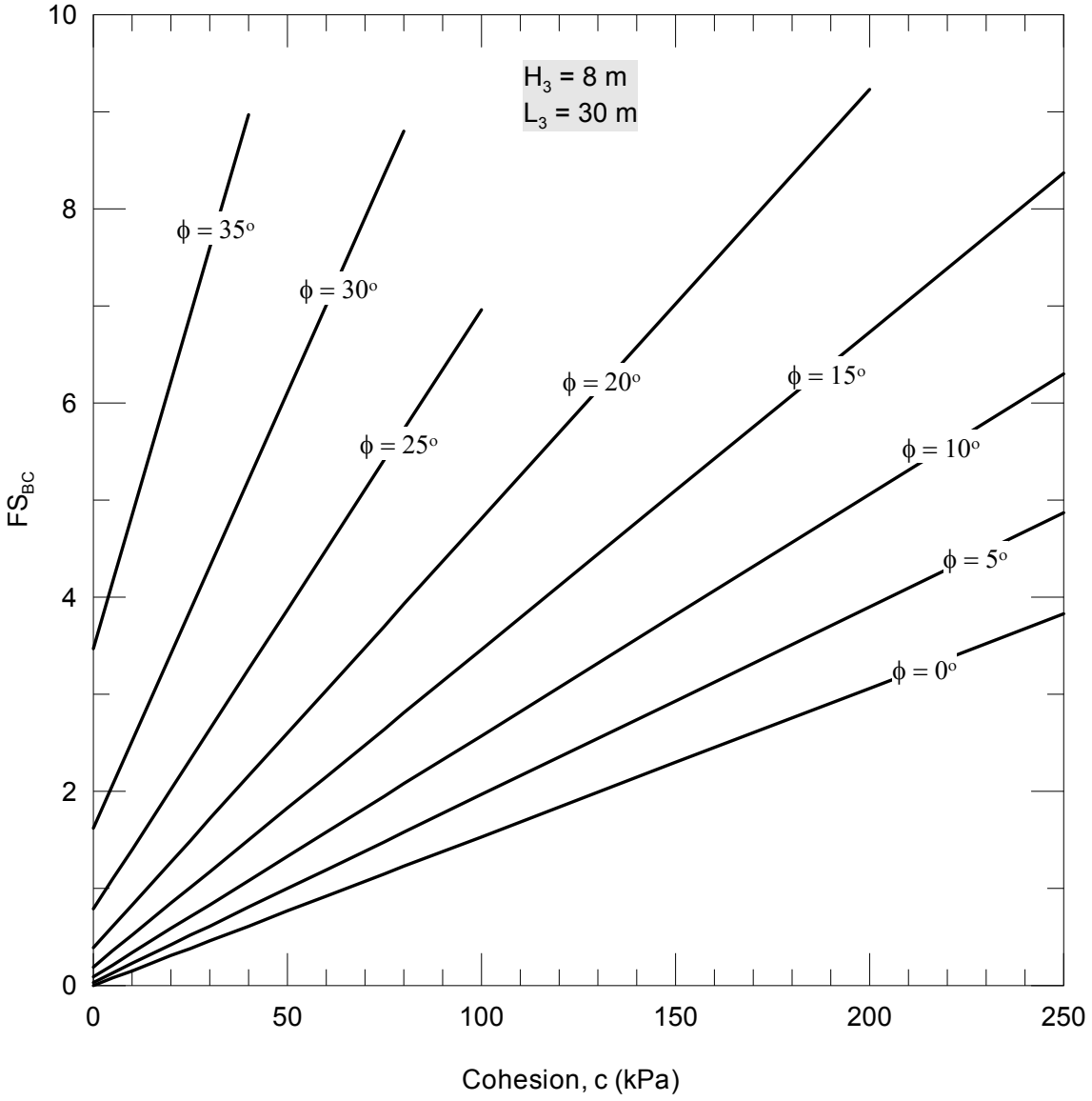

Figure 3.6 Variation of FS_{BC} for different shear strength properties of the foundation soil profile (for the H_3 - L_3 case)

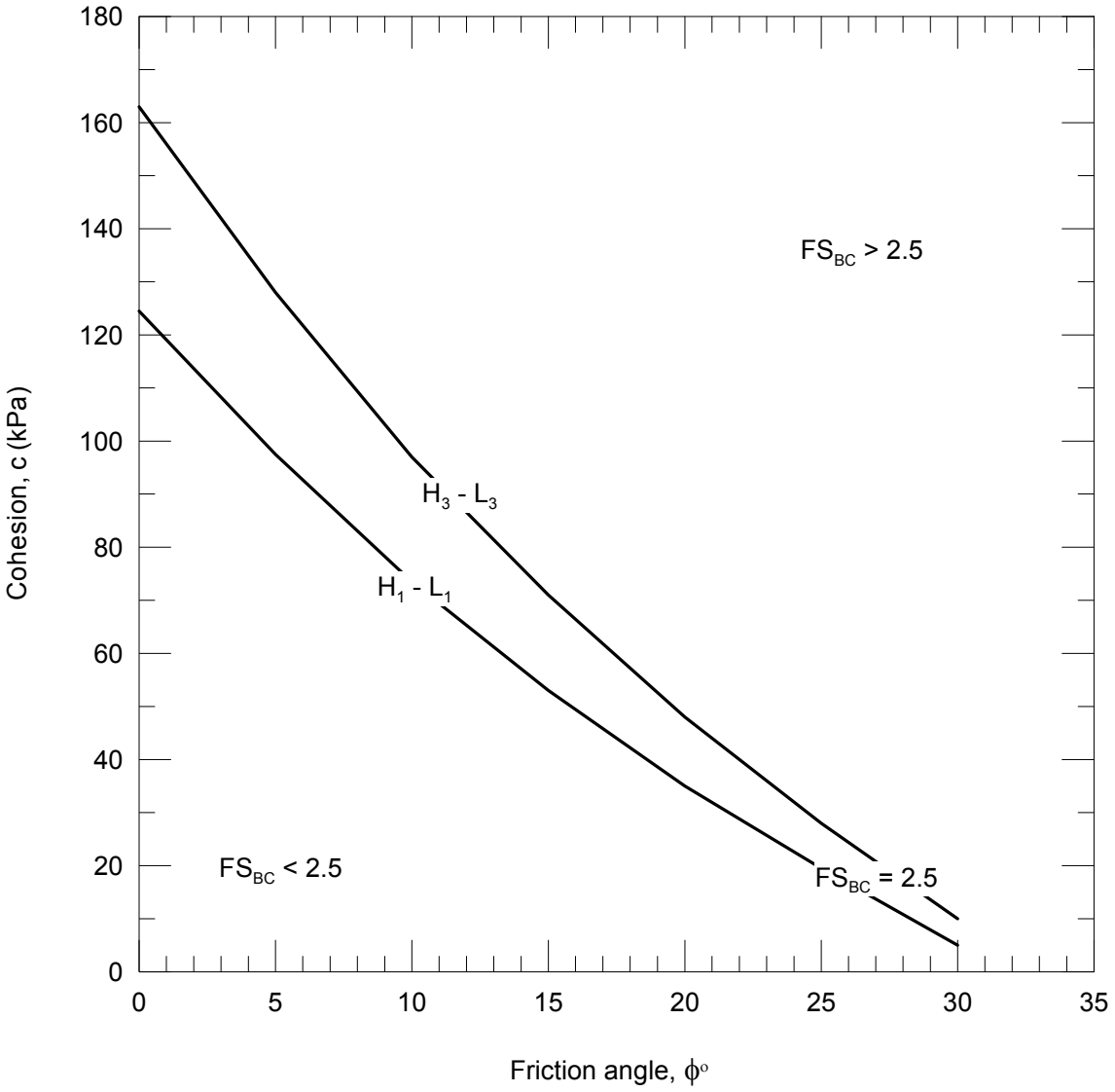

Figure 3.7 Critical lines of the bearing capacity failure mode for the two extreme cases in terms of span length and wall height

CHAPTER 4. FINITE ELEMENT ANALYSIS

4.1. Introduction

The previous chapter examined the ultimate limit states of MSE bridge abutments with predefined geometric and loading conditions, according to conventional methods of design. These methods, based on limit equilibrium principles, provide results in terms of internal and external stability of the MSE structure. However, they do not provide any information regarding serviceability limit states, such as the settlements of the foundation soil due to surcharge from the wall and the bridge. In order to assess the performance of MSE abutments with respect to settlements, the finite element method of analysis was used. This type of analysis was performed for the cases that were identified as more interesting according to the results in terms of bearing capacity of the foundation soil (Table 4.1). Specifically, the cases that were analyzed were the ones with FS_{BC} = 2.5, which is the minimum recommendation according to FHWA and AASHTO guidelines.

The well known program Plaxis was used for the finite element analysis (Brinkgreve, 2002). Plaxis is a state-of the art program, developed at the Technical University of Delft (The Netherlands) specifically for analyzing geomechanics and soil-structure interaction problems using the finite element method. Its development started in 1987, and since then the program has been extensively tested in academia and industry (references). Its capabilities to simulate stage construction and interface response between soil and other material were critical features for the application considered in this study.

The finite element analysis was performed in plane strain conditions, using 15-node triangular elements. Each element contains 12 stress points. The overall

geometry of the model needed to be big enough, so that the boundaries do not affect the deformations. In this context, for all five examined cases, the geometry extended to a distance four times the height of the MSE wall (without the abutment) in depth, and four times the width of the MSE wall, behind the MSE wall. The left boundary was taken equal to half the length of the span for each case. In terms of boundary conditions, as shown in Figure 4.1, horizontal fixities ($u_x = 0$) were applied on the left and right geometric boundaries, and full fixities ($u_x = u_y = 0$) on the bottom geometric boundary.

4.2. Structural elements modeling

4.2.1. Steel strips

As already stated in previous chapters, in terms of reinforcement, the current study considers galvanized mild steel strips, with typical properties given in Table 4.2.

On Plaxis, the reinforcement elements are modeled by line elements (called by the program “geogrid” elements). These elements are slender structures with a normal stiffness but with no bending stiffness, therefore they can sustain only tensile forces but not compressive forces. The line elements have translational degrees of freedom in each node. For the 15-node soil elements, each line element has 5 nodes, as shown in Figure 4.2. Note that the axial forces are evaluated at the Newton-Cotes stress points, which coincide with the nodes.

The only material property of a line element is an elastic normal (axial) stiffness EA, which based on the properties of Table 4.2, would be:

$$(EA)_S = 200{,}000\,\frac{MN}{m^2} \times 0.0002\,m^2 \Rightarrow (EA)_S = 40{,}000\,kN$$

However, in order to model the reinforcement strips on plane strain conditions, an approximation has to be made. This is so because in reality the strips are distinct elements and the problem of soil reinforcement using such elements is a 3-D problem (Figure 4.3). In plane strain analysis, the strips are considered continuous in the out-of-plane direction, i.e. the problem is treated in 2-D conditions (Figure 4.3). In order to model them properly, one has to determine the equivalent properties to a distinct strip of a sheet such as the one shown in Figure 4.3. To do so, the properties have to be normalized per linear meter.

The axial stiffness, S, of one unique strip is given by:

$$S = \frac{E_S A_S}{L_S}$$

For N distinct strips per linear meter, the equivalent stiffness S_N of that group of strips is given by:

$$S_N = \sum_{i=1}^{N} \frac{E_i A_i}{L_i} = N \frac{E_S A_S}{L_S}$$

where N is the total number of strips per linear meter,
A_s is the cross sectional area of the strip,
E_s is the elasticity modulus of the strip, and
L_s is the length of the strip.

On plane strain analysis, we practically substitute the N distinct strips by one sheet – strip, such as the one shown in Figure 4.3, whose equivalent stiffness is given by:

$$S_{eq} = \frac{E_{eq}A_{eq}}{L_{eq}}$$

Then, the condition that must be satisfied is:

$$S_N = S_{eq}$$

i.e. we want the equivalent steel sheet that has a width of one linear meter (and with which we model the discrete reinforcements elements) to have an axial stiffness equal to the summation of the axial stiffnesses of the individual strips that are contained within one linear meter. So we have:

$$S_N = S_{eq} \Rightarrow N\frac{E_s A_s}{\cancel{L_s}} = \frac{E_{eq}A_{eq}}{\cancel{L_{eq}}} \Rightarrow NE_sA_s = E_{eq}A_{eq} \Rightarrow \left(EA\right)_{eq} = N\cdot\left(EA\right)_S$$

If S_h is the horizontal spacing of the strips on 3-D analysis, then N is given by:

$$N = \frac{1}{S_h}$$

and the above relation can be written as following:

$$\left(EA\right)_{eq} = \frac{1}{S_h}\left(EA\right)_S$$

If we are interested in finding the equivalent thickness of the steel sheet:

$$\left(EA\right)_{eq} = N\left(EA\right)_S \Rightarrow \left(E\times bh\right)_{eq} = N\left(E\times bh\right)_S \Rightarrow$$

$$(E \times 1m \times h)_{eq} = N \times E \times 50mm \times 4mm \Rightarrow$$

$$E \times 1000\cancel{mm} \times h_{eq} = N \times E \times 50\cancel{mm} \times 4mm \Rightarrow \; h_{eq} = 0.2\,N\,(mm)$$

For instance, in the case of S_h = 0.75 m and N = 1.33 strips per linear meter, the equivalent thickness of a steel sheet is 0.27 mm (instead of 4 mm, which is the real thickness of one strip). Based on the above equations, Table 4.3 provides equivalent stiffness for a number of cases of different reinforcement densities, i.e. different horizontal spacing of the reinforcement strips.

As stated in CHAPTER 3, the horizontal distance of strips in the current study is S_h = 0.5m, so the equivalent stiffness that is used in the finite element analysis is 80,000 kN per linear meter.

4.2.2. Facing panels

Different type of facing options can be employed in reinforced soil structures. The current study considers the well known segmental precast concrete panels. Their basic properties are summarized in Table 4.4.

In order to model the facing panels on Plaxis we are using what the program calls “plates”. Plates are structural objects used to model slender structures in the ground with a significant flexural rigidity (bending stiffness) and a normal stiffness. For example, plates can be used to simulate the influence of walls, plates, shells, or linings extending in the z-direction. The most important parameters are the flexural rigidity (bending stiffness) EI and the axial stiffness EA. From these two parameters an equivalent plate thickness d_{eq} is calculated from the equation:

$$d_{eq} = \sqrt{12\frac{EI}{EA}}$$

Plates in the 2D finite element model are composed of beam elements (line elements) with three degree of freedoms per node: two translational (u_x, u_y) and one rotational (φ_z). In the 15-node soil elements that are employed in this study, each beam element is defined by five nodes (Figure 4.4). The beam elements are based on Mindlin's beam theory. This theory allows for beam deflections due to shearing as well as bending. In addition, the element can change length when an axial force is applied. Beam elements can become plastic if a prescribed maximum bending moment or maximum axial force is reached. Bending moments and axial forces are evaluated from the stresses at the stress points. A 5-node beam element contains four pairs of Gaussian stress points. Within each pair, stress points are located at a distance $1/2\,d_{eq}\sqrt{3}$ above and below the plate center-line.

The cross sectional area of the panels, perpendicular to the axial forces, and for one linear meter of wall, is:

$$A = 1\,m \times 0.14\,m \Rightarrow A = 0.14\,m^2$$

Then the axial stiffness is given by:

$$EA = 25{,}000\,\frac{MN}{m^2} \times 0.14\,m^2 \Rightarrow$$

$$EA = 3{,}500{,}000\,kN \text{ per linear meter of wall}$$

Since the thickness of the panels are d = 0.14 m, we can easily find the bending stiffness (per linear meter of wall) using the equation:

$$EI = EA\,\frac{d^2}{12} = 3{,}500{,}000\,kN \times \frac{0.14^2\,m^2}{12} \Rightarrow$$

$EI = 5{,}716.7\ kNm^2$ per linear meter of wall

The weight of the panels for one linear meter of wall (and one meter height) is given by:

$$w = 23.5\frac{kN}{m^3} \times 0.14\,m \times 1m = 3.29\frac{kN}{m} \text{ per linear meter of wall}$$

Table 4.5 summarizes the facing panels properties, as input to Plaxis.

4.2.3. EPDM bearing pads

In order to prevent direct contact and possible damage of the concrete facing panels as they seat on the top of each other, joint elements that are usually called bearing pads and are fabricated from EPDM (Ethylene Propylene Diene Monomer) rubber are installed in between them. These elements provide the needed balance between compressibility under increased load and the ability to maintain the panel joint in an open condition. Two options were examined on Plaxis in order to model the EPDM pads: as plate elements or as hinges. A hinge is a plate connection that allows for a discontinuous rotation in the point of connection (joint). This means that the plate ends can rotate freely with respect to each other. However, this option does not reflect the compressibility that develops between the panels due to the presence of the rubber pads. Therefore, the EPDM pads were modeled as plates.

Based on studies by RECo, the EPDM pads demonstrate a two-phase stress-strain behavior (RECo, 2000). Low loading produces a relatively large value of strain, corresponding in the field to a flattening of the ribs. As the load increases, corresponding to an increasing height of panels above the bearing pad elevation, the strain rate diminishes as the bearing load is distributed into the full thickness of the pad. Testing indicates only 10 to 15% thickness loss for pads at the

bottom of a wall 10.5 m high. Ergun (2002) provides a plot of load – deformation curves of pads based on experimental results (Figure 4.5). Based on this plot, an average value for the Young modulus of the bearing pads was calculated and used it in the current model.

The Young modulus is calculated based on a compressive load equal to 50 kN and a deformation of 7.5 mm (i.e. the average between the two curves).

$$E = \frac{\sigma}{\varepsilon} \Rightarrow E = \frac{N/A}{\Delta h/h}$$

The area of one bearing pad is given by:

$$A = 100\,mm \times 85\,mm = 8500\,mm^2 \Rightarrow A = 0.0085\,m^2$$

So the Young modulus is equal to:

$$E = \frac{50\,kN/0.0085\,m^2}{7.5\,mm/20\,mm} \Rightarrow E = 15686\,\frac{kN}{m^2}$$

Due to software constrains related to the scale of the problem, the bearing pads are modeled with a height equal to 60 mm, instead of 20 mm, as shown in Figure 4.6. We want the deformation on the 60 mm pad to be equal to the deformation of the 20 mm pad, i.e. we want $\Delta h_{20} = \Delta h_{60}$.

Since it is $\varepsilon = \frac{\sigma}{E}$ and $\varepsilon = \frac{\Delta h}{h}$ we have:

$$\Delta h_{20} = \Delta h_{60} \Rightarrow \varepsilon_{20} h_{20} = \varepsilon_{60} h_{60} \Rightarrow \varepsilon_{20} 20 = \varepsilon_{60} 60 \Rightarrow \varepsilon_{20} = 3\,\varepsilon_{60} \Rightarrow$$

$$\frac{\sigma_{20}}{E_{20}} = 3\,\frac{\sigma_{60}}{E_{60}} \Rightarrow E_{60} = 3\,E_{20}$$

So the elastic modulus of the 60 mm high bearing pad shall be 3 times the modulus of the 20 mm high bearing pad. This means it is:

$$E_{60} = 47{,}058 \frac{kN}{m^2}.$$

The cross sectional area of the pad is:

$$A = 100\,mm \times 85\,mm = 8500\,mm^2 \Rightarrow A = 0.0085\,m^2$$

So the axial stiffness is given by:

$$(EA)_{60} = 0.0085\,m^2 \times 47{,}058 \frac{kN}{m^2} = 399.93\,kN \Rightarrow$$

$$(EA)_{60} = 400.0\,kN\,\text{per linear meter}$$

The above refers to one single bearing pad with dimensions 100 mm x 85 mm x 60 mm. Since our model is a plane strain model, we need to model the pad with a linear sheet:

$$(EA)_{eq} = N(EA)_{PAD,60}$$

Assuming we have two bearing pads per panel, the number of pads per linear meter of wall is:

$$N = \frac{2}{1.5} = \frac{1}{0.75} = \frac{4}{3}$$

So,

$$(EA)_{eq} = \frac{4}{3} \times 400 = 533.3\,\text{kN per linear meter}$$

To get the bending stiffness per linear meter, since we know the thickness of the panels (d = 0.085 m):

$$EI = EA\frac{d^2}{12} = 533.3\,\text{kN} \times \frac{0.085^2\,\text{m}^2}{12} = 0.321\,\text{kNm}^2 \Rightarrow$$

$$EI = 0.321\,\text{kNm}^2 \text{ per linear meter}$$

Table 4.6 summarizes the properties of the EPDM pads as these are used as input on Plaxis. Note that we assume the pads are weightless and that the Poisson's ratio is very high.

4.2.4. Strip footing (bridge seat)

The bridge seat is modeled with 15-nodes triangular linear elastic non-porous elements (Figure 4.7). The numerical integration of these elements involves 12 Gaussian stress points. The unit weight is taken equal to 23.5 kN/m^3. The Poisson's ration and Young modulus are taken equal to 0.20 and 25,000,000

4.2.5. Leveling pad

The leveling pad is typically non-reinforced concrete and its purpose is to serve as a guide for the facing panels erection. The leveling pad is not intended as a structural foundation support. Its dimensions are typically 150 mm thickness (height) and 300 mm width. The leveling pad was modeled in the exact same way, and with the same properties, as the bridge seat.

4.3. Interfaces modeling

4.3.1. General

The interaction between soil and reinforcement elements, as well as between soil and other structural elements, were modeled by interface elements. For the 15-node soil elements that are used in the current study, each interface element has five pair of nodes (five nodes on one side of the geometry and five on the other). Note that the interface elements have zero thickness, i.e. the coordinates of each pair are identical. Their stiffness matrix is obtained by means of Newton Cotes integration. Therefore, the position of the five stress points coincides with the five node pairs (Figure 4.8).

The behavior of the interfaces is described by an elastic – plastic model and the Coulomb criterion is used to distinguish between elastic behavior, where small displacements can occur within the interface, and plastic interface behavior, where permanent slip may occur. So, the interface remains elastic when:

$$|\tau| < \sigma_n \tan\varphi_i + c_i$$

and moves into plastic region when:

$$|\tau| = \sigma_n \tan\varphi_i + c_i$$

where φ_i and c_i are the friction angle and the cohesive intercept of the interface, respectively. These two parameters are linearly related to the strength parameters of the soil layer by the following relations:

$$\tan\varphi_i = R_{inter} \times \tan\varphi_{soil}$$

$$c_i = R_{inter} \times c_{soil}$$

where R_{inter} is the so-called strength reduction factor with

$$0.01 \leq R_{inter} \leq 1$$

The dilatancy angle of the interface is given by the following relation:

$$\psi_i = \begin{cases} 0 & \text{for } R_{inter} < 1 \\ \psi_{soil} & \text{for } R_{inter} = 1 \end{cases}$$

When the interface is elastic, then both slipping or overlapping may occur. By slipping it is meant a relative movement parallel to the interface, and by overlapping a relative displacement perpendicular to the interface. The magnitudes of these displacements are given by the following expressions:

$$\text{Elastic gap displacement} = \frac{\sigma\, t_i}{E_{oed,i}}$$

$$\text{Elastic slip displacement} = \frac{\tau\, t_i}{G_i}$$

where G_i is the shear modulus of the interface, $E_{oed,i}$ is the one-dimensional compression modulus of the interface, and t_i is the virtual thickness of the interface. The compression and shear moduli are given by the following expressions:

$$E = 2G_i \frac{1 - v_i}{1 - 2v_i}$$

$$G_i = R_{inter}^{\ 2}\, G_{soil} \le G_{soil}$$

$$v_i = 0.45$$

4.3.2. Soil – strip interface modeling

The real problem of strip to soil interface friction is shown schematically in Figure 4.9a. An apparent friction, δ, which for overburden up to 6 m is higher than the friction φ of the soil itself, is mobilized in the area surrounding each strip. The coefficient of apparent friction, f, is given by:

$$f = \begin{cases} \tan\delta = 1.2 + \log c_u & \text{at the top of the structure} \\ \tan\varphi & \text{at a depth of 6 m and below} \end{cases}$$

where c_u and φ are the coefficient of uniformity and the friction angle, respectively, of the reinforced soil. Note that the maximum value that f can take is equal to 2. The above relation, for c_u = 4, is presented graphically in Figure 4.10.

As already explained in previous paragraphs, the current analysis is performed for plane strain conditions, which practically means that we represent the three dimensional problem of the apparent coefficient of friction into a two dimensional problem. This is presented schematically in Figure 4.9b. In order to do so, we must determine the equivalent coefficient of apparent friction. Assuming we have N strips (of width b = 50 mm) per linear meter of wall, the tensile force of these N strips is given by:

$$T_{strips/meter} = 2\, b\, N\, \sigma'_{AV}\, \tan\delta\, l_a$$

where σ'_{AV} is the average effective stress applied on a reinforcement layer, and l_a is the length of the reinforcement within the resistive area. Then the tensile

forces developed on the remaining soil to soil interface (that has a length equal to 1 – b N) due to the friction angle of the soil φ are given by:

$$T_{soil/meter} = 2\left(1 - b\,N\right)\sigma'_{AV}\,\tan\varphi\,l_a$$

The equivalent tensile forces developed on one strip (of width B = 1 m) are given by:

$$T_{plate/meter} = 2\,B\,\sigma'_{AV}\,\tan\delta^{*}\,l_a$$

We want this equivalent tensile force to be equal to the summation of the tensile forces developed on the strip to soil and soil to soil interfaces. This means that we have:

$$T_{strips/meter} + T_{soil/meter} = T_{plate/meter} \Rightarrow$$

$$2\,b\,N\,\sigma'_{AV}\,\tan\delta\,l_a + 2\left(1 - b\,N\right)\sigma'_{AV}\,\tan\varphi\,l_a = 2\,B\,\sigma'_{AV}\,\tan\delta^{*}\,l_a \Rightarrow$$

$$\left(0.05\right)N\,\tan\delta + \left(1 - 0.05N\right)\tan\varphi = \left(1\right)\tan\delta^{*} \Rightarrow$$

$$\tan\delta^{*} = 0.05N\,\tan\delta + \left(1 - 0.05N\right)\tan\varphi$$

So, the equivalent coefficient of apparent friction for the plane strain analysis is given by:

$$f^{*} = \begin{cases} \tan\delta^{*} = 0.05N\,\tan\delta + \left(1 - 0.05N\right)\tan\varphi & \text{at the top of the structure} \\ \tan\varphi & \text{at a depth of 6 m and below} \end{cases}$$

Based on the above equation, Table 4.7 provides the values of equivalent apparent coefficients of friction, for N = 2 strips per linear meter (i.e. S_h = 0.5m) and for varying depth.

So, in order to model the equivalent apparent friction angles along the soil – strip interfaces, we need strength reduction factors that are actually higher than one. However, as already explained earlier, Plaxis does not allow these factors to get values higher than one. For simplicity purposes, it was decided that all interfaces will be modeled using R = 1, since this is anyway an assumption on the safe side.

4.3.3. Soil – concrete interface modeling

Soil to concrete interfaces always demonstrate reduced strength behavior with respect to soil to soil interfaces. Typical factors for decreasing the friction angle and the cohesive intercept along such interfaces are provided in the literature. For this study a factor of 2/3 is used. So, the interfaces properties are given by the following relations:

$$\tan\varphi_i = R_{inter} \times \tan\varphi_{soil} \Rightarrow \tan\varphi_i = \frac{2}{3} \times \tan\varphi_{soil}$$

$$c_i = R_{inter} \times c_{soil} \Rightarrow c_i = \frac{2}{3} \times c_{soil}$$

4.4. Soil modeling

Soil is modeled with 15-nodes triangular linear elastic non-porous elements (Figure 4.7). The numerical integration of these elements involves 12 Gaussian stress points. Two different constitutive models were used in the current study: the Mohr – Coulomb model, and the Hardening Soil model. The Hardening Soil model is a double stiffness model with isotropic hardening. Its advantages

compared to Duncan – Chung's hyperbolic model are that it uses the theory of plasticity rather than elasticity, it includes soil dilatancy, and it introduces a yield cap. Compared to an elastic – perfectly plastic model, its yield surface is not fixed in terms of principal stress state but it can expand due to plastic straining. In the The Hardening Soil model distinction is made between two types of straining: shear hardening that models irreversible strains due to primary deviatoric loading, and compression hardening that models strains due to primary compression loading.

The basic constitutive equations of the Hardening Soil model are presented in the following paragraphs. For the sake of convenience, equations are presented for TX CD conditions ($\sigma'_2 = \sigma'_3$). The relationships between axial strain ε_1 and deviatoric stress q is approximated by a hyperbola (Kondner and Zelasko, 1963):

$$\varepsilon_1 = \frac{q_\alpha}{2E_{50}} \cdot \frac{q}{q_\alpha - q} \Rightarrow \varepsilon_1 = \frac{q_\alpha}{2E_{50}} \cdot \frac{q}{1 - \frac{q}{q_\alpha}} \qquad [1]$$

where ε_1 is the axial strain,

q_α is the asymptotic value of shear strength,

E_{50} is the stiffness modulus for primary loading, and

q is the deviatoric stress that for TX conditions is given by $q = \sigma'_1 - \sigma'_3$.

The asymptotic value of shear strength is related to the ultimate deviatoric stress q_f with the following equation:

$$q_f = R_f \times q_\alpha$$

where R_f is the failure ratio that must be less than 1.
A suitable value is usually $R_f = 0.9$. Apparently, it is always:

$q < q_f$

The ultimate deviatoric stress, derived from the Mohr – Coulomb criterion, is given by:

$$q_f = \frac{6 \sin\varphi_p}{3 - \sin\varphi_p}\left(p' + c \cdot \cot\varphi\right)$$

where p' is the mean stress given by:

$$p' = \frac{\sigma'_1 + \sigma'_2 + \sigma'_3}{3} = \frac{\sigma'_1 + 2\sigma'_3}{3}$$

Going back to Eq. [1], as soon as $q = q_f$, the failure criterion is satisfied and perfectly plastic yielding occurs as this is described by the Mohr Coulomb model.

Stiffness for primary loading

The highly non-linear stress – strain behavior for primary loading is modeled using a stiffness modulus, E_{50}, that depends on the confining stress, σ'_3. This is given by:

$$E_{50} = E_{50}^{ref}\left(\frac{\sigma'_3 + c \cdot \cot\varphi}{p^{ref} + c \cdot \cot\varphi}\right)^m$$

where E_{50}^{ref} is the reference stiffness modulus for a specific reference stress, p^{ref},

p^{ref} is the reference stress for which E_{50}^{ref} is defined,

σ'_3 is the effective confining stress, and

m is a unitless numbers that defines the dependency of E_{50} to the confining stress.

For c = 0, such as in sands and normally consolidated clays, the above equations gives:

$$E_{50} = E_{50}^{ref}\left(\frac{\sigma'_3}{p^{ref}}\right)^m$$

In order to simulate a logarithmic stress dependency, as observed for soft clays, it shall be m = 1. Then the above can be written as:

$$E_{50} = E_{50}^{ref}\frac{\sigma'_3}{p^{ref}}$$

For other type of soils, Janbu (1963) reported values of approximately 0.5 for Norwegian sands and silts, and Von Soos (1983) reported values between 0.5 and 1 for various types of soils.

Stiffness for unloading / reloading:

For unloading / reloading purposes, another stiffness modulus, E_{ur}, that also depends on the confining stress is used. This is given by:

$$E_{ur} = E_{ur}^{ref}\left(\frac{\sigma'_3 + c\cdot\cot\varphi}{p^{ref} + c\cdot\cot\varphi}\right)^m$$

where E_{ur}^{ref} is the reference Young modulus for unloading / reloading for a specific reference stress, p^{ref}.

By using the reference Young modulus, the unloading / reloading path is modeled as purely (non-linear) elastic.

The elastic components of strain ε^e are calculated based on a Hookean type of elastic relation using the above equation (for p^{ref} = 100 kPa) and:

$$G_{ur} = \frac{1}{2(1+v_{ur})} E_{ur}$$

where G_{ur} is the uloading / reloading shear modulus, and

v_{ur} is the unloading / reloading Poisson's ration (constant).

For TX conditions, it is $\sigma'_2 = \sigma'_3$ = constant, so it is also E_{ur} = constant. Then the elastic strains are given by:

$$\varepsilon_1^e = \frac{q}{E_{ur}} \qquad \text{and} \qquad \varepsilon_2^e = \varepsilon_3^e = v_{ur} \frac{q}{E_{ur}}$$

Stiffness for oedometer loading:

For compression loading, a third stiffness modulus, E_{oed}, that also depends on the confining stress is used. This is given by:

$$E_{oed} = E_{oed}^{ref} \left(\frac{\sigma'_3 + c \cdot \cot\varphi}{p^{ref} + c \cdot \cot\varphi} \right)^m$$

where E_{oed}^{ref} is the reference modulus for compression loading for a specific reference stress, p^{ref}.

Yield surface, failure condition, hardening law

For TX conditions, the two hardening laws are given by:

$$f_{12} = \frac{q_\alpha}{2E_{50}} \cdot \frac{(\sigma'_1 - \sigma'_2)}{q_\alpha - (\sigma'_1 - \sigma'_2)} - \frac{2(\sigma'_1 - \sigma'_2)}{E_{ur}} - \gamma^p$$

$$f_{13} = \frac{q_\alpha}{2E_{50}} \cdot \frac{(\sigma'_1 - \sigma'_3)}{q_\alpha - (\sigma'_1 - \sigma'_3)} - \frac{2(\sigma'_1 - \sigma'_3)}{E_{ur}} - \gamma^p$$

where γ^p is the measure of plastic shear strain and the relevant parameter for frictional hardening.

The plastic shear strain is given by:

$$\gamma^p = \varepsilon_1^p - \varepsilon_2^p - \varepsilon_3^p = \varepsilon_1^p + \left(\varepsilon_1^p - \varepsilon_1^p\right) - \varepsilon_2^p - \varepsilon_3^p = 2\varepsilon_1^p - \left(\varepsilon_1^p + \varepsilon_2^p + \varepsilon_3^p\right) \Rightarrow$$

$$\gamma^p = 2\varepsilon_1^p - \varepsilon_v^p \Rightarrow \gamma^p \approx 2\varepsilon_1^p$$

Note that the plastic volumetric strain ε_v^p is never exactly zero, however for hard soils it is $\varepsilon_1^p \gg \varepsilon_v^p$, so the above approximation is generally accurate.

For a constant value of γ^p, the yield condition can be visualized in p' – q plane by means of a yield locus. Apparently the shape of the yield loci depends also on the parameter m. For m = 1, straight lines are obtained, while for m < 1 slightly curved lines are obtained.

Flow rule, plastic potential functions

The relationship between rates of plastic strain and $\dot{\gamma}^p$ is given by:

$$\dot{\varepsilon}_v^p = \sin\psi_m \dot{\gamma}^p \qquad \text{(flow rule)}$$

where ψ_m is the mobilized dilatancy angle given by:

$$\sin\psi_m = \frac{\sin\varphi_m - \sin\varphi_{cv}}{1 - \sin\varphi_m \sin\varphi_{cv}}$$

where φ_m is the mobilized friction angle, and

φ_{cv} is the critical state friction angle.

The mobilized friction angle is given by:

$$\sin\varphi_m = \frac{\sigma_1' - \sigma_3'}{\sigma_1' + \sigma_3' - 2c \cdot \cot\varphi}$$

At failure, when the mobilized friction angle equals the failure angle φ, then:

$$\sin\psi = \frac{\sin\varphi - \sin\varphi_{cv}}{1 - \sin\varphi \sin\varphi_{cv}}$$

or equivalently:

$$\sin\varphi_{cv} = \frac{\sin\varphi - \sin\psi}{1 - \sin\varphi \sin\psi}$$

In Plaxis, one has to provide input data on the ultimate friction angle φ and ultimate dilatancy angle ψ, and the program calculates the critical state friction angle.

The plastic potential functions are given by (non-associated flow rule):

$$g_{12} = \frac{1}{2}(\sigma'_1 - \sigma'_2) - \frac{1}{2}(\sigma'_1 + \sigma'_2)\sin\psi$$

$$g_{13} = \frac{1}{2}(\sigma'_1 - \sigma'_3) - \frac{1}{2}(\sigma'_1 + \sigma'_3)\sin\psi$$

Table 4.1 Bearing capacity safety factors according to conventional design methods (with bold the cases analyzed with the finite elements)

	S_1	S_2	S_3
H_1 - L_1	6.8	2.8	2.7
H_1 - L_2	6.5	2.6	2.6
H_1 - L_3	6.2	**2.5**	**2.5**
H_2 - L_1	6.3	2.6	**2.5**
H_2 - L_2	6.1	**2.5**	2.4
H_2 - L_3	5.8	2.4	2.3
H_3 - L_1	5.8	**2.5**	2.3
H_3 - L_2	5.6	2.4	2.2
H_3 - L_3	5.4	2.3	2.1

Table 4.2 Basic properties of steel strips

Property	Symbol	Vale
Width	b	50 mm
Thickness	t	4 mm
Cross sectional area	A	0.0002 m^2
Modulus of elasticity	E	200,000 MPa
Poisson's ration	v	0.30
Yield strength	F_y	450 MPa
Ultimate tensile strength	F_U	520 MPa

Table 4.3 Equivalent axial stiffness

S_h (m)	N	h_{eq} (mm)	$(EA)_{eq}$ (kN)
0.75	4/3	0.27	53,333
0.50	6/3	0.40	80,000
0.375	8/3	0.53	106,667

Table 4.4 Basic properties of facing panels

Property	Symbol	Value
Height	h	1.50 m
Width	w	1.50 m
Thickness	d	0.14 m
Modulus of elasticity	E	25,000 MPa
Poisson's ratio	v	0.20
Unit weight	γ	23.5 kN/m^3
28-day compressive strength	f_c'	28 MPa

Table 4.5 Properties of facing panels (as input to Plaxis)

Material type	Elastic	
Property	Value	Units
EA	3,500,000	kN/m
EI	5,716.7	kNm^2/m
d	0.14	m
w	3.29	kN/m/n
v	0.20	

Table 4.6 Properties of EPDM pads (as input to Plaxis)

Material type	Elastic	
Property	Value	Units
EA	533.3	kN/m
EI	0.321	kNm^2/m
d	0.085	m
w	0	kN/m/n
v	0.495	

Table 4.7 Equivalent apparent friction for plane strain analysis and corresponding strength reduction factors (for 2 strips per linear meter)

z (m)	δ^* (^{o})	R_{inter}
0	38.2	1.17
1	37.5	1.14
2	36.9	1.11
3	36.2	1.08
4	35.5	1.06
5	34.7	1.03
6	34	1
7	34	1
8	34	1

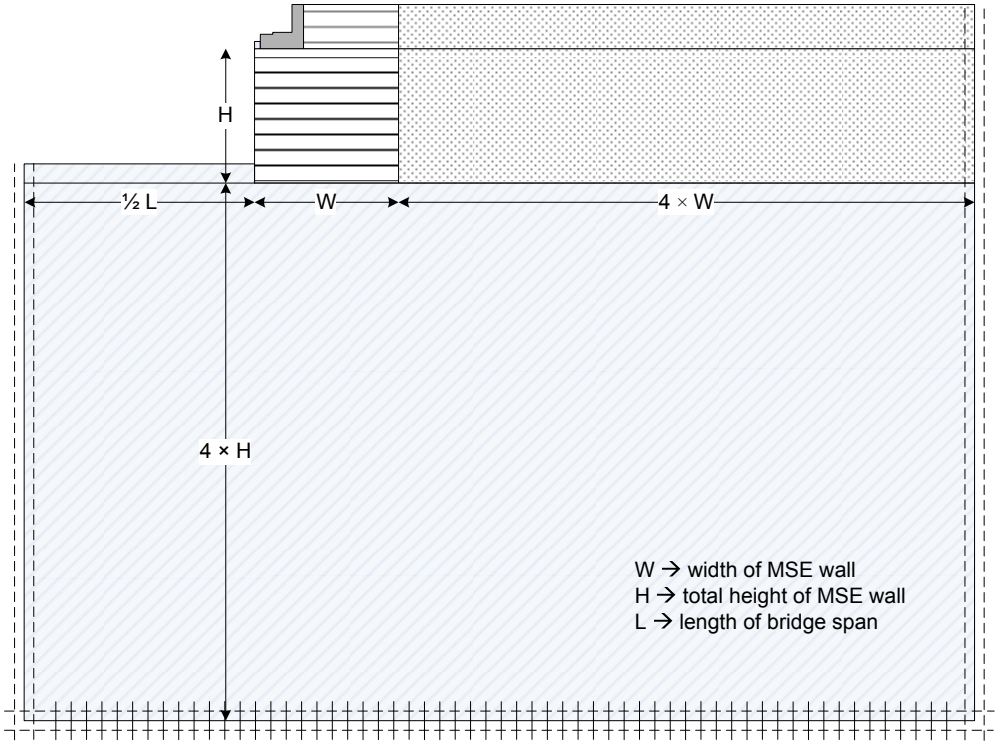

Figure 4.1 Geometry and boundary conditions in the finite element analysis

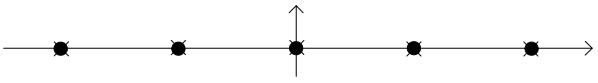

Figure 4.2 Position of nodes and stress points in a 5-node geogrid element

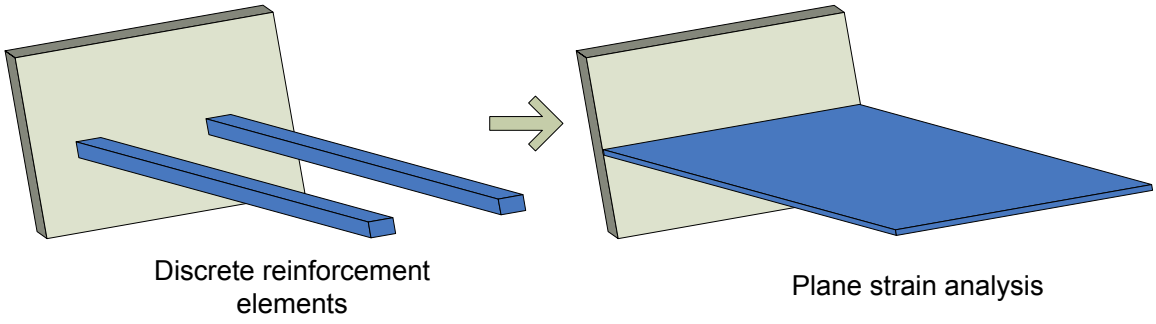

Figure 4.3 Representation of 3-D and 2-D (plane strain) analysis

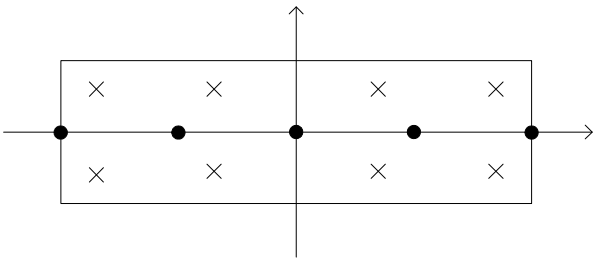

Figure 4.4 Position of nodes and stress points in a 5-node beam element

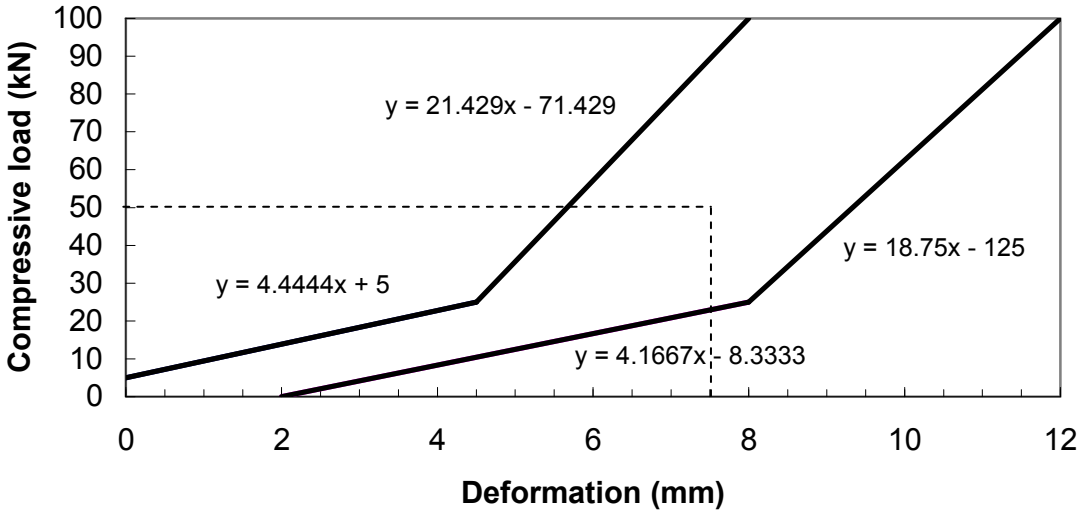

Figure 4.5 Envelope of load – deformation behavior of a typical EPDM pad (based Ergun)

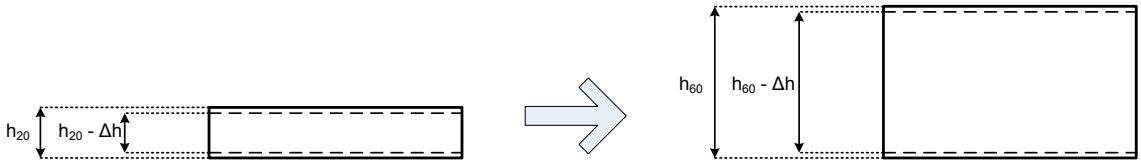

Figure 4.6 Modeling of EPDM pads in finite elements

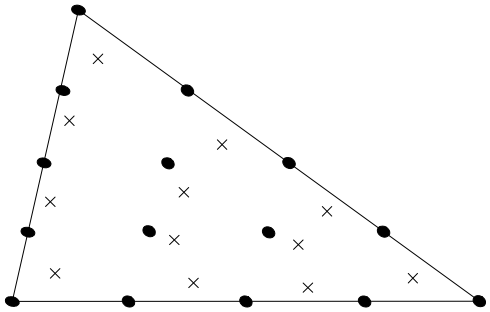

Figure 4.7 Position of nodes and stress points on a 15-node triangular element

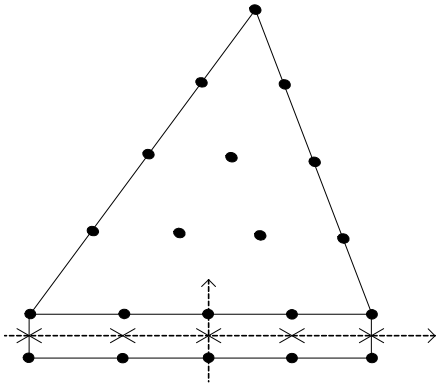

Figure 4.8 Distribution of nodes and stress points of interface elements with respect to the soil element (in reality, in the finite element analysis the coordinates of each pair of nodes are identical)

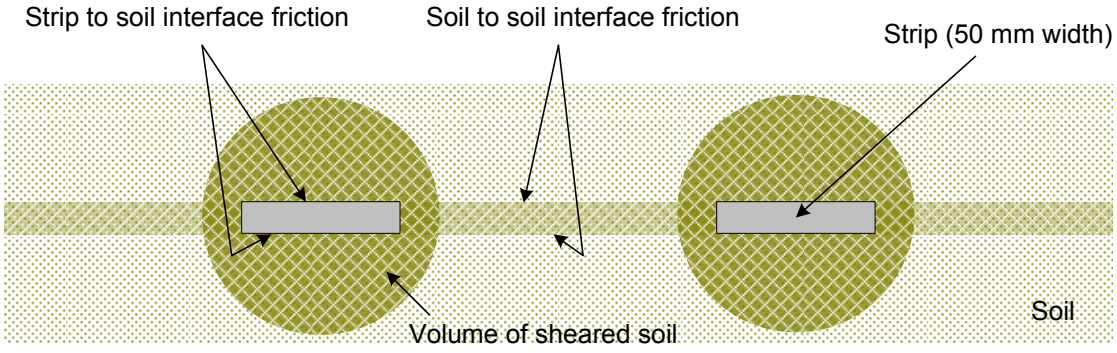

a.

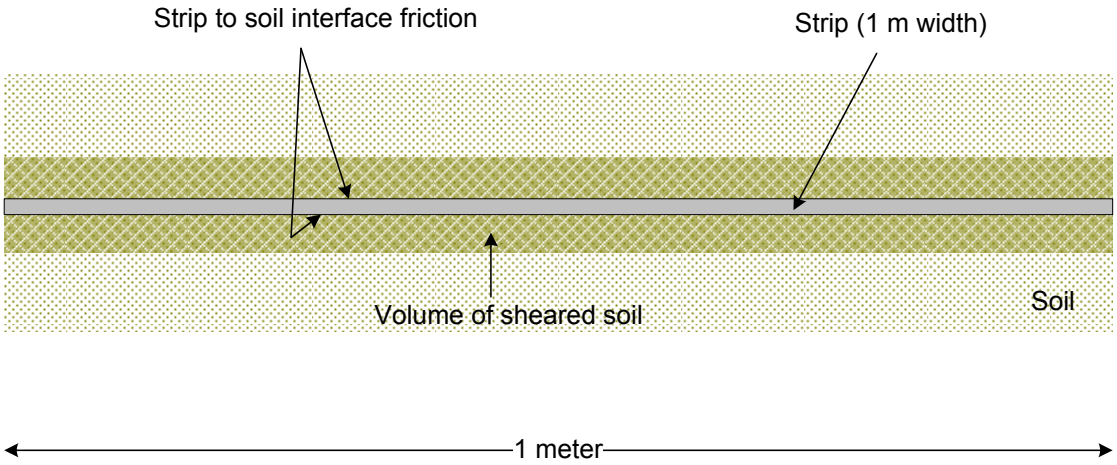

b.

Figure 4.9 (a) Representation of the 3-D apparent coefficient of friction phenomenon. (b) Representation of the apparent coefficient on a 2-D (plane strain) analysis

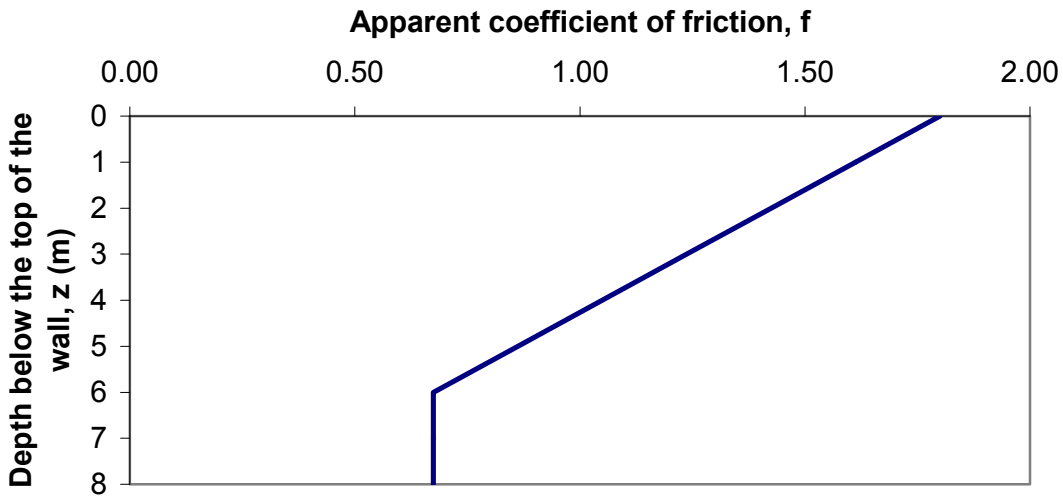

Figure 4.10 Variation of coefficient of apparent friction with overburden pressure

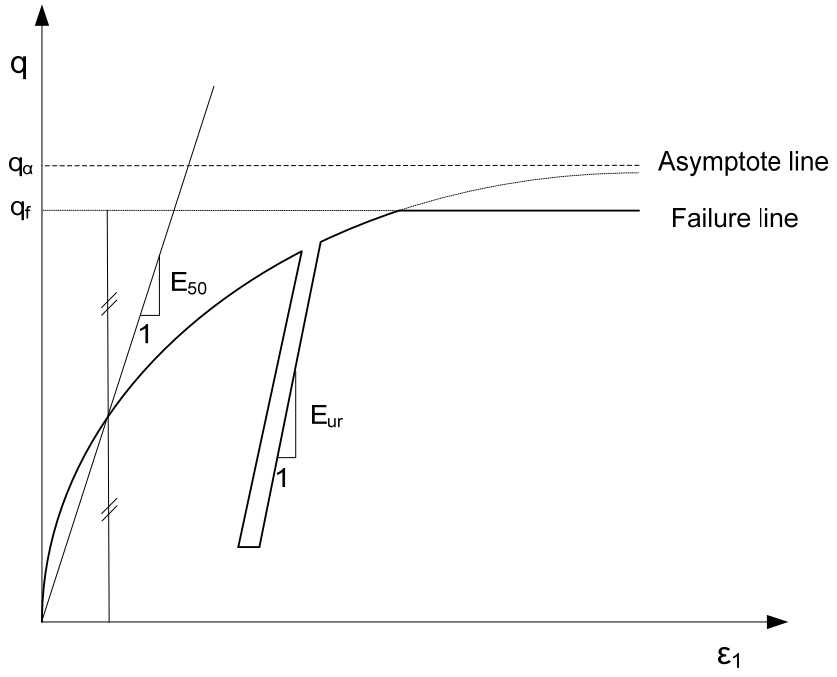

Figure 4.11 Graphical representation of the hyperbolic stress - strain relation

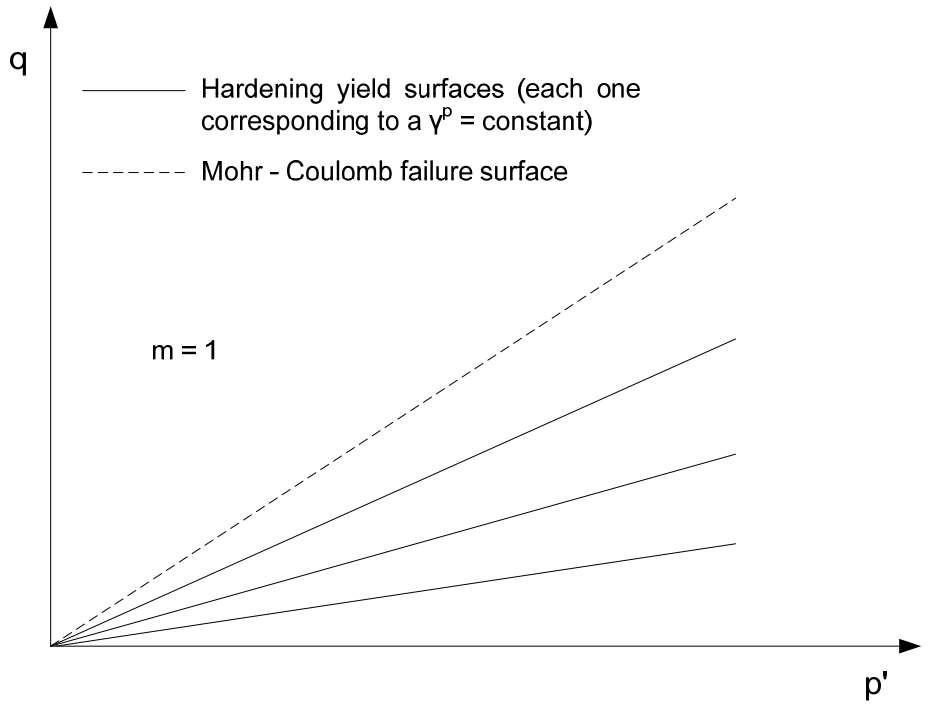

Figure 4.12 Shear hardening yield surfaces

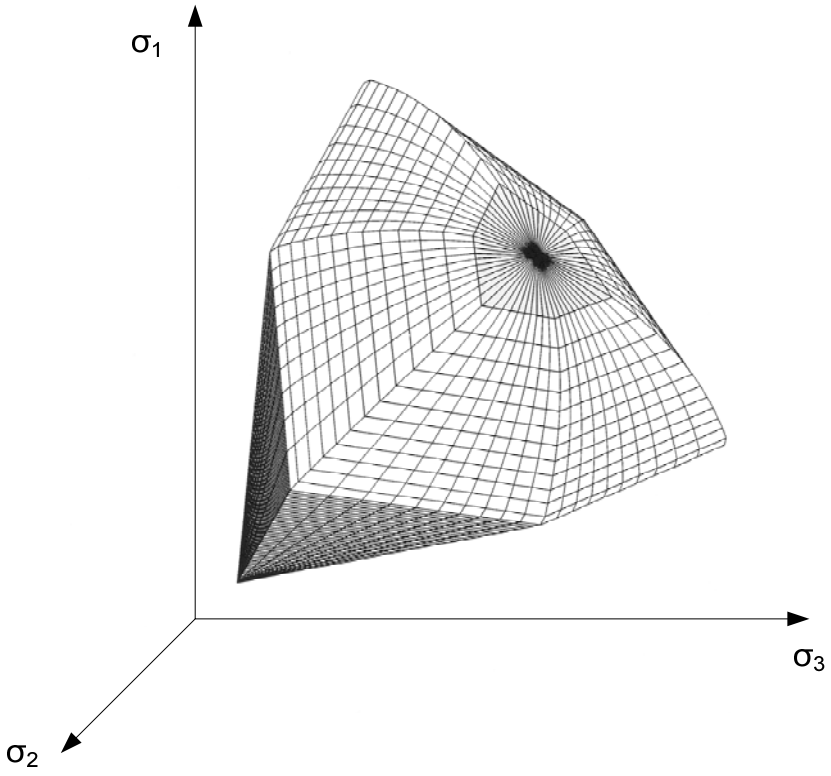

Figure 4.13 Hardening Soil model yield contours (modified after Brinkgreve, 2002)

CHAPTER 5. DEFORMATIONS OF MSE BRIDGE ABUTMENTS

5.1. Introduction

Based on the results of conventional design methods that were presented in CHAPTER 3, five different case examples were examined using the finite element method. These cases were selected based on the bearing capacity safety factors (Table 3.4). To be more specific, analysis was performed for those examples whose FS_{BC} was equal to 2.5, and their geometric characteristics are summarized in Table 5.1. Two different types of analysis were performed for each case.

First, foundation soil was assumed a fully permeable material, so the resulting vertical displacements correspond to immediate settlements of the system due to MSE wall self-weight and bridge loads. In this case, all involved soil layers, i.e. reinforced, retained, and foundation, were modeled as elastic – perfectly plastic Mohr Coulomb material. In the second type of analysis, a layer of non-permeable compressible soil is introduced as part of the foundation profile. This type of soil, corresponding to a normally consolidated clay, was modeled as a hardening material, using the available on Plaxis Hardening Soil constitutive model. Magnitudes and time rates of consolidation settlements were investigated in this second type of analysis.

5.2. Initial conditions and stage construction

As shown in Figure 5.1, for all examined cases, groundwater level was placed at the ground surface, and the unit weight of water was taken equal to 10 kN/m^3. Vertical and horizontal effective stresses at a point are given by K_0 conditions:

$$\sigma'_{v,0} = \sum \text{Mweight} \left(\sum_i \gamma_i h_i - p_w \right)$$

$$\sigma'_{h,0} = K_0 \sigma'_{v,0}$$

where $\sum \text{Mweight}$ is the proportion of gravity that is applied, with values between 0 and 1. In the current study it was $\sum \text{Mweight} = 1$, implying that the full soil weight was activated.

γ_i is the unit weight of individual layers,

h_i is the layer depth,

p_w is the initial pore pressure in the stress point, and

K_0 is the coefficient of earth pressure at rest.

The default value of K_0 is given by Jaky's formula (1946):

$$K_0 = 1 - \sin\varphi$$

So, in our case for S_2 it is $K_0 = 0.5$ and for S_3 it is $K_0 = 0.658$.

5.3. Magnitude of settlements

5.3.1. Immediate and consolidation settlements

Table 5.2 provides the values of the Mohr Coulomb parameters that were used in the assessment of settlements in fully permeable foundation material. Note that parametric studies in terms of the Young modulus of the foundation profile were performed, in order to cover a wide range of cases with respect to the compressibility of the foundation soil. Specifically, for each of the five studied cases shown in Table 5.1, analysis was performed for values of E equal to 25,000, 50,000, and 100,000 kPa. A second type of analysis was performed by

introducing a non-permeable compressible layer as part of the foundation profile. This type of analysis was used to assess the magnitude and time rate of consolidation settlements. The compressible layer was modeled using the Hardening Soil model and its constitutive parameters are given in Table 5.3. In the following Figures, the analyzed examples are notated as Hi – Li – Si for the cases where the foundation soil is fully permeable, and as Hi – Li – Si* when the compressible material is included in the analysis.

Figure 5.2 shows schematically two critical construction stages: (a) just before and (b) immediately after the application of the concentrated vertical and horizontal loads from the bridge, i.e. at the end of construction activities. Figure 5.3 and Figure 5.4 show the resulting settlements at the end of the above stages for one of the examined cases (H_3 - L_1 - S_2 with E_{S2} = 25,000 kPa). Also, Figure 5.5 to Figure 5.9 provide the magnitudes of the vertical displacements along the top of the structure for the same construction stages, for all five examined cases. Displacements on each case are shown for the three different values of the Young modulus of the foundation soil that were previously mentioned. Last, Figure 5.10 to Figure 5.14 illustrate the magnitudes of consolidation settlements for the same construction stages.

With respect to the situation before the application of the bridge loads The following comments can be made:

Settlements demonstrate a tendency to increase with horizontal distance from the wall's facing. This is demonstrated clearly in Figure 5.3, and the same trend was observed in all examined cases. This fact is mostly due to the geometry of the problem: specifically, due to the proximity of the foundation soil beneath the MSE mass to an area with less overburdens than the soil beneath the retained mass (Figure 5.1). In addition, the MSE mass is more rigid, and therefore prone to smaller settlements itself, due to the presence of the steel strips. However, the transition between reinforced and retained fill (indicated as point B in Figure 5.2) is smooth.

For the same geometry and loading conditions, settlements depend significantly on the compressibility of the foundation soil. For the permeable cases, it is shown that as the Young modulus decreases from 100,000 kPa to 25,000 kPa, the settlements increase (Figure 5.5 to Figure 5.9). For example, Figure 5.9 shows that the resulting settlements at point B (with reference to Figure 5.2) are 4.7 cm, 7.6 cm, and 13.3 cm for 10,000 kPa, 50,000 kPa and 25,000 kPa, respectively. For the cases that the 3-m thick compressible material is introduced the settlements are naturally much higher (Figure 5.10 to Figure 5.14)

Settlements depend on the height of the MSE abutment, as well. As expected, the taller the system, the larger the settlements at any given point, especially for foundation soils of high compressibility.

With respect to the situation after the application of the bridge loads, the following comments can be made: Overall, the impact of concentrated loads from the bridge is not significant with respect to the resulting settlements.

In terms of relative increase (%), the shorter walls are affected more by the bridge loads, compared to the taller ones. It is so for two reasons. First, because in the analyzed cases, shorter walls are subjected to larger loads. Second, because the taller the wall is, the greater the distance until the foundation soil and therefore the loads are more widely distributed at the base of the wall.

For the same geometric conditions, the relative impact of the concentrated loads near the facing, decreases as the stiffness of the foundation soil decreases. This means that for the analyzed cases, the settlements are controlled to a greater extent by the stiffness of the foundation soil, rather than the superstructure loads.

In addition it is note that the impact of the loads dissipates as we move away from the facing along the horizontal axis. However, the increase in settlements close to the facing, due to the superstructure loads compensates for the difference in settlements that was observed between the reinforced and the retained fill before the application of the loads. In other words, the differential

settlement between the facing and the back of the wall are smaller after the application of the loads.

5.3.2. Impact of the bridge loads on the immediate settlements

Settlements occur due to self-weight, compaction efforts, and bridge loads. This means that proper adjustments made during the construction process can compensate for elevation losses due to settlements caused by the self-weight of the MSE wall and compaction efforts. In this way, the final settlements would be the ones exclusively due to the concentrated loads from the bridge.

Figure 5.15 shows the distribution of settlements for one of the examined cases (again, H_3 - L_1 - S_2 with E_{S2} = 25,000 kPa). This Figure clearly shows that the impact of the loads on the settlements is very small. For illustration purposes, Figure 5.16 shows the same thing, but the scale here is in mm. Figure 5.17 to Figure 5.19 present the relative vertical displacements along the top of the MSE wall and the embankment, after the application of the bridge loads. In other words, assuming that the occurring settlements until the application of the bridge loads are compensated before the loads are applied, then these would be the magnitudes of the settlements at the end of the project. As expected, the impact of the loads is larger near the facing of the wall. The true impact of the loads in terms of settlements magnitude is relatively small, ranging from 0.5 to 2 cm and with an average of approximately 1.1 cm.

5.4. Facing panel horizontal displacements

The movements of the facing panels do not have a serious impact on the structural integrity of the wall, but they shall be relatively limited in order to satisfy aesthetic requirements.

Figure 5.21 shows the horizontal movements of the facing panels for one of the examined cases (H_1 - L_3 - S_2 with E = 100,000 kPa) and for different construction stages. Specifically, line 1 indicates the movements upon the

completion of the MSE wall, line 2 indicates the movements after the footing and the fill behind it are put in place (but without any load from the bridge yet), line 3 the movements after the application of the vertical concentrated load, and line 4 the movements after the application of the horizontal concentrated load. So, line 4 indicates the movements at the end of the project.

As shown in Figure 5.21, the different stages reflect on the magnitude of the movements, especially near the top of the wall. Similar trends were observed for all cases examined.

In terms of magnitudes, the horizontal movements of the panels ranged between approximately 0.7 and 1.6 cm, with an average 1.1 cm, with respect to their original position. With respect to each other, the relative movements are even smaller.

Another observation is that for the same geometric conditions, and for decreasing stiffness of the foundation soil, the movements of the lower panels increase with a simultaneous decrease of the movements of the top panels.

5.5. Time rates of consolidation settlements

Dissipation of excess pore pressures depends on the coefficient of consolidation c_v of the clay layer and the length of the drainage path. This study was based on the assumption of double drained 3-m thick clay layers. For such layers, the results indicate that for coefficients of consolidation larger than approximately 10^{-3} cm^2/s (10^{-6} ft^2/s) a great fraction of excess pore pressures has already dissipated by the time that bridge loads are applied. Figure 5.22 shows the dissipation of excess pore pressures with time for one of the analyzed examples ($H_1 – L_3 – S_2$*). The same trend was observed in all five examples that include an impermeable layer as part of the foundation profile. Note that the above c_v value is of the same order of magnitude to values reported in the literature for glacial lake clays or silty clays in midwest. In terms of settlements magnitudes, it was found that by the end of construction, consolidation settlements were completed by 87 to 92 % (Figure 5.23 to Figure 5.27). This means that no waiting periods

for consolidation to occur need to be accounted in the construction process, since only a small fraction of settlement has not occurred by the end of construction. In terms of absolute values, the maximum remaining settlement after the end of construction was found to be approximately 2 cm (0.8 in). However, the above conclusion is not valid when coefficients of consolidation were decreased by one order of magnitude. For example, one case analyzed with c_v equal to 10^{-4} cm^2/s indicated that only 50 % of consolidation settlement had occurred by the end of construction (Figure 5.28 and Figure 5.29). In that case, the time required for complete consolidation to occur was almost one year after the end of construction. So, in such cases the construction sequence needs to be modified in order to take into account consolidation settlements. For instance, this could mean either including long waiting periods that would allow larger fractions of consolidation to occur before the application of bridge loads (as in Figure 5.30 and Figure 5.31), or using preloading techniques that would accelerate the rate of consolidation.

Table 5.1. Geometric characteristics of cases analyzed with the FEM

Case	Span length (m)	Total height of MSE wall (m)	Width of MSE wall (m)
H_1 - L_3 - S_2	30	6	7
H_1 - L_3 - S_3	30	6	7
H_2 - L_1 - S_3	24	7	7.5
H_2 - L_2 - S_2	24	7	7.5
H_3 - L_1 - S_2	18	8	8

Table 5.2. Mohr Coulomb model parameters

Soil layer	c (kPa)	φ (^{o})	ψ (^{o})	E (kPa)	v (-)
Reinforced soil	0	34	7	50,000	0.306
Retained soil	0	30	6	40,000	0.320
Foundation soil S_2	5	30	0	varied [(1)]	0.350
Foundation soil S_3	40	20	0	varied [(1)]	0.350

[(1)] 100,000 - 50,000 - 25,000 kPa

Table 5.3. Hardening Soil model parameters

E_{50}^{ref} (kN/m^2)	1840
E_{oed}^{ref} (kN/m^2)	1840
E_{ur}^{ref} (kN/m^2)	16560
p_{ref} (kN/m^2)	100
c_{ref} (kN/m^2)	0.1
φ (^{o})	29
ψ (^{o})	0
v_{ur} (-)	0.2
m (-)	1
K_0^{nc} (-)	0.515
R_f (-)	0.9
$k_x = k_y$ (cm/s)	5×10^{-7}
c_v (cm^2/s)	12×10^{-4}

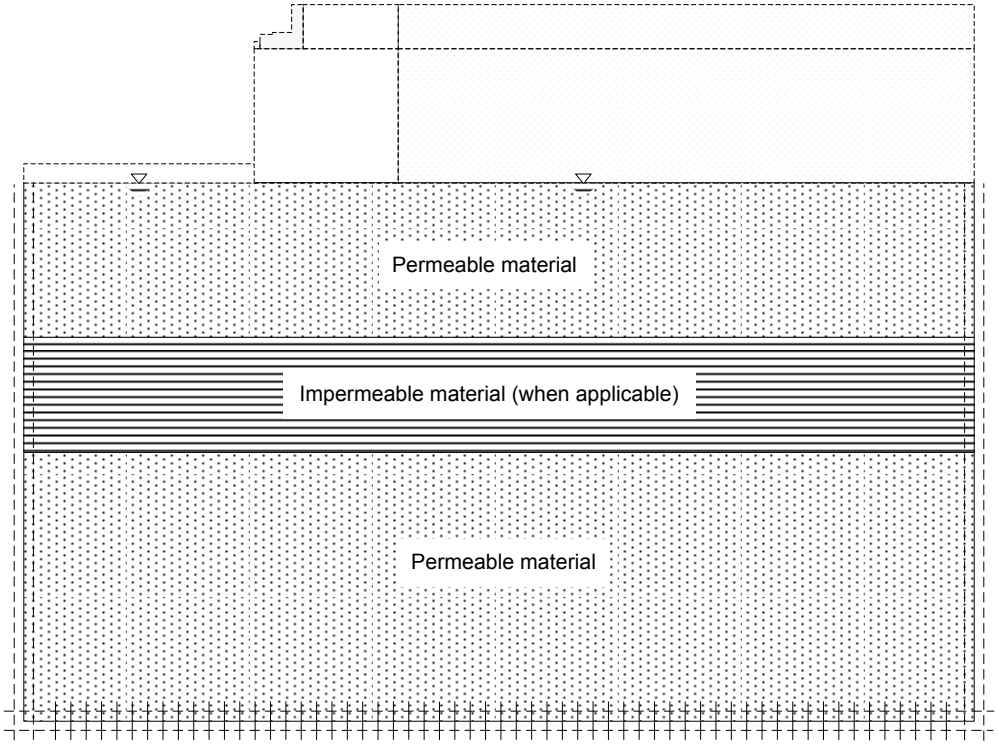

Figure 5.1. Initial conditions

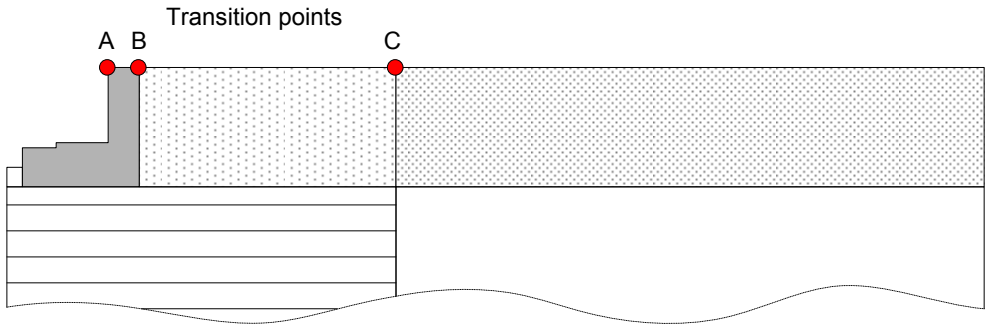

a. Before the application of bridge loads

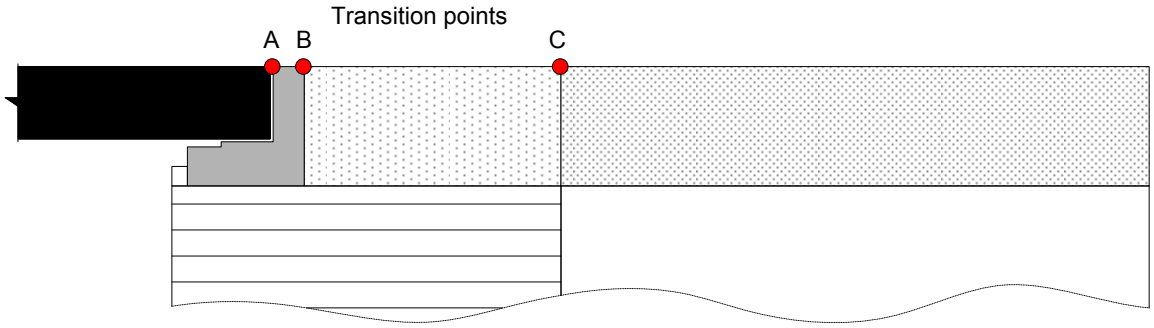

b. After the application of bridge loads

Figure 5.2. Geometry at the top of the structure indicating the transition points

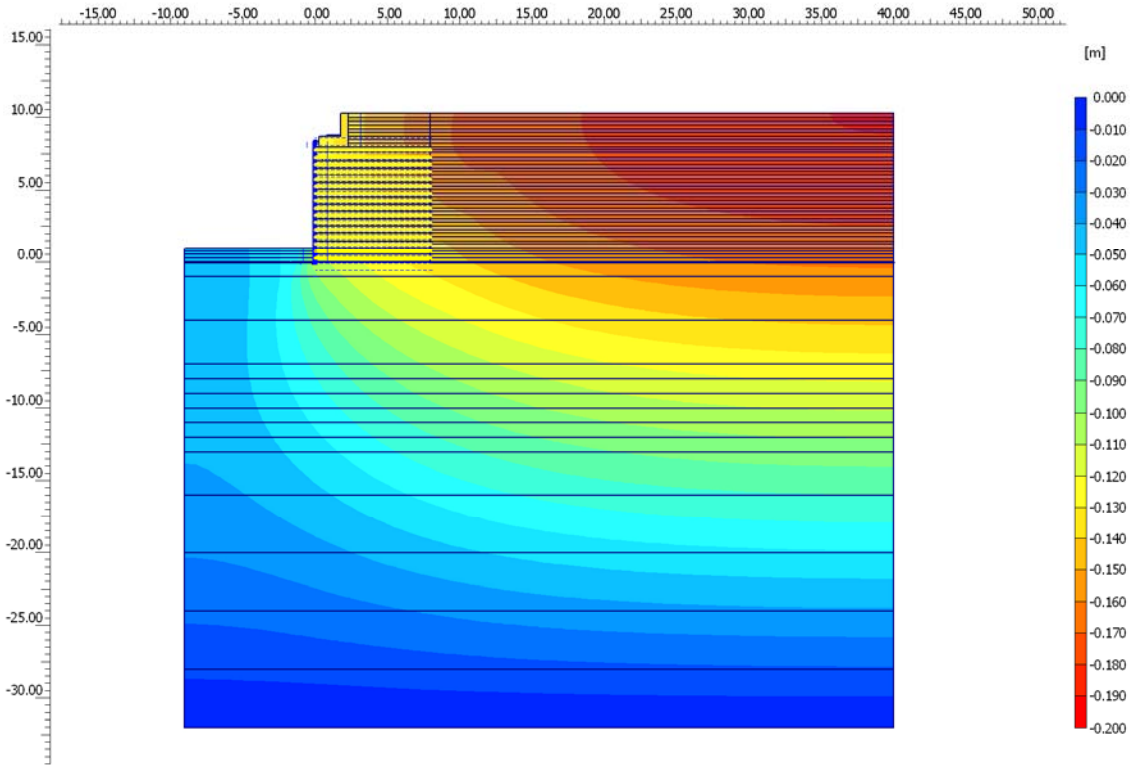

Figure 5.3 Settlements due to MSE self-weight (H_3 - L_1 - S_2, E = 25,000 kPa)

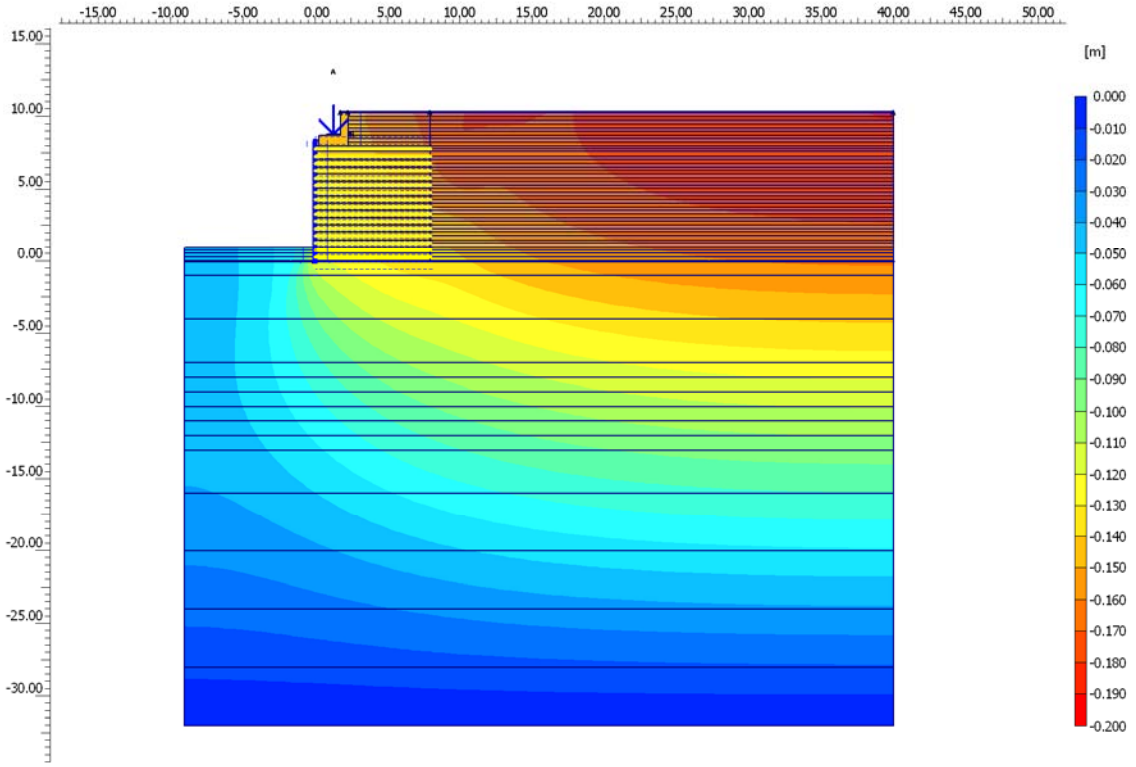

Figure 5.4 Settlements due to MSE self-weight and bridge loads (for H_3 - L_1 - S_2, E = 25,000 kPa)

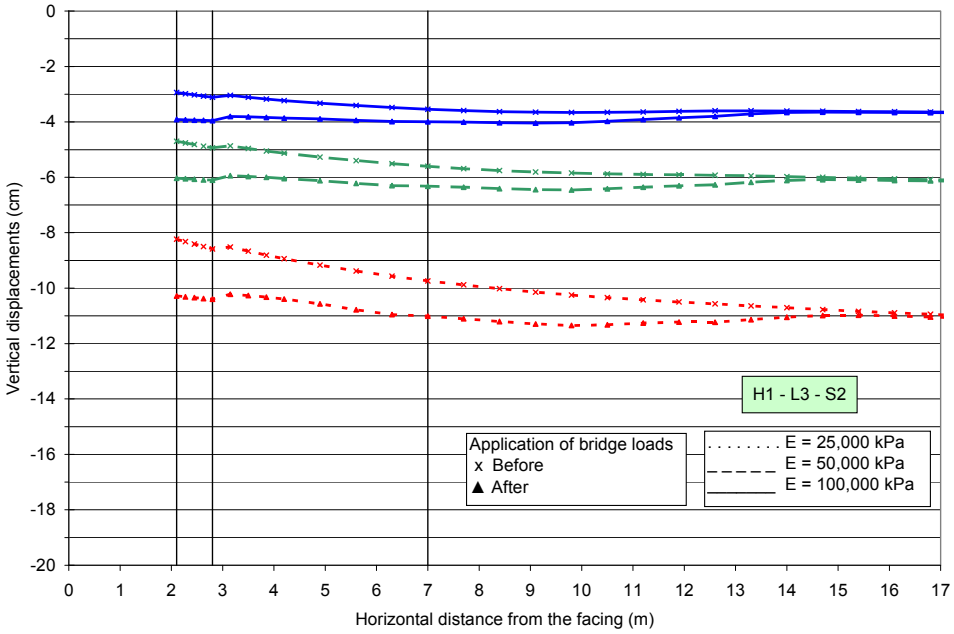

Figure 5.5. Settlements at the surface (H_1 - L_3 - S_2)

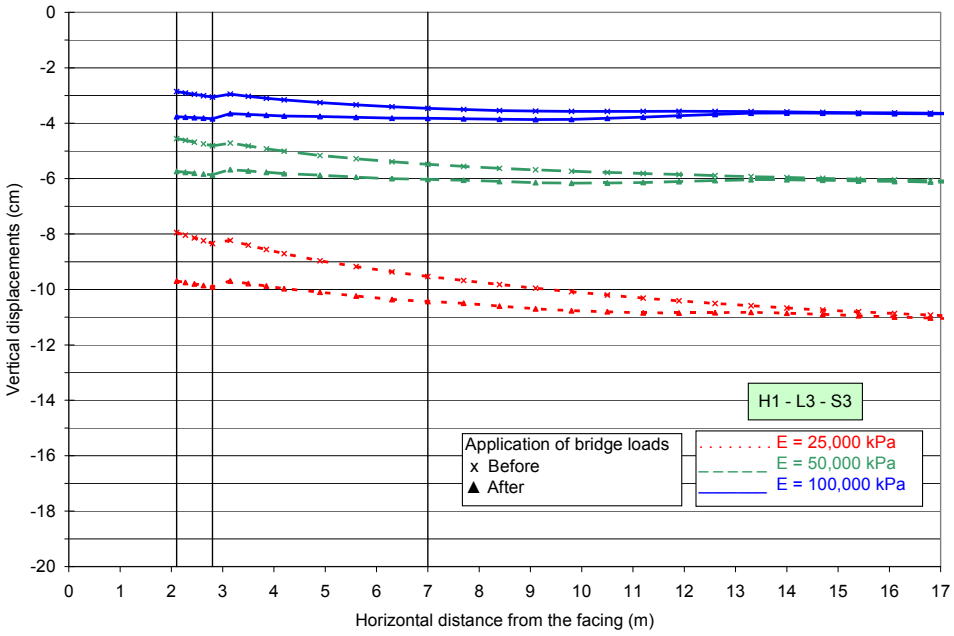

Figure 5.6. Settlements at the surface (H_1 - L_3 - S_3)

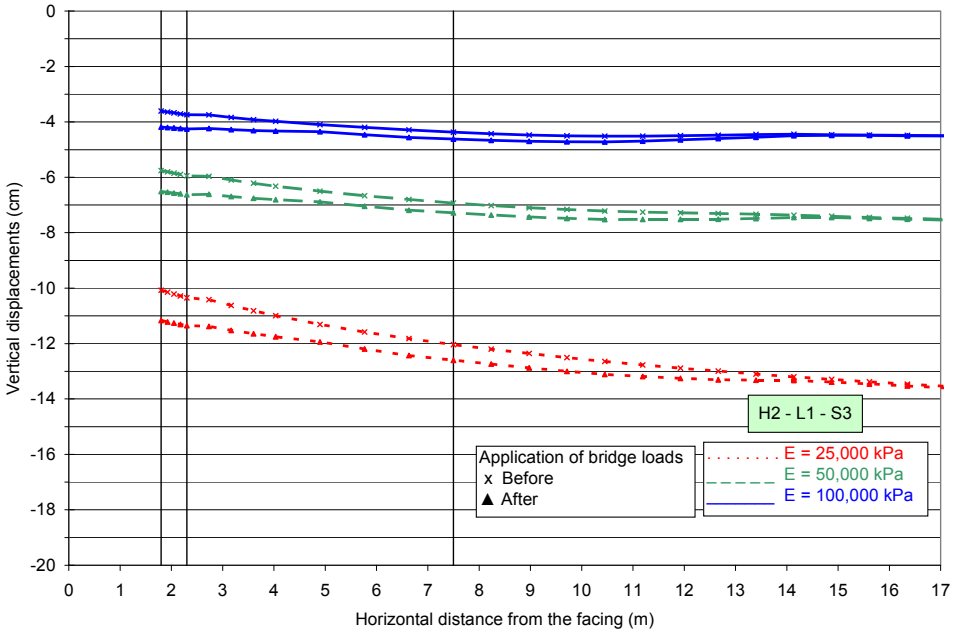

Figure 5.7. Settlements at the surface (H_2 - L_1 - S_3)

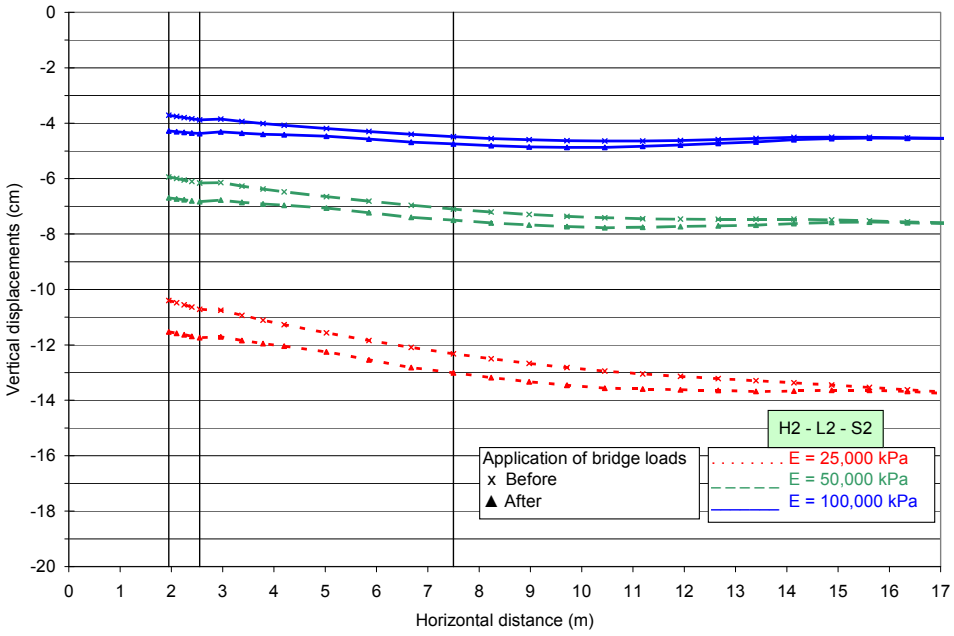

Figure 5.8. Settlements at the surface (H_2 - L_2 - S_2)

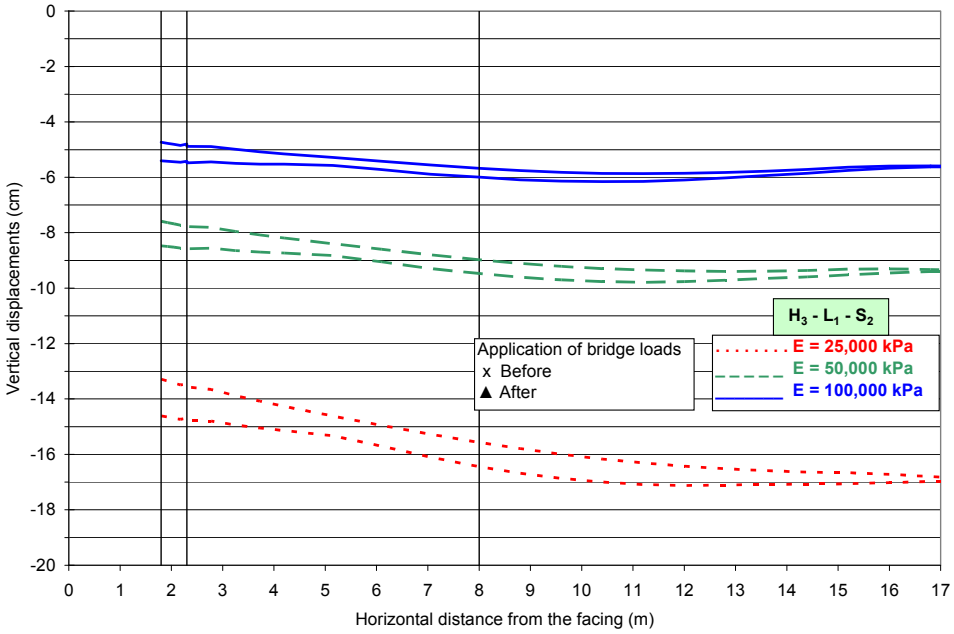

Figure 5.9. Settlements at the surface (H_3 - L_1 - S_2)

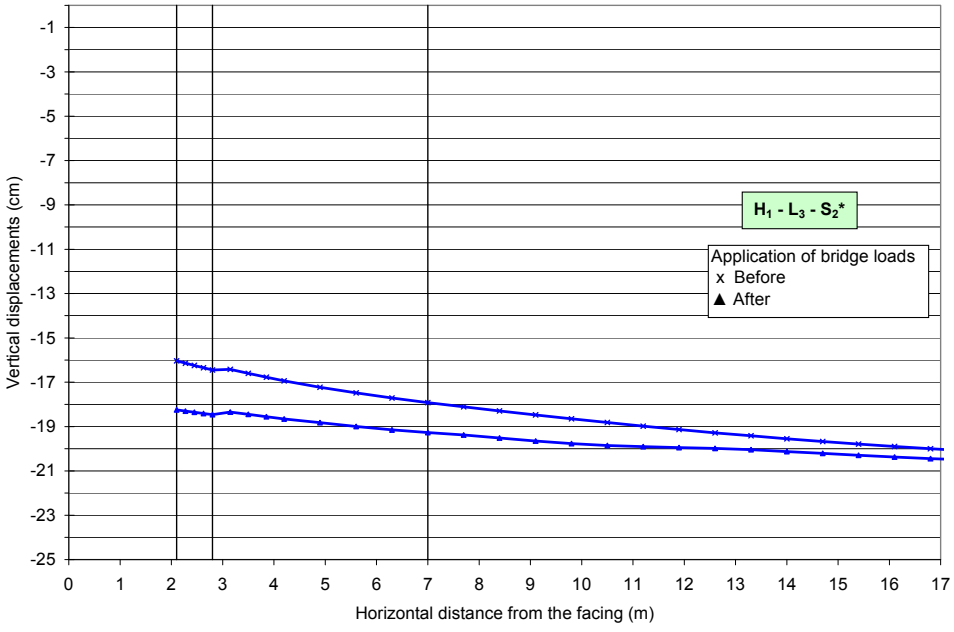

Figure 5.10. Settlements at the surface (H_1 - L_3 - S_2*)

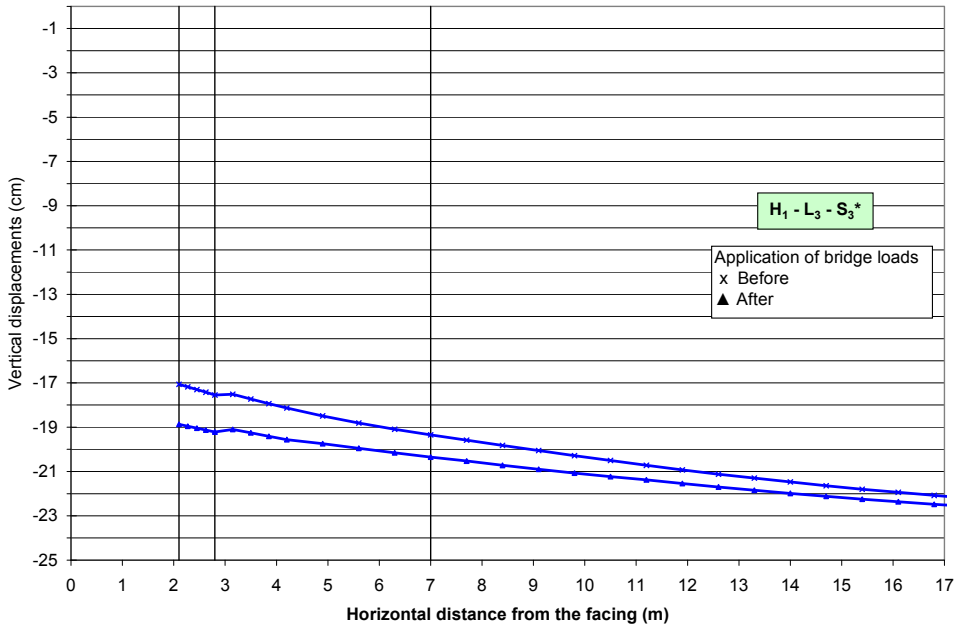

Figure 5.11. Settlements at the surface (H_1 - L_3 - S_3*)

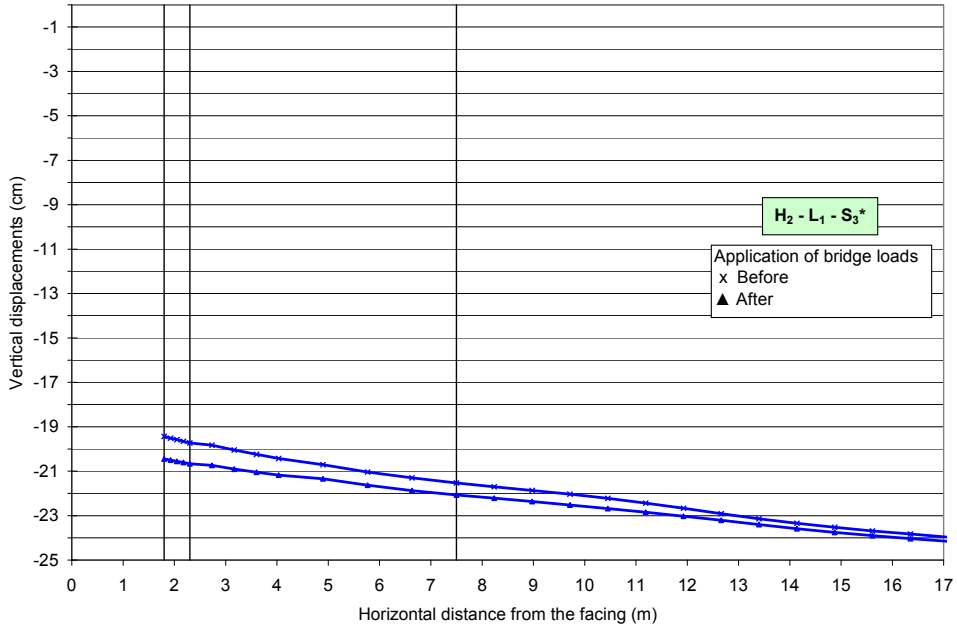

Figure 5.12. Settlements at the surface (H_2 - L_1 - S_3*)

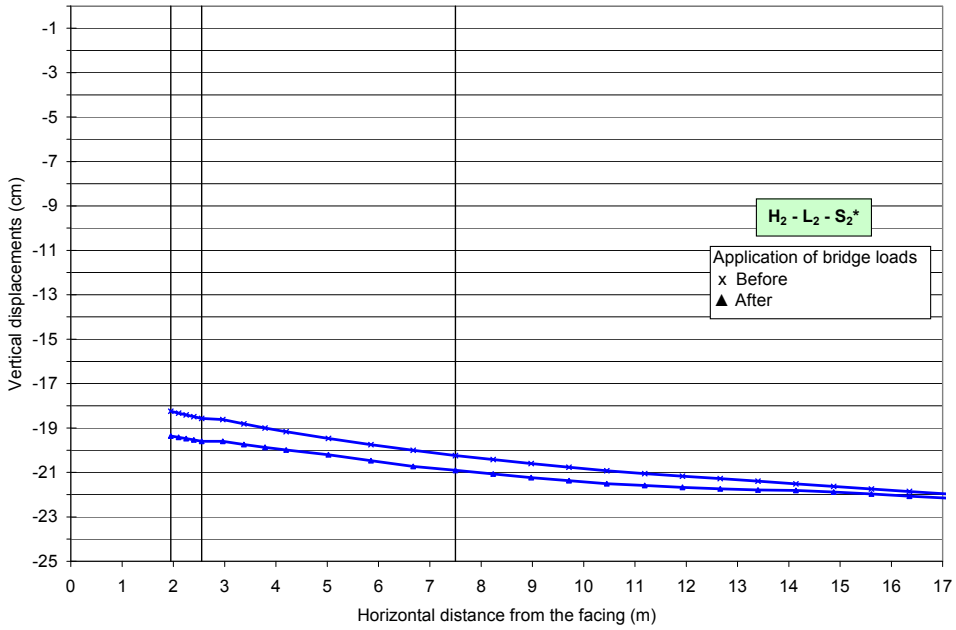

Figure 5.13. Settlements at the surface (H_2 - L_2 - S_2*)

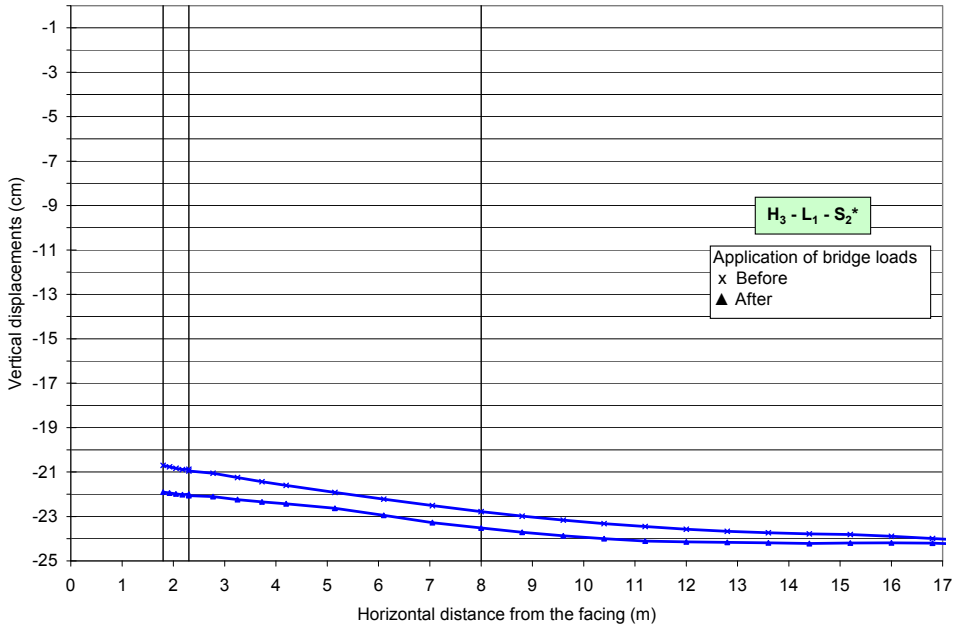

Figure 5.14. Settlements at the surface (H_3 - L_1 - S_2*)

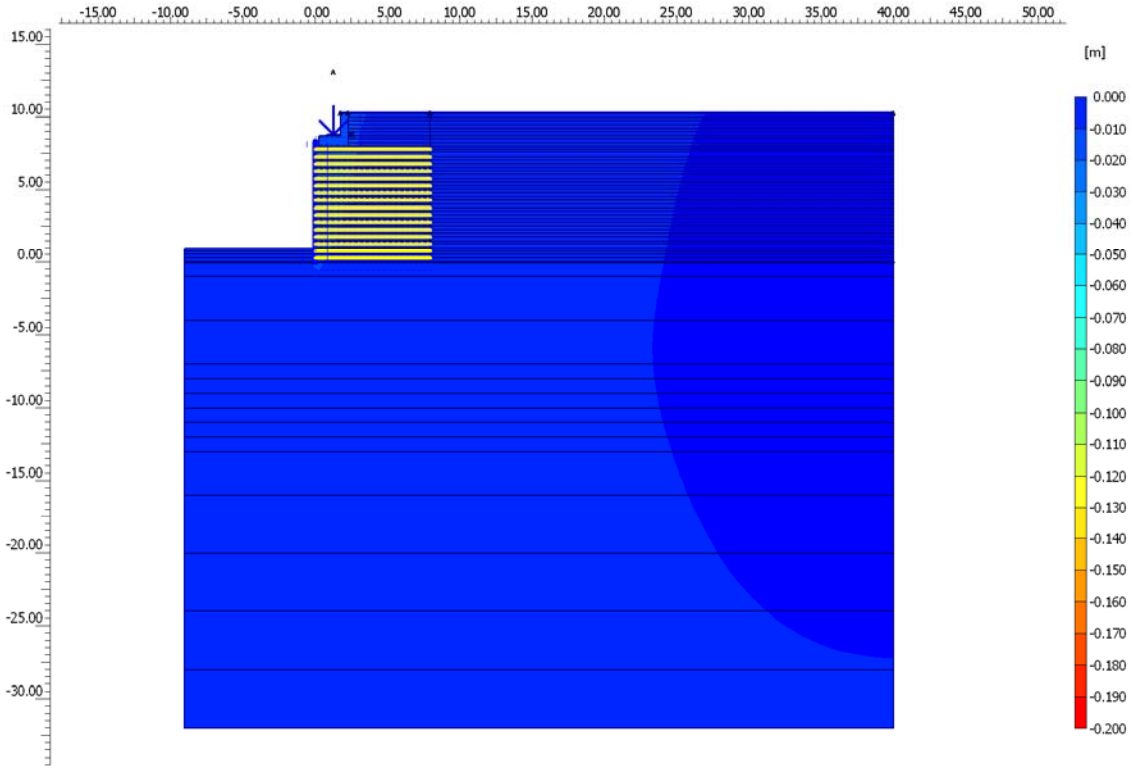

Figure 5.15 Settlements only due to bridge loads (H_3 - L_1 - S_2, E = 25,000 kPa)

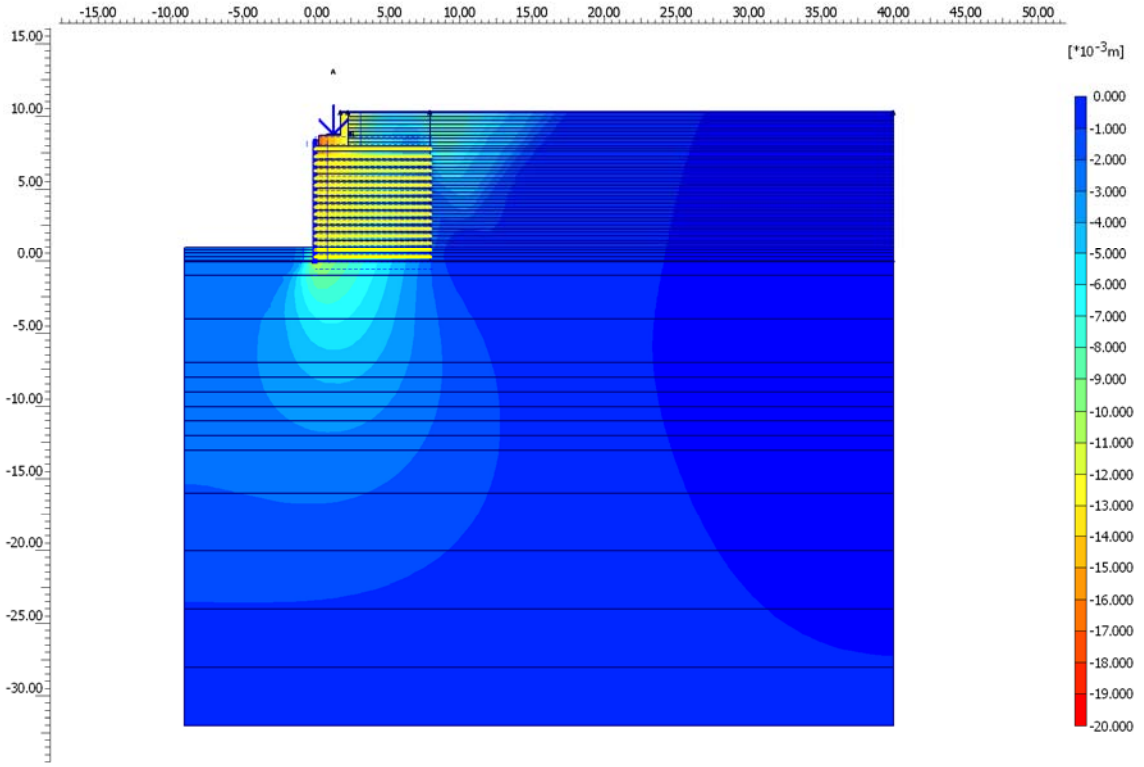

Figure 5.16 Settlements only due to bridge loads in mm (H_3 - L_1 - S_2, E = 25,000 kPa)

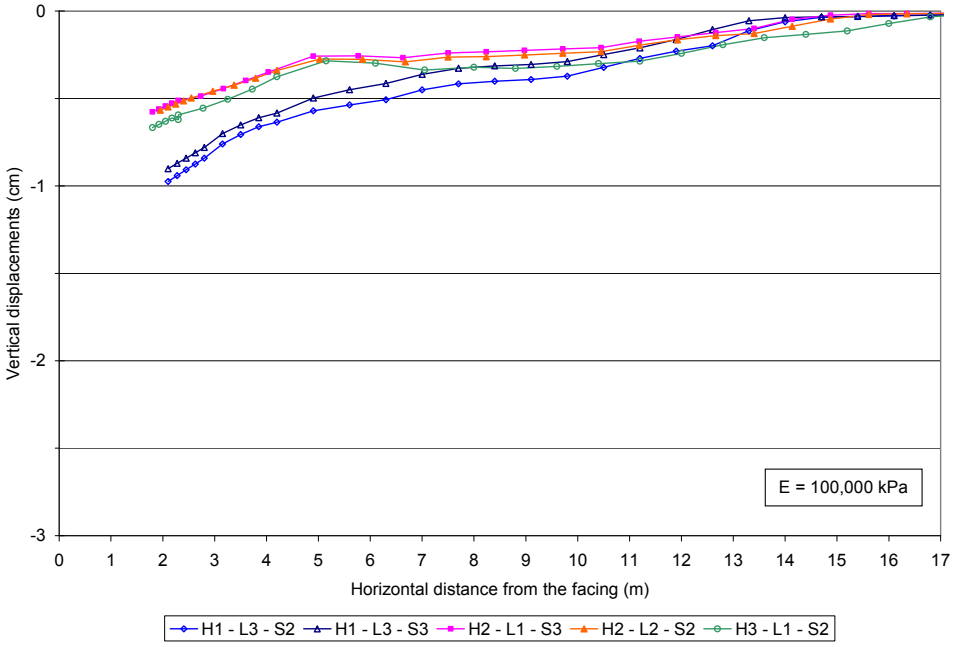

Figure 5.17. Settlements at the surface due to bridge loads

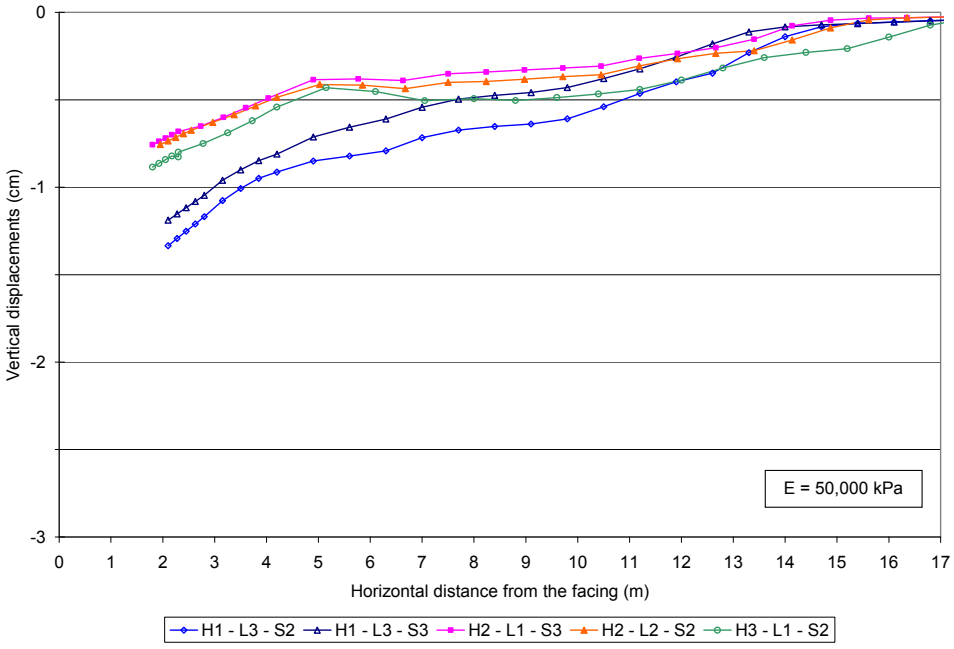

Figure 5.18. Settlements at the surface due to bridge loads

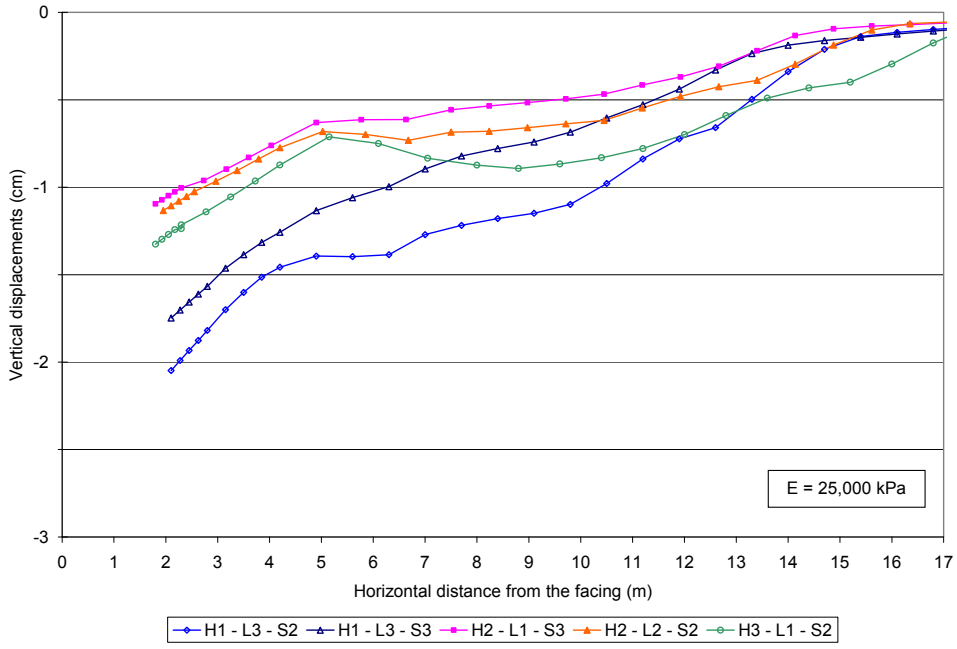

Figure 5.19. Settlements at the surface due to bridge loads

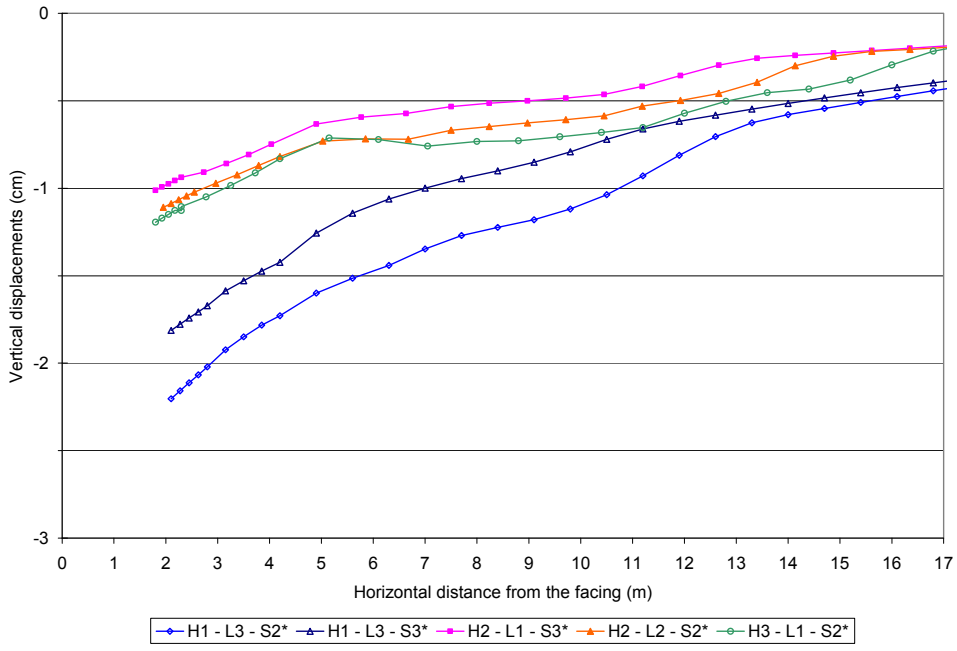

Figure 5.20. Settlements at the surface due to bridge loads

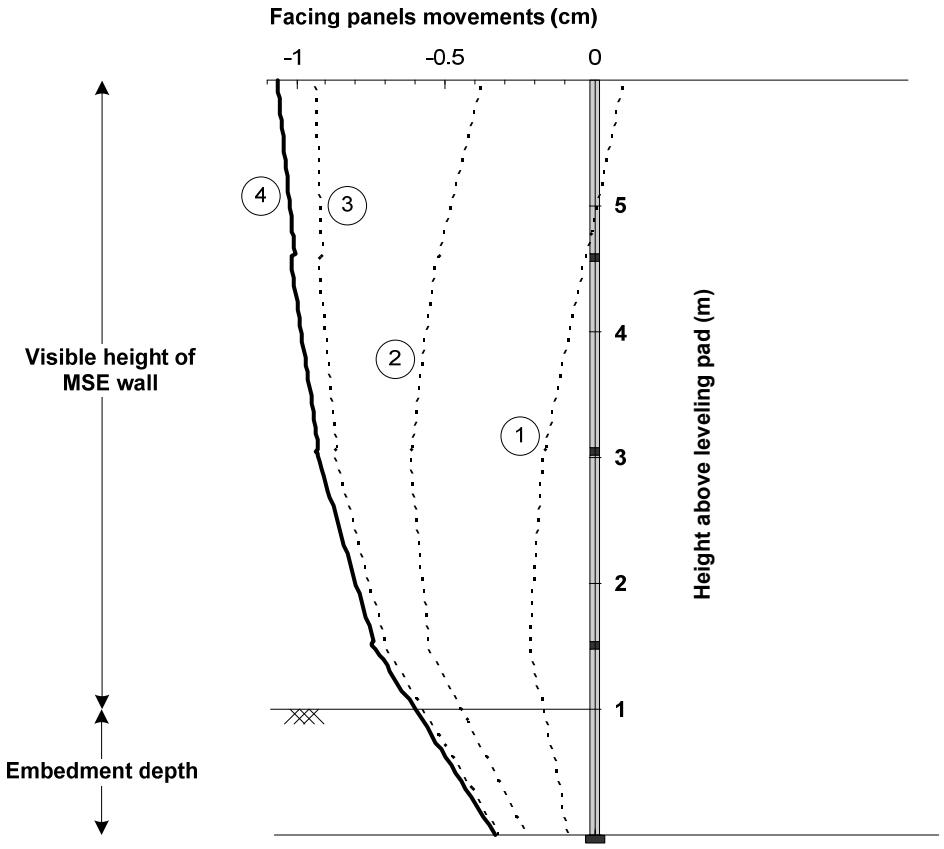

Figure 5.21. Horizontal movements of facing panels (H_1 - L_3 - S_2, E = 100,000 kPa)

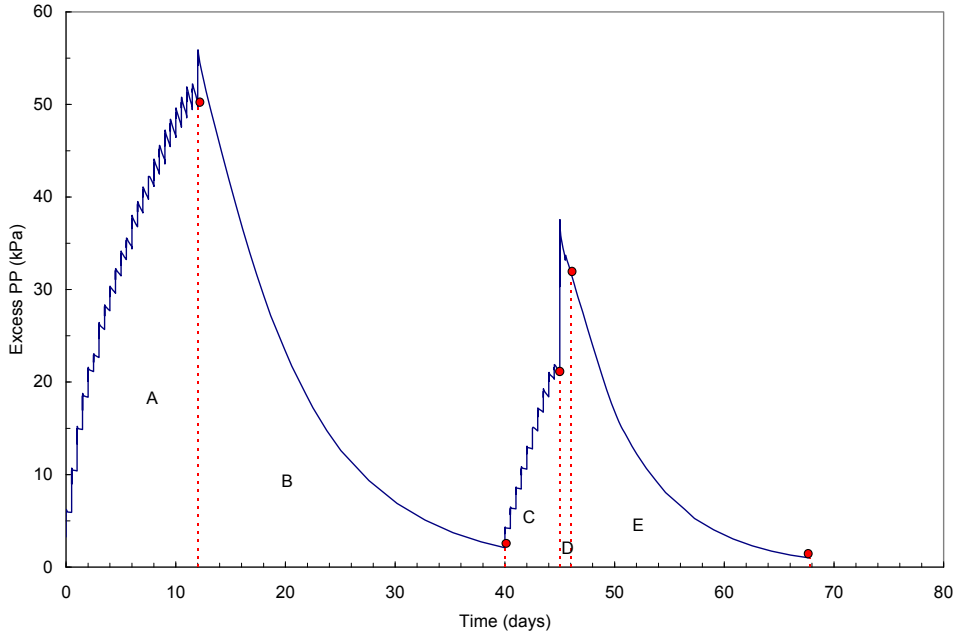

Figure 5.22. Dissipation of excess pore pressures (H1 - L3 - S2*)

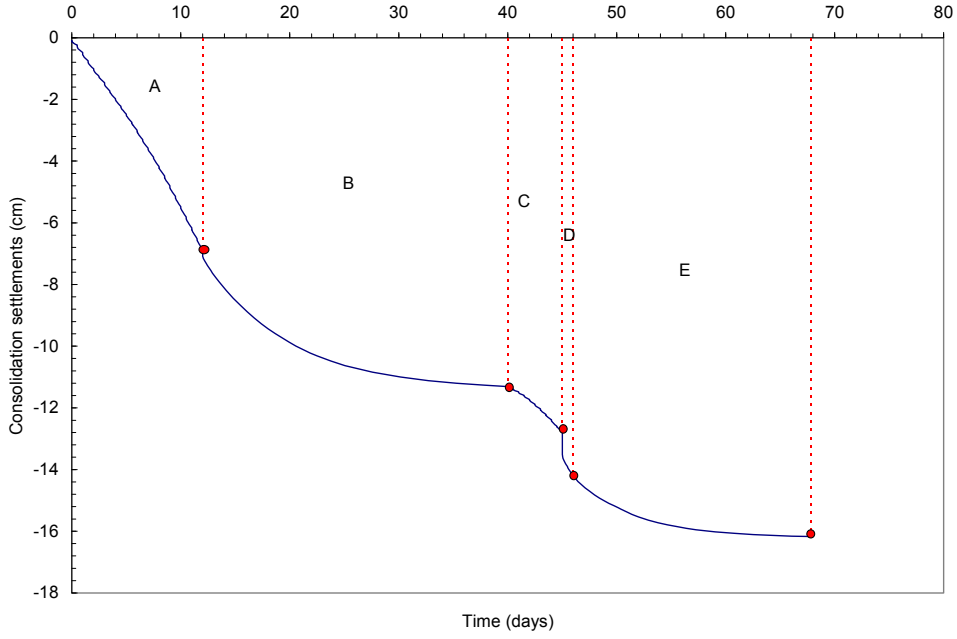

Figure 5.23. Consolidation settlement at the leveling pad (H_1 - L_3 - S_2*)

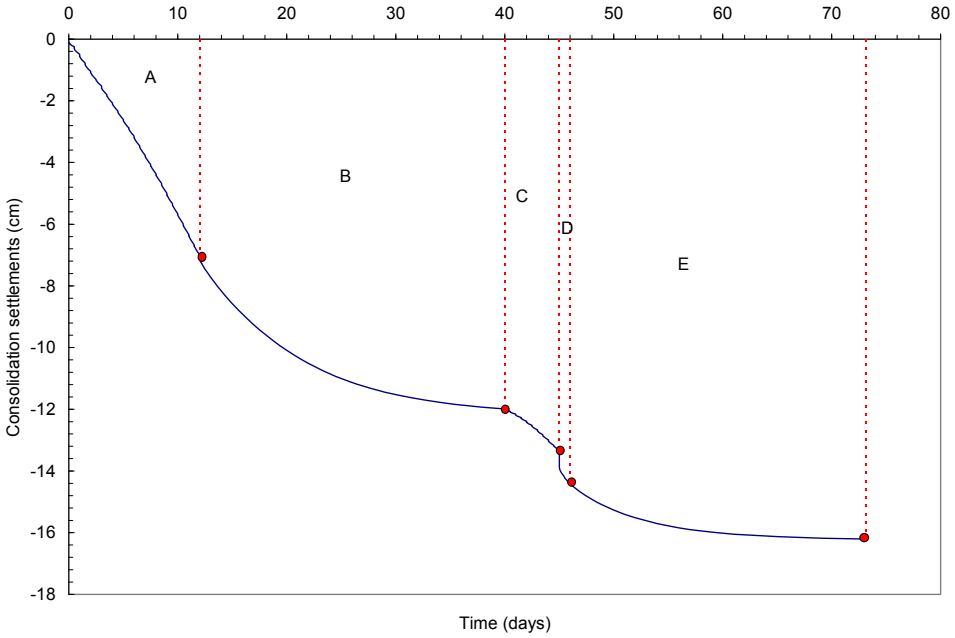

Figure 5.24. Consolidation settlement at the leveling pad (H_1 - L_3 - S_3*)

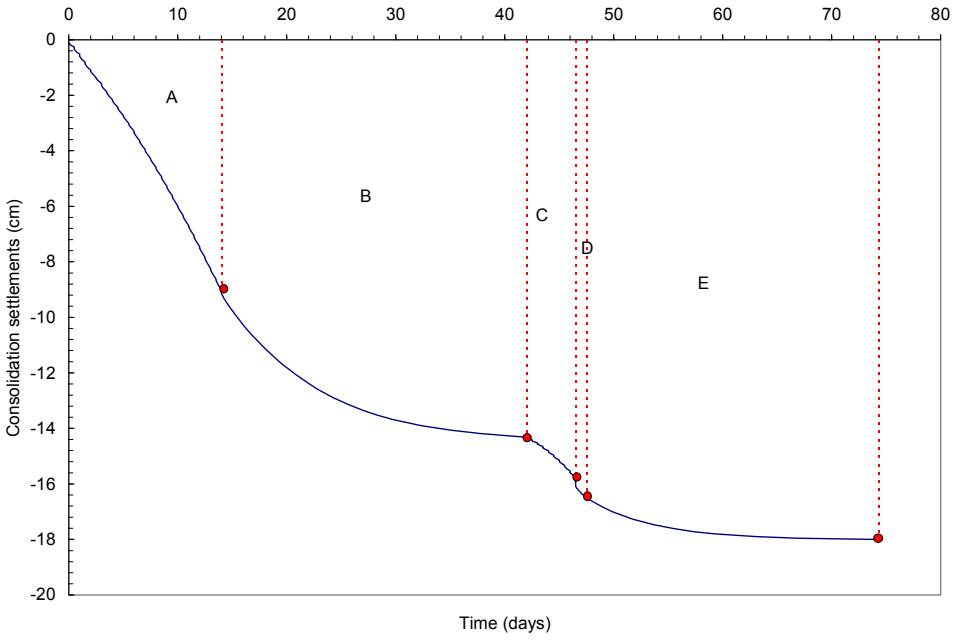

Figure 5.25. Consolidation settlement at the leveling pad (H_2 - L_1 - S_3*)

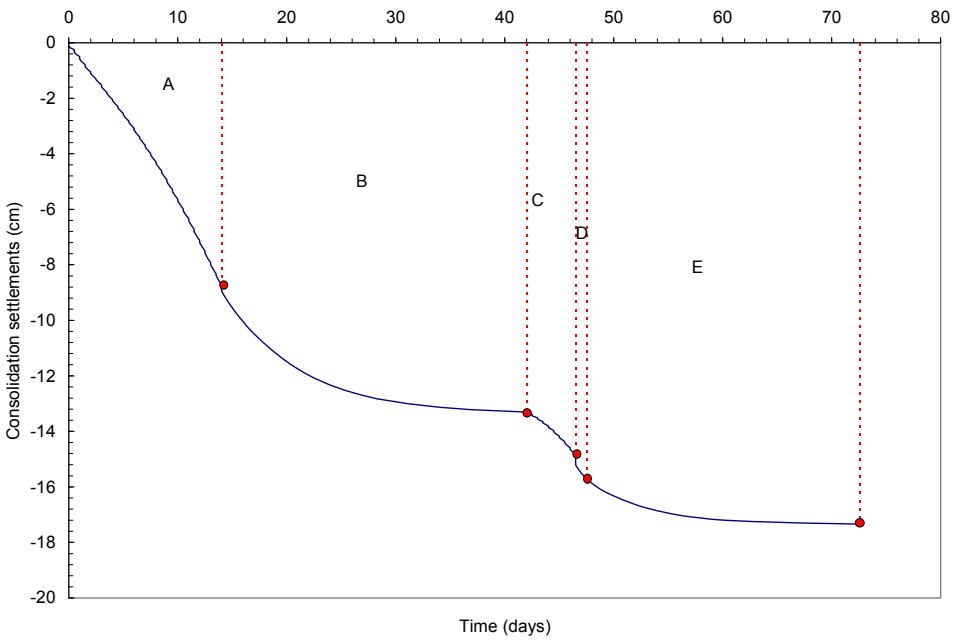

Figure 5.26. Consolidation settlement at the leveling pad (H_2 - L_2 - S_2*)

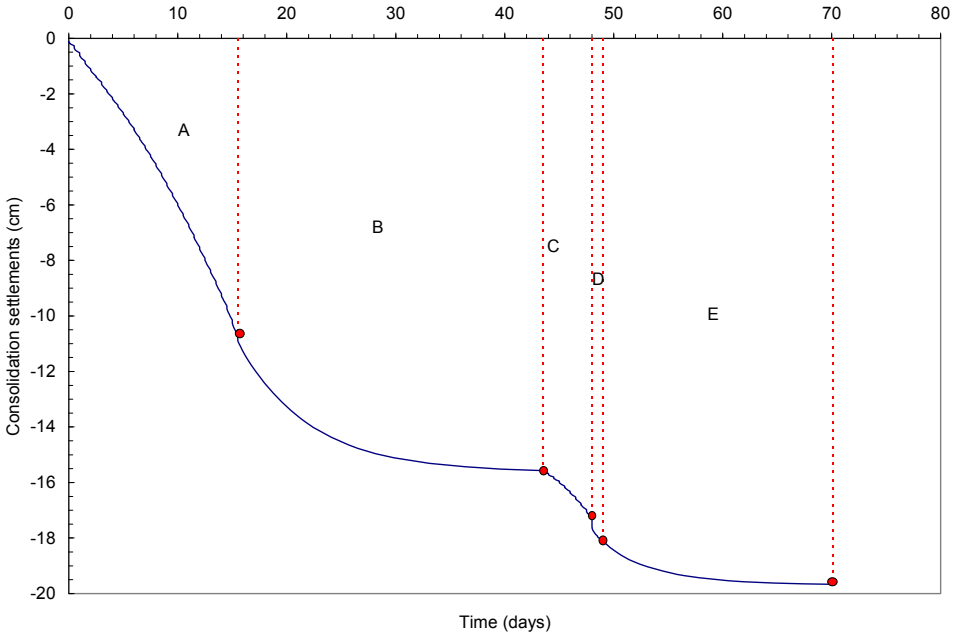

Figure 5.27. Consolidation settlement at the leveling pad (H_3 - L_1 - S_2*)

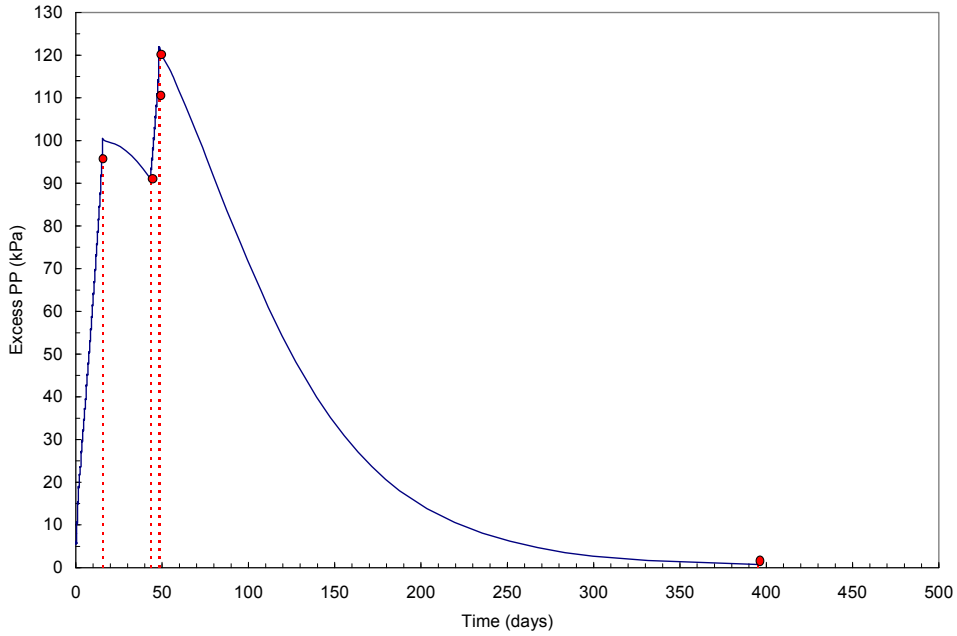

Figure 5.28. Dissipation of excess pore pressures (H_3 - L_1 - S_2*)

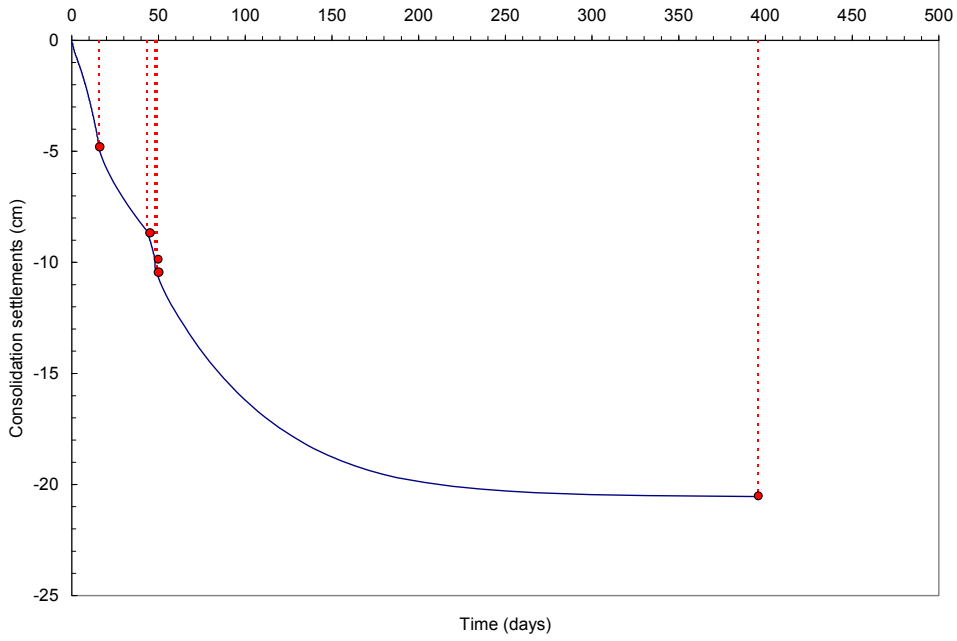

Figure 5.29. Consolidation settlement at the leveling pad (H_3 - L_1 - S_2*)

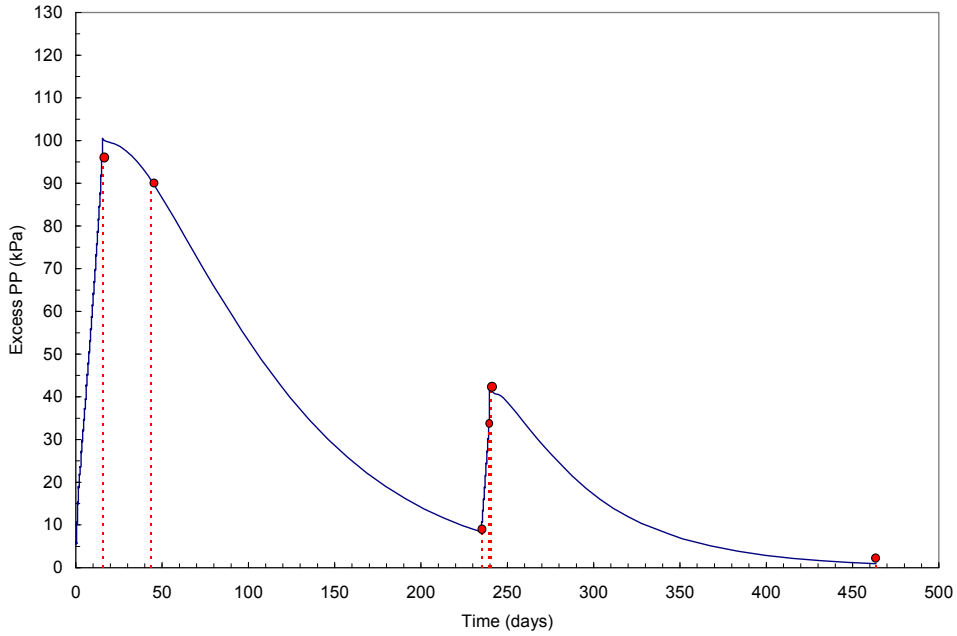

Figure 5.30. Dissipation of excess pore pressures (H_3 - L_1 - S_2*)

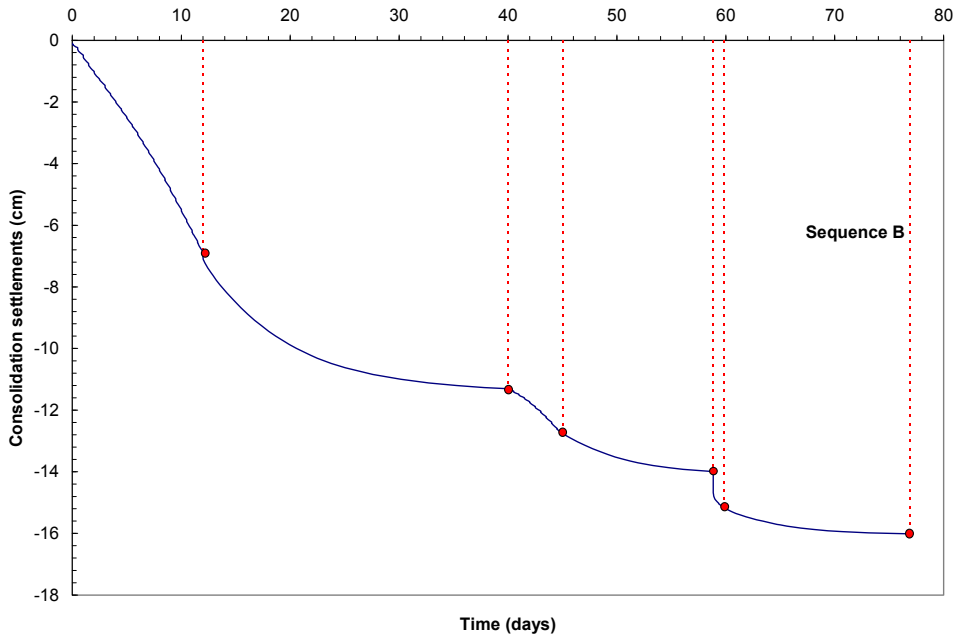

Figure 5.31. Consolidation settlement at the leveling pad (H_3 - L_1 - S_2*)

CHAPTER 6. CONCLUSIONS AND RECOMMENDATIONS

6.1. Statement of the problem and objectives of the study

Mechanically Stabilized Earth (MSE) walls, a technically and economically attractive alternative to traditional reinforced concrete retaining walls, have been increasingly used by INDOT as the solution of choice for bridge abutment retaining walls. Current practice in Indiana highways is to support independently the bridge on piles. However, this type of design presents the following shortcomings:

1. It is a source of considerable complication in the construction process, because it requires the piles to cross the reinforced soil fill.
2. The bridge support is rigid in comparison to the surrounding MSE wall. This difference of rigidity may generate detrimental differential movements between the bridge structure, the MSE wall, and the approach embankment, and therefore contribute in particular to creating the so-called “bump” at the bridge / embankment transition.
3. The cost of MSE bridge abutment is considerably increased by the use of deep foundations.

In a number of cases, these problems may be avoided or minimized if the MSE fill is designed not only to retain the approach embankment, but also to support the bridge. In this type of design, the bridge seat lays on a strip footing that is directly constructed on the top of the reinforced fill.

The objective of this study was to investigate on the possible use of MSE bridge abutments as direct support of bridges on Indiana highways and to lead to drafting guidelines for INDOT engineers to decide in which cases such a solution would be applicable.

6.2. Summary of findings from this study

6.2.1. Literature Review

An extensive review on the topic of MSE walls used as direct bridge abutments, was performed based on literature and other accessible data. The outcomes of this review are the following:

MSE walls have been successfully used as direct bridge abutments for more than thirty years. From 1969 to 1977, a series of structures, either experimental prototypes or in-service abutments, were constructed mainly in France and provided the opportunity to investigate the effect of concentrated loads on a MSE structure. Those real scale investigations were performed in conjunction with laboratory and numerical studies. In the US, the first MSE walls used as direct bridge abutments were constructed in 1974 in Nevada. Nowadays, numerous such structures exist around the world. In the vast majority of these structures, metallic reinforcement has been used. Many examples can be found in the US, too, where the configuration of directly supporting a bridge on MSE structures is acknowledged in FHWA and AASHTO guidelines and design methods are readily available.

The effects of concentrated loads on a MSE structure can be summarized as following: First, the loads increase the magnitude of tensile stresses within the MSE mass. Results from the early studies have indicated that concentrated loads dissipate throughout the soil mass with depth, following approximately Boussinesq's distribution. The simpler and more conservative 2V:1H distribution was adapted for design purposes. Second, the loads influence the locus of points of maximum tensile stresses within the MSE mass. Compared to conventional MSE walls, the locus may change depending mainly on the geometry of the footing by deviating so that it intersects the back of the bridge seat.

In principle, design methods for MSE walls used as direct bridge abutments are similar with the design methods for conventional MSE walls. These are the result of soil classical plasticity theories (i.e. Coulomb's and Rankine's),

combined with empirical knowledge accumulated over the past three decades. The methods are based on limit equilibrium principles and address ultimate limits of resistance with respect to external and internal stability following a semi-empirical approach. In terms of external stability, MSE bridge abutments are analyzed similarly to typical MSE walls, i.e. the reinforced fill is assumed to behave as a rigid body for the purpose of limit equilibrium considerations. Stability must be verified with respect to overturning around the toe, sliding on the base, and bearing capacity of the foundation soil. Particularly regarding the bearing capacity, AASHTO and FHWA guidelines recommend that the ratio of width over height of MSE bridge abutments has to be larger than that of equivalent MSE walls used only as retaining structures. In terms of internal stability, safety must be verified with respect to tensile and pull out failure of the reinforcement elements. The impact of the bridge loads is reflected in the provided equations for internal stability calculations, from which it is implied that the reinforcement density requirements are increased compared to conventional MSE walls.

In addition to external and internal stability, design considerations for MSE bridge abutments include the stability of the bridge seat on top of the MSE mass. The bridge seat must meet the typical criteria for a strip footing against sliding, overturning, and bearing capacity failure modes. Particularly with respect to the latter one, bearing pressure applied on the MSE mass shall be limited to 200 kPa. Finally, especially in cases that the MSE structure is built on weak foundation soil conditions or on sloping ground, overall stability control shall be performed using slope stability analysis methods, such as rotational or wedge analysis.

With respect to deformation issues, the following statements can be made: Generally, one primary advantage of MSE walls compared to reinforced concrete walls, is their ability to withstand differential settlements without structural distress. Nevertheless, in case of MSE bridge abutments, settlements have to be examined carefully and on a case by case basis, in order to determine their effect

on the superstructure. Uniform settlements are usually of little concern to the structural integrity of the abutment. However, if they are excessively large, they may cause practical problems, such as bridge beam encroaching on the required clearances. Differential settlements can cause serious problems, even in small amounts. In this context, FHWA and AASHTO guidelines provide criteria for allowable differential settlements with respect to longitudinal angular distortion, i.e. the ratio of differential settlements over the bridge span length. In addition, some researchers have suggested criteria with respect to allowable differential movements between the bridge seat, the retaining wall, and the approach embankment. However, these usually refer to abutments rigidly founded on piles. In the case of abutments directly founded on MSE walls, differential movements between the bridge deck and the approach embankment are not expected to be significant, because the deck is practically supported by the embankment itself.

As last part of the literature review, an effort was made in order to classify information on documented performance of MSE bridge abutments, based on published data. Although the review clearly indicated that building MSE walls for direct use of bridge abutments is not an unusual design practice, the extent and quality of available data does not allow for accurate comparative studies, that would lead to safe conclusions regarding the applicability of such a solution for Indiana bridges. Therefore, recommendations cannot be formulated based exclusively on this data, and a robust in-depth study was necessary. This study was composed of two parts. First, analysis was performed based on conventional methods of design in order to assess the performance of MSE bridge abutments with respect to external and internal stability. Consequently, based on the obtained results finite element analysis was performed in order to investigate deformation issues. Summaries and conclusions of the two types of analysis are discussed in the following sections.

6.2.2. Analysis based on conventional methods of design

The purpose of this part of the study was to investigate the performance of MSE bridge abutments based on conventional design methods, and to identify cases where the criteria for ultimate limits of resistance with respect to external and internal stability are satisfied. The program *MSEW v.2.0* was used for the analysis. This is an interactive software for the design and analysis of generic MSE structures following the design guidelines of FHWA. In fact, the first version of the program, v.1.0, is designed exclusively for use by State and Federal Highway Agencies.

INDOT's interest, expressed in early stages of the project, was in single span bridges with span length between 18 and 30 m (60 and 100 ft), and visible height of MSE abutment walls between 5 and 7 m (16 and 23 ft). Based on these ranges a decision was made to examine all possible combinations of examples with 18, 24, and 30 m spans and 5, 6, and 7 m visible heights. This resulted in nine cases with respect to geometric characteristics of the abutment – bridge system. In all occasions, embedment depth was set at 1 m (3 ft) below ground surface. Vertical and horizontal concentrated loads transmitted from the bridge to the MSE walls, as well as uniformly distributed loads, were calculated according to AASHTO specifications. Finally, it was decided that each of the nine geometric cases would be examined for three different soil profiles. In the absence of any field or laboratory data, soil profiles were attempted to resemble typical profiles found in Indiana. These data were selected at the beginning of the project in agreement with the SAC. These are intended to represent a range of shear strength and compressibility characteristics, but were not derived from actual tests. Undrained triaxial tests are required when the bearing layer is made of saturated fine-grained soil, drained triaxial or direct shear tests are applicable otherwise. Overall, the above methodology resulted in analyzing twenty seven different cases, based on variation of loading, geometric, and foundation soil conditions. The major conclusions drawn from the analyses are summarized in the next paragraphs.

In terms of external stability, early results indicated that MSE structures shall not be used as direct bridge abutments in cases where soft soil layers, such as normally consolidated clays, are present near the surface. In such occasions, a design configuration including piles shall be used. In more competent foundation profiles, the application of bridge loads on top of MSE walls has an impact on the design width of the wall, i.e. the required design of reinforcement elements. Specifically, for the case examples analyzed in this study, in order to maintain bearing capacity factors above the minimum recommendations, the ratio of width over total height of the wall was taken equal to 1 – 1.15. It is noted that in some occasions, where the foundation soil was very competent, this ratio could have been smaller. However, the width of the base for each of the nine different in terms of geometry examples, was derived with respect to the worst soil conditions. In addition, it is noted that for conventional retaining structures the ratio of width over total height of the wall is usually taken equal to 0.7 or greater. For the specific site and geometry conditions that were assumed in the study, bearing capacity controlled the design. Specifically, in 8 out of 27 case examples, bearing capacity safety factor was (slightly) below 2.5, which is the recommended minimum value by AASHTO. On the other hand, safety factors against sliding and overturning were in all cases well above the minimum recommendations, and therefore these two modes of failure do not cause serious concerns. So, overall, the decisive factor is the bearing capacity, which as expected is significantly affected by foundation soil conditions. When these conditions are marginal, loading and geometric characteristics can play an important role, too. Sensitivity analyses with respect to shear strength properties of the foundation soil were performed and charts in terms of bearing capacity safety factors were produced. Given the conditions assumed in this study, these charts may be used as preliminary decision tools regarding whether or not piles can be eliminated.

In terms of internal stability, bridge loads have an impact on the required density of the reinforcement, i.e. the vertical and horizontal spacing of the strips.

In order to maintain safety factors against tensile and pull out failure above the minimum recommendations, horizontal and vertical spacing was taken equal to 0.50 m (20 in). For conventional walls without any surcharge loads, typical vertical and horizontal spacing usually starts from around 0.75 m (30 in). The results also indicated that special attention needs to be paid in the strips immediately below the bridge seat. Overall, it can be stated that the presence of bridge loads on top of MSE walls increases the required density of reinforcement elements. However, an appropriate internal design reveals the exact density requirements, and as long as this is performed, tensile and pull out failure modes are not expected to cause serious problems.

Summarizing, the results of the analysis with respect to the ultimate limit states of external and internal stability, confirm the recommendations already provided in the AASHTO and FHWA guidelines. The currently available methods of design take into consideration the impact of bridge loads, when these are present, and therefore provide the necessary means to decide whether or not an MSE wall used as direct bridge abutment can be designed with safety. When this is the case, the recommendations also provide the means in order to perform an accurate design with respect to external and internal stability based on the project's site conditions.

6.2.3. Analysis based on the finite element method

Conventional design methods of MSE structures address ultimate limit states of resistance. However, using MSE walls as direct bridge abutments also requires their high performance, over the long term, with respect to deformations. In this context, an aspect that needed investigation was the analysis of stresses and strains under service loads. This type of analysis was performed using the finite element method and provided a better insight regarding the performance of the structure, particularly with respect to settlements over time and under service load conditions. *Plaxis v. 8.2* was used for the finite element analysis. This is a state-of-the-art program, developed specifically for analyzing geomechanics and

soil - structure interaction problems, that has been validated over the last twenty years in academia and industry. Its capabilities to simulate stage construction and interface response between soil and other material were critical features for the application considered in this study.

Analysis was performed in plane strain (2-D) conditions. In reality, likewise most geotechnical problems, mechanically stabilized earth is a 3-D problem. However, computer resources for real three dimensional analyses are considerable and usually unavailable. Due to this reason, in the literature MSE structures are typically modeled, based on approximations, in two dimensions. Comparisons between results from instrumented real-scale structures and numerical simulations, suggest that this approximation is relative reliable, when performed in the appropriate manner. Even in this case, modeling an MSE structure with finite elements is nevertheless a complicated problem, due to the presence (and interaction with each other) of many elements of totally different nature: soil, reinforcing strips, concrete facing panels, and EPDM pads.

In this study, soil was modeled with 15-node triangular elements using two constitutive models. Mohr-Coulomb was used for the reinforced backfill, the approach embankment, and part of the foundation soil. The “Hardening Soil” model, one of the advanced models available on Plaxis, was used for the normally consolidated clay layer, when such a layer was included in the foundation profile (but not immediately below the structure). This advanced model takes into consideration the effects of confinement and stress history on the soil moduli. It accounts separately for both plastic straining due to deviatoric loading and plastic straining due to primary compression by using two appropriate moduli (E_{50}^{ref} and E_{oed}^{ref}). A third modulus (E_{ur}^{ref}) allows for elastic loading – unloading of the soil. Failure of the soil occurs according to Mohr-Coulomb criterion using the traditional shear strength parameters (c, φ, and ψ). In the absence of experimental data, values for the constitutive model parameters were derived based on published data for case examples referring to Indiana, and correlations available in the literature.

Simulations were performed for the examples that, based on the results of conventional design methods, were identified as more interesting. Specifically, analysis was performed for those cases on which FS_{BC} = 2.5. Those were five cases, and two different type of analysis was performed for each one of them. First, foundation soil was assumed a permeable material, so the resulting vertical displacements correspond to immediate settlements of the system due to MSE wall self-weight and bridge loads. Second, a layer of non-permeable compressible soil was introduced in the foundation profile. Magnitudes and time rates of consolidation settlements were investigated in this second type of analysis. In all cases, the construction sequence of MSE structures in practice was taken into consideration during the numerical simulations. Execution of simulations followed the typical stage construction composed of the subsequent repetitive steps: erection of one row of facing panels, placement of one layer of backfill, placement of one layer of reinforcement, and so on. The results of the analyses in terms of deformations are summarized in the next paragraphs.

Settlements of MSE walls used as direct bridge abutments occur due to self-weight of the MSE structure, compaction efforts, and bridge loads. Overall, the magnitude of settlements due to the above depend significantly on the compressibility of the foundation soil. In this study, four different foundation profiles were analyzed for each of the examined examples: three profiles included a homogeneous permeable material with Young moduli varying between 100,000, 50,000 and 25,000 kPa (14,500, 7,250 and 3625 psi), while the fourth profile introduced a non-permeable compressible layer with compression index equal to 0.250. The resulting maximum settlements along the top of the MSE structure were 6, 9.5, 16.5, and 24 cm (2.35, 3.75, 6.5 and 9.5 in), respectively. It is underlined here that these values refer to settlements due to both MSE self-weight and bridge loads.

Settlements depend on the height of the structure, as well. It was found that larger settlements appear in the taller walls, although these were subjected to smaller bridge loads compared to the short walls. The impact of wall's height was

found to increase with increasing compressibility of the foundation soil. Finally, settlements were found to depend on the magnitude of bridge loads. However, for the case examples analyzed in this study, varying the bridge loads had a smaller impact than varying foundation soil compressibility or height of the structure.

As already stated, total settlements are due to self-weight of the MSE structure and bridge loads. An important conclusion of this study is that the fraction of settlements that are caused due to the bridge loads is small with respect to the settlements caused by the MSE self-weight. For instance, for the examples that involved a 3-m thick clay layer as part of the foundation profile (those were the examples with the larger total settlements, i.e. up to 24 cm), the application of bridge loads increased the settlements by 5 to 14 % near the facing of the wall and by 2 to 8 % at the back of the wall. This means that proper adjustments during the construction process and before the application of the bridge loads, can compensate for elevation losses due to settlements caused by the self-weight of the MSE wall. If such adjustments are assumed, then final settlements just below the bridge seat range between 0.5 and 2.5 cm (0.2 and 1.0 in).

Another important conclusion drawn from the results was related to the uniformity of the resulting settlements at the top of the MSE bridge abutment. Specifically, it was found that the settlements are relatively uniform and that transitions between approach embankment / reinforced fill and reinforced fill / bridge deck are smooth. In other words, the so-called “bump” that often appears at these transitions when the bridge seat is founded on piles, seems to be eliminated in the configuration under study.

Regarding time rates of consolidation, the following comments can be made. Apparently, dissipation of excess pore pressures depends on the coefficient of consolidation c_v of the clay layer and the length of the drainage path. This study was based on the assumption of double drained 3-m thick clay layers. For such layers, the results indicate that for coefficients of consolidation larger than

approximately 10^{-3} cm^2/s (10^{-6} ft^2/s) a great fraction of excess pore pressures has already dissipated by the time that bridge loads are applied. Note that the above c_v value is of the same order of magnitude to values reported in the literature for glacial lake clays or silty clays in midwest. In terms of settlements magnitudes, it was found that by the end of construction, consolidation settlements were completed by 87 to 92 %. This means that no waiting periods for consolidation to occur need to be accounted in the construction process, since only a small fraction of settlement has not occurred by the end of construction. In terms of absolute values, the maximum remaining settlement after the end of construction was found to be approximately 2 cm (0.8 in). However, the above conclusion is not valid when coefficients of consolidation were decreased by one order of magnitude. For example, one case analyzed with c_v equal to 10^{-4} cm^2/s indicated that only 50 % of consolidation settlement had occurred by the end of construction. In that case, the time required for complete consolidation to occur was almost one year after the end of construction. So, in such cases the construction sequence needs to be modified in order to take into account consolidation settlements. For instance, this could mean either including long waiting periods that would allow larger fractions of consolidation to occur before the application of bridge loads, or using preloading techniques that would accelerate the rate of consolidation.

Overall, the finite element analysis indicated that under certain conditions, settlements and more generally deformation issues, may not be a rejecting factor against designing MSE structures as direct bridge abutments. Of course, a decision whether or not such a solution is applicable shall always be based on detailed site investigation and project by project analysis. In summary, for the range of geometric conditions, and material and foundation soil conditions simulated in the finite element analysis, the computational results indicate that:

- Stress levels in the MSE structure and foundation soil would be acceptable.

- Deformation field in terms of total and differential settlement, including total and differential settlement in the transition zone and horizontal deflection of the facing, would not be excessive.

6.3. Recommendations

On the basis of this study, it appears that use of MSE walls as direct bridge abutments (i.e. without piles) would be reliable under certain conditions. These conditions are the following:

- For the range of geometric conditions investigated (18 to 30 m span length and 5 to 7 m visible height), the foundation soil has adequate bearing capacity when subjected to all dead and live loads.
- The largest part of the consolidation settlement (if any) is expected to be completed by the end of construction (for instance, 85 % of the primary consolidation).

. Although conclusions are based on case examples that reflect relatively typical situations, for this type of structures a project by project study shall be made. Given that the general criteria of this study (loading and geometric conditions, foundation soil characteristics) are met, the following recommendations are made:

1. Perform a detailed site investigation. Sites with soft layers near the surface shall be excluded and abutments on piles shall be preferred in such cases. In the present context, soft layer near the surface means a deposit whose shear strength will make bearing capacity inadequate, or a deposit that will induce consolidation settlement that will continue to occur after the end of construction, or a deposit that will undergo secondary compression. A detailed site investigation is a site characterization according to standards of critical foundation work. It is not within the scope of the study to discuss site characterization procedures.
2. Design using current procedures that address external and internal stability. Make sure that provisions mentioned in the recommendations are satisfied.

For example, as stated in FHWA and AASHTO guidelines, the bridge seat shall be designed so that the contact pressure is less than 200 kPa and the bearing centerline is located at least one meter from the facing.

3. Using classical methods of settlements' calculations, verify that differential settlements between abutments, and between MSE fill - approach embankment - bridge seat do not exceed the appropriate limits. Overall, we recommend that 85 % of total consolidation has occurred by the end of construction.
4. The results of the study do not indicate that any change to current specs for MSE structures is required. Therefore, it is recommended construction with strict adherence to the specifications governing selection, placement and compaction of backfill material, and collection and removal of water.

6.4. Anticipated Benefits and Implementation

Using MSE structures as direct bridge abutments would be a significant simplification in the design and construction of current systems and would lead to faster construction of highway bridge infrastructures. Additionally, it would result in construction cost savings due to elimination of deep foundations. Finally, this solution would contribute to better compatibility of deformation between the components of bridge abutment systems, thus minimize the effects of differential settlements and the undesirable "bump" at bridge / embankment transitions. Cost savings in maintenance and retrofitting would also result.

Conclusions and recommendations of the study are based on case examples. However, several assumptions and simplifications were made in the course of the study and are inherent to the analysis. Therefore, uncertainty is still to be expected and it would be safe to verify the previous conclusions by monitoring the performance of an actual structure. It is recommended to construct a pilot project. The following are suggested as implementation items:

i. Selection of a bridge for a pilot project with the following characteristics:

- Single span length between 18 and 30 m (60 and 100 ft).
- Visible height of the abutment walls between 5 and 7 m (16.5 and 23 ft).
- Foundation soil with adequate bearing capacity for direct abutment, and at least 85 % of the consolidation settlement completed by the end of construction.
- Both abutments will be MSE structures: one with no pile (direct MSE abutment) and the other with piles (mixed MSE abutment).

ii. Instrumentation of both abutments and approach embankments on each side and monitoring during and after construction for vertical deformation (abutments and transition zones) and horizontal deformation (facings).

iii. Comparison of both types of design on the basis of observed performance and construction cost.

LIST OF REFERENCES

AASHTO (2002). Standard Specifications for Highway Bridges, 17th edition. Published by the American Association of State Highway and Transportation Officials, USA.

AASHTO (2004). LRFD Bridge Design Specifications, 3rd edition. Published by the American Association of State Highway and Transportation Officials, USA.

Abu-Hejleh, N., Zornberg, J.G., Wang, T. and Watcharamonthien, J. (2002). Monitored Displacements of Unique Geosynthetic-Reinforced Soil Bridge Abutments. Geosynthetics International, IFAI, Vol. 9, No 1, pp. 71-95.

ADAMA Engineering Inc. (2004). MSEW (2.0). Newark, Delaware, USA.

Allen, T.M. and Bathurst, R.J. (2001). Prediction of Soil Reinforcement Loads in Mechanically Stabilized Earth Walls. Report WA-RD 522.1 Final Research Report, Washington State Department of Transportation, Olympia, WA.

Anderson, P.L., Brabant, P.E., (2005). Increased Use of MSE Abutments. In: Proceedings of the 22nd Annual International Bridge Conference, Pittsburgh, PA, June 13 – 15 2005.

Bastick, M.J. (1985). Behavior of Reinforced Earth Abutments – Summary of the Research Results. Report No. 37 (unpublished). Terre Armée Internationale.

Boyd, M.S. (1988). Reinforced earth bridge abutments. In: International Geotechnical Symposium on Theory and Application of Earth Reinforcement. Fukuoka, Japan, 5-7 October 1988, Balkema, 499-503.

Brabant, K. (2001). Mechanically Stabilized Earth Walls for Support of Highway Bridges. The Reinforced Earth Company. Unpublished Report.

Briaud, J.L., James, R.W., Hoffman, S.B. (1997). Settlement of Bridge Approaches (The Bump at the End of the Bridge). NCHRP Synthesis of Highway Practice 234. Transportation Research Board, Washington, DC.

Cheung, K.-C. Peters, D., Blackler, A. (????). The Design and Construction of a Bridge with MSE Abutments on Seismically Liquefiable Soil.

Cheung, K.-C., Peters, D. (????). New Zealand Experience on Economical Design of Reinforced Earth Embankments on Liquefiable Soil.

Christopher, B.R. (1993). Deformation Response and Wall Stiffness in Relation to Reinforced Soil Wall Design. Ph.D. Thesis, School of Civil Engineering, Purdue University, West Lafayette, IN.

Christopher, B.R., Gill, S.A., Giroud, J.-P., Juran, I., Mitchell, J.K., Schlosser, F., and Dunnicliff, J. (1990). Reinforced Soil Structures, Volume 1: Design and Construction Guidelines. Report FHWA-RD-89-043, Federal Highway Administration (FHWA), Washington, D.C.

Egan, P.D. (1984). Design and performance of reinforced earth bridge abutments. In: Proceedings of the 1st International Bridge Conference, Pittsburgh, PA, 92-98.

Elias, V. and Egan, P.D. (1985). Use of “Reinforced Earth” for Retained Embankments in Railroad Applications. Transportation Research Record, Vol. 1030, pp. 21-28.

Elias, V., Christopher, B.R., Berg, R.R. (2001). Mechanically stabilized earth walls and reinforced soil slopes – Design & construction guidelines. Publication No. FHWA-NHI-00-043. Published by the US Department of Transportation, Federal Highway Administration, Washington D.C., March 2001, USA.

Fannin, R.J. (2001). Field Observations on the Load-strain-time Behaviour of Geogrid Reinforcement. Canadian Geotechnical Journal, Vol. 31, pp. 564-569.

French Ministry of Transportation (1979). Les Ouvrages en Terre Armee – Recommendations et regles de l’art (Reinforced Earth Structures – Guidelines and State-of the Art). LCPC / SETRA. Ministere des Transports, Paris (in French).

GangaRao, H.V.S., Moulton, L.K. (1981). Tolerable movement criteria for highway bridges. Public Roads, 44 (4), 140-147.

Goughnour, R.D., DiMaggio, J.A. (1979). Soil-reinforcement methods on highway projects. In: Proceedings, Symposium on Earth Reinforcement, ASCE Annual Convention, Pittsburg, PA, April 27 1978, 371-399.

Groupe TAI (Undated). Reinforced Earth Bridge Abutments. Terre Armée Internationale.

Hanna, B.E. (1977). The Use of Reinforced Earth Walls as Bridge Abutments. Proceedings, 28th Annual Highway Geology Symposium. South Dacota School of Mines & Technology. Rapid City, South Dacota, August 10-12 1977, 57-60.

Hoppe, E.J. (1999). Guidelines for the use, design, and construction of bridge approach slabs - Final report. Virginia Transportation Research Council, VTRC 00-R4.

Ingold, T.S. (1982). Reinforced Earth. Thomas Telford Ltd., London.

Jones, C.J.F.P. (1996). Earth reinforcement & soil structures. Thomas Telford Ltd., (new edition).

Juran, I., Schlosser, F. (1979). Theoretical analysis of failure in reinforced earth structures. In: Proceedings, Symposium on Earth Reinforcement, ASCE Annual Convention, Pittsburg, PA, April 27 1978, 528-555.

Juran, I., Schlosser, F., Long, N.T., Legeay, G. (1979). Full Scale Experiment on a Reinforced Earth Bridge Abutment in Lille. In: Proceedings, Symposium on Earth Reinforcement, ASCE Annual Convention, Pittsburg, PA, April 27 1978, 556-584.

Keller, G.R. and Devin, S.C. (2003). Geosynthetic-Reinforced Soil Bridge Abutments. Transportation Research Record, No 1819, pp. 362-368.

Kim, J.S. and Baker, R.M. (2002). Effect of Live Load Surcharge on Retaining Walls and Abutments. Journal of Geotechnical and Geoenvironmental Engineering, ASCE, Vol. 128, No 10, pp. 803-813.

Kumada, T., Otani, Y., Matsui, T. (1992). Practice and design of reinforced-earth bridge abutments on soft ground. Proceedings, International Symposium on Earth Reinforcement Practise, November 11-13 1991. Editors: Ochiai, Hayashi, and Otani. Balkema, 373-378.

Lee, K.L., Adams, B., Vagneron, J. (1973). Reinforced Earth Retaining Walls. ASCE Journal of the Soil Mechanics and Foundations Division, 99 (10), 745-764.

Lee, K.Z.Z., Wu, J.T.H. (2004). A synthesis of case histories on GRS bridge-supporting structures with flexible facing. Geotextiles and Geomembranes, 22 (4), 181-204.

Long, J.H., Olson, S.M, & Stark, T.D. (1998). Differential Movement at Embankment / Bridge Structure Interface in Illinois. Transportation Research Board, Washington, DC.

McKittrick, D. (1979). Design, construction, technology and performance of reinforced earth structures. In: Proceedings, Symposium on Earth

Reinforcement, ASCE Annual Convention, Pittsburg, PA, April 27 1978, 596-617.

Mitchell, J.K. (1984). Earth Walls. TR News, Transportation Research Board, Washington, D.C., Vol. 114, pp. 24-31.

Mitchell, J.K., Christopher, B.R. (1990). North American Practice in Reinforced Soil Systems. In: Design and Performance of Earth Retaining Structures, GSP No. 25, ASCE, 332-346.

Moulton, L.K., GangaRao, H.V.S., Halvorsen, G.T. (1985). Tolerable movement criteria for highway bridges. Report No. FHWA/RD-85/107. October 1985. U.S. Department of Transportation, Federal Highway Administration, Washington D.C.

Moulton, L.K., Kula, J.R. (1980). Bridge movements and their effects. Public Roads, 44 (2), 62-75.

RECO (2000). Design manual for reinforced earth walls. The Reinforced Earth Company. Vienna, VA, USA.

Runser, D.J., Fox, P.J. and Bourdeau, P.L. (2001), “Field Performance of a 17m Reinforced Soil Retaining Wall”, Geosynthetics International, IFAI, Vol. 8, No 5, pp. 367-391.

Schlosser, F. (1990). Mechanically Stabilized Earth Retaining Structures in Europe. In: Design and Performance of Earth Retaining Structures, GSP No. 25, ASCE, 347-378.

Schlosser, F., Guilloux, A. (1981). Le frottement dans le reinforcement des sols. Révue Française de Géotechnique, 16: 66-77.

Schlosser, F., Bastick, M. (1991). Reinforced Earth. In: Foundation Engineering Handbook, 2nd edition. Editor: H.-Y. Fang. Chapman & Hall, New York, 778-795.

Schlosser, F., Elias, V. (1979). Friction in reinforced earth. In: Proceedings, Symposium on Earth Reinforcement, ASCE Annual Convention, Pittsburg, PA, April 27 1978, 735-762.

Schlosser, F., Long, N.T. (1974). Recent results in French research on reinforced earth. Journal of Construction Division, ASCE, 100 (CO3): 223-237.

Schlosser, F., Vidal, H. (1969). La Terre armée. Bulletin de Liaison des Laboratoires Routiers – Ponts et Chaussées No. 41, Réference No. 797, 101-144.

Seow, K., Noël, B. (1994). Application of the reinforced earth bridge abutments in the maritime. In: Proceedings of the 4th International Conference on Short and Medium Span Bridges: Developments in Short and Medium Span Bridge Engineering. Halifax, Nova Scotia, 1173-1183.

Skinner, G.D., Rowe, R.K. (2005). Design and behavior of a geosynthetic reinforced retaining wall and bridge abutment on a yielding foundation. Geotextiles and Geomembranes, 23 (3), 234-260.

Vidal, H. (1969). The principle of Reinforced Earth. Highway Research Record No. 282 (1659), 1-16.

APPENDICES

Appendix A. Case studies of MSE bridge abutments found in the literature

#	Area	Wall geometry (L for reinforcement)	Abutment geometry	Bridge geometry	Soil profile	Settements / Deformations	Description / Comments	Reference
1	Strasbourg, France	Around 3.5m (H). [?]		Single span.			1969. First bridge abutments ever. Owner: Electricité de France (engineering department). Design by La Terre Armeé, Paris. Two abutments for a bridge to carry very heavy truck loads on a service road leading to hydroelectric dams on the Rhine River. Abutmentswere both technically and economically succesful.	Groupe TAI (undated)
2	Thionville, France	18m (H)		78m long prestressed concrete viaduct. Abutment supports span of 38m.			1972. First highway abutment. It crosses the Moselle River on the Nancy - Luxemburg Highway and it supports the end span of the viaduct.	Groupe TAI (undated), Boyd 1988
3	Dunkirk, France	15m (H) x 550m (W) x 16m (L) [height: up to 15m]					1970. Double-sided wall to support a traveling gantry crane applying loads of 280 and 380 kN/m, 0.8 and 2.7m respectively back from the face (wheel loads in exess of 1,000 tons).	Groupe TAI (undated), Boyd 1988
4	Angers, France						1977	Groupe TAI (undated), Boyd 1988
5	Lille, France	5.6m (H), 15m (L)		Single span, 19m			1973. Full scale experiment by the French Road Research Laboratory.	Juran et al 1979, Groupe TAI (undated), Brabant 2001, Boyd 1988
6	Amersfoort, Netherlands	6.20m (H), 8m (L)	2.7m (W), 2m (H). Distance from facing = 0.3m			Measured movements of the facing were less than 0.1mm.	1984. Built for the Ministry of Public Affairs/ Department of Bridges. Eigh (8) levels of reinforcement. Conclusions → the stiffness of the foundation soil at the base gealy reduces the tension in the lower levels of reinforcement strips.	Groupe TAI (undated)
7	Triel, France						1975. Experimental wall by Terre Armeé. Surcharge loading was increased to 90kPa over a 2m width behind the facing.	Groupe TAI (undated), Boyd 1988

8	Millville, USA	L/H = 0.45					Experimental wall by The Reinforced Earth Company.Surcharge loading increased to 40kPa over a width of 1.5m.Length of reinforcement = 2.7m.	Groupe TAI (undated)
9	Fremersdorf, Germany	7.30m (H)					1980. A localized, temporary load of 650kN was placed on the reinforced volume at a point slightly further behind the wall facing than usual for a Reinforced Earth abutment load.	Groupe TAI (undated)
10	Fontainebleau, France	6.80m (H), 4.60m (L)	1.50m (W), 1.50m (H). Distance from facing = 0.25m				1988. Experimental large narrow wall.	Groupe TAI (undated)
11	Val d' Esnoms, France			Single span and the abutment is high relavent to the span (light bridge).	Compressible soils.	Sufficient period of time was allowed for settlement and consolidation of the foundation due to the weight of the Reinforced Earth mass prior to placement of the beam seat and superstructure.	Nancy-Dijon Freeway.	Groupe TAI (undated)
12	Vallon des Acacias, France	17m (H)		Single span and the abutment is high relavent to the span (light bridge).	Compressible soils (alluvial deposits).	Abutments settled 40-70cm and experience 1.5% differential settlement without damage. The 9.5m roadway spans were installed several months later and exhibited no significant movement.	Nice, Côte d' Azur Freeway.	Groupe TAI (undated)
13	Antoing, Belgium	7m (H), 8m (L)	1.75m (W)	Single span, 14.30m (L)	Compressible soils (5m of loose, clayey sand).	65mm of settlement under the RE structure (180kPa). Second phase → superstructure, increase in load by 65kPa causing additional homogeneous settlement of 25mm.		Groupe TAI (undated)
14	Dijon - Geneva Highway, France			Two span.	Highly compressible soils.			Groupe TAI (undated)

15	Ring de Kortrijk, Belgium	5.7m (H), 6.9m (L)		Highly compressible soils: 4m of clayey hydraulic soil (with pek resistance as low as 6bars). Below it is the very thick Flanders clay.	Very good results: 50mm settlement during construction of abutments, and 35mm after placement of superstructure.	Soil improvement took place by substitution of the 4m of the compressible soil.	Groupe TAI (undated)
16	Grossbliederstroff Bridge, Germany	6m (H), 7.2m (L)	29m span.	Highly (exceptionally) compressible soils: 10m clayey alluvial deposits of mixed quality.	Superstructure heavy related to weight of the abutments, so most settlement would be due to this. Due to soil, expectations were for 15cm settlement or more. Stone columns [d=0.8m, H=10m, spaced every 1.5m] were used for soil improvement. Final settlement 5 cm.	Crosses the Saar River at the French-German border.	Groupe TAI (undated)
17	Champlain, Canada		76m length, three independent spans (35-6-35).	24m of compressible clay.	Anticipated settlement 30-45cm. Temporary surcharge of 6.4m thick for two years before construction of the wall and abutments. When w→25cm, fill was partially removed and RE walls were constructed. Five years after construction of bridge w=3cm, causing no problems.	Overpass of highway A40.	Groupe TAI (undated)
18	Rocquencourt, France			8-10m of uncompacted fill which consolidates quickly.		Precharged the site simultaneously with the final RE structure and a temporary topping of concrete blocks (could also be fill). Topping is designed to stand for all or part of the future superstructure's weight. Consolidation is accelerated and if schedule permits, final settlement can be reached before rodaway is built.	Groupe TAI (undated)

19	Wells, Maine, USA	27m (31.4m slantwise), single span. 59o-28' skew.	More than 40m of relatively loose sand and wet clay of average consistency.	Anticipated settlement around 63cm (25"). Preloading for approx. one year with 3.3m of clay additional to RE structure (prior to construction of the abutment seats) produced approximately one third, i.e. 22cm (8 1/2"), of the anticipated long term settlement.After removing the preload and constructing the abutment seat and bridge, an additional 15cm (6 1/2") of settlement occurred within the first two years of service. Approximately 30cm (12") settlement was additionally expected over the next ten years. Provisions were made in the design and construction of the bridge and substructure to allow for jacks to raise the bridge to maintain the design profile elevations. Gages to monitor lateral movement were installed, and essentially no lateral movement of the wall panels has been measured.	1980. US Route 1 bridge over Boston - Maine Railroad.	Groupe TAI (undated), Brabant 2001, Karasopoulos (1984), Egan 1984

20	Lovelock, Nevada, USA		Width: 2' 9". Distance from facing = 1'	Precast bridge span of 70'.	0-40/50': Fine sandy silts and clays, low platicity silty clays, and clayey silts. 50'-100': clean sand. 100'-300': highly compressible and very weak organic and inorganic clays and silts having low permeability. Groundwater at 12'.	Preload by the construction of the embankment itself. Primary consolidation (two years) would take place during this phase. Indeed it was completed by 90% after 2 years when the settlement rate had decreased to 0.2'/year. Since the placement of the RE abutments there has been further settlement of 0.5' and the predicted future setlement was 0.5' for the next 20 years.	1974. First US abutment, constructed for Nevada Department of Highways. 80,079ft2 of abutment walls. Located on I-80 in an area where it crosses Big Meadow Ranch Road, northeast of Reno, near Lovelock. The bridge seat had a uniform bearing pressure of 3KSF. Stresses at the base of the RE structure were 1.5KSF. Maximum unit horizontal stresses in the zone of influence of the bridge seat were 1.4KSF.	Hanna 1977, Brabant 2001
21	Conrail, Gang Mills, (Steuben County) NY	7.5m (25') (H), 7.5m (25') (W), 9.75m (32') (L)	Stub abutments, 5.8m (19') wide and 5.2m (17') in height including the back wall. The stub abutments bear directly on the Reinforced Earth volume.	Single span bridge constructed of steel plate girders, spanning 72.6m (238') over five sets of Conrail tracks.		Due to the enormous load of the 12m (40') high embankments, a 30-day waiting period was required after embankment construction before constructing the stub abutments. Settlement of the embankment was monitored during construction and during the waiting period to determine when it was permissible to construct the abutment seats.	2000. Route 417. The longest span supported by MSE abutment in US (New York Department of Transportation). Wall construction started during the summer of 1999 and bridge construction was completed in early 2000. Special design considerations included: i) Use of extremely large stub abutment footings ii) Support of very high bridge loads iii) Minimal embedment of the wall to reduce excavation, and iv) Settlement monitoring during construction and the 30 day waiting period.	Brabant 2001, reinforcedearth.com
22	Burlington, Vermont					Was expected to settle approximately 15cm (6").The actual settlement exceeded 40cm (16") prior to the construction of the seats. The elevations of the bidge pedestal were adjusted to compensate for the settlement.	Abutment for a railroad unloading trestle.	Brabant 2001

23	Tahuna Bridge, New Zealand	8m (H), 12m (L)		Slghtly skewed two 19m spans bridge carrying 2 lanes of rural traffic.	Alluvial deposit of over 40m thick which is susceptible to seismic liquefaction.			2003	Cheung and Peters 2002, Cheung et al 2003
24	Islip, NY		3m wide spread footings.	Single span steel girder bridge spanning 27m. The alignment of the bridge is at a 40 degree skew to the railroad.			Route 27A, over the Long Island Railroad. Special design considerations include: i) Acute corner design which requires tying two of the wall faces together within the acute corner area. ii) Specially designed parapets with architectural features to match other structures in the area. iii) A 1.5-meter deep strip free zone beyond the sidewalk for future utilities to be added.iv) Precast facing panels with an Ashlar Stone finish to enhance the beauty of the structure and, v) Precast coping units to provide a finished appearance to the abutment walls.		reinforcedearth.com
25	Reno Junction, Wyoming			Sngle bridge, 90' steel span (clear distance between RE structures = 78'). Clearance of 30'.				Wyoming Highway Department.	Hanna 1977
26	I-40 Gallup, New Mexico				Foundation similar to Lovelock, NV: weak compressible material of a former channel Rio Puerco.	Construction in two stages: First construction of embankment including RE walls. A 6-month period of no activity will follow where primary consolidation of up to 2' is expected. 60% of the total ultimate consolidation will occur during this period wth further settlement expected over a 20-years period.	New Mexico State Highway Department. Final elevations of bridges wrt the top of the RE abutments will be established after the initial settlement period and structures and remaining roadway will be constructed.		Hanna 1977
27	Anchor Dam, Wyoming	Maximum height 15'.	Small abutments.					First US stream crossing of a bidge with RE abutments. Site near Thermopolis.	Hanna 1977

28	Libby Dam, Montana (I)		43' clearance between abutments.		US Army Corps of Engineers. Burlington Northern main line.	Hanna 1977
29	Libby Dam, Montana (II)		43' clearance between abutments.		US Army Corps of Engineers. Montana State Highway.	Hanna 1977
30	Yamanokami river, Japan	3m (H), 8m (L)		60m of highly compressible soft ground.	Highway abutment, Yamanokami river, northern part of Lake Kawaguchi, Yamanashi Prefecture.Preloading was employed to restrict settlement to the minimum after the erection of the superstructure. Preloading continued till completio of 90% of anticipated consolidation settlement.	Kumada et al 1992
31	Swanport Deviation at Murray Bridge, Australia	6m (H), 12m (L), 400m2	The deck of prestressed concrete girders spanning 13.5m is supported on a sill beam 1.8m wide and 1m below road surface level.	Sandy to plastic clay.	First abutment built in Australia. Bridge over Mulgundawah Road. Concrete facings panels. Plain reinforcement with 80x3mm section and 12m length. Total horizontal stresses (inluding earth pressure) at the bearing level on the sill were 43kN/m (square o the abutment) and effective vertical pressure of 160kPa at the base of the sill beam. Backfill material: sand with φ=35o.	Boyd et al 1978
32	Botany, Australia	7.5m (H), 12m (L), 3350m2 (total)	Post tensioned concrete deck spanning 27m (or 20?) supportd on a sill beam 2.4m wide and variable depth up to 1.4m below road surface.	Sand	Railway overpass stucture. Concrete facings panels. Ribbed reinforcement with 40x5mm and 60x5mm section. The bridge loadings applied at bearing level on the sill eam are 345kN/m vertical and 8.5kN/m horizontal. The addition of earth pressure results in a total horizontal load of 39kN/m (square to the abutment) and vertical pressure of 180kPa at the base of the sill beam. Backfill material: sand.	Boyd et al 1978
33	Del Park Road Bridge, Pinjarra, Australia	10.7m (H), 9m (L), 495m2	Two span concrete deck. Each span of 11m is supported on a sill beam 1.6m wide and 1.9m below road suface level.	Clay	Steel facings panels. Ribbed reinforcement with 40x5mm and 60x5mm section.Total horizontal load (including earth pressure) is 28kN/m (square to the abutment) and vertical pressure is 130kPa at the base of te sill beam. Backfill material: bauxite fill.	Boyd et al 1978
34	Pt. Germein Overpass, Australia	6.75m (H), 666m2			South Australia. To be costructed by the time of publication.	Boyd et al 1978

35	Tuggeranong Parkway Cotter Road Bridge, Australia	6.75m (H), 1065m2					To be costructed by the time of publication.	Boyd et al 1978
36	Bedford Waterfront, Canada	7.5m (H), up to 9m (L), 533m2		Single span, 32m long.	Thin layer of silty sand on top of the bedrock.	Post construction settlements were minimal.	Nine levels of reinforcement vertically spaced at 0.75m. The maximum loads transmitted to he RE mass by the bridge seat for different loading cases were 240kPa vertical load and 21kN/l.m horizontal load.	Seow and Noel 1994
37	Highway 104 New-Glasgow	9m (H)		Single span, 30m long.			Crosses the West River. Not yet constructed by the time of publication.	Seow and Noel 1994
38	Glendale/Duke Connector, Bedford, Canada	9m (H)		Single span, 30m long.			Not yet constructed by the time of publication.	Seow and Noel 1994
39	Bilbao - Behobie highway, Spain						The abutment settled 1050mm without distress.	Boyd 1988
40	Oregon, USA			Single span, 55m long.	Compressible soils.	Accomodation of 300mm of settlements without loss of structural integrity.		Boyd 1988
41	Field River, Australia		Abutment height 22m (apparently including RE structure)		Extremely variable foundation profile, including an ancient river bed and existing poorly compacted embankment material.	The structure movements are within the limits required for the bridge.	Constructed by the Highways Department of South Australia. Expensive foundation treatment was avoided due to use of RE abutment.	Boyd 1988
42	River Torrens, South Australia		Abutment height 7.7m	Single span (?), 42m long.	Poor foundation material.		Railway bridge. Existing structures precluded the use of piles.	Boyd 1988
43	Queensland, Australia		Abutment height 14.5m	Single steel span, 16.3m long.			Designed to support 300tn coal dump trucks unloading at the rate of 2000tn per hour.	Boyd 1988

Appendix B. Derivation of vertical dead and live concentrated loads

The calculation of the vertical dead and live loads was performed by Mr. Randy Strain from the Design Division of the INDoT (August 2005). Sixteen different cases based on span length, type of beam, efficient spacing, etc. were examined. Detailed results of the analysis are shown in the following Table.

Table B.1 Vertical dead and live loads for different spans, beams, and efficiency spacing

Case #	Overall width (ft)	Beam spacing	Type of beam	Span Length (ft)	# of beams	DL / beam (kips)	LL / beam (kips)	DL+LL / beam (kips)	DL (kips)	LL (kips)	DL + LL (kips)	DL / feet	LL / feet	DL+LL / feet
1	39	6@6 + 2x1.5	II I-beam	60	7	41.44	60.19	101.63	290.08	421.33	711.41	7.44	10.80	18.24
2	39	5@7 + 2x2	II I-beam	60	6	46.46	70.64	117.1	278.76	423.84	702.6	7.15	10.87	18.02
3	39	3@12 + 2x1.5	III I-beam	70	4	87.99	110.22	198.21	351.96	440.88	792.84	9.02	11.30	20.33
4	39	4@9 + 2x1.5	III I-beam	70	5	71.89	89.53	161.42	359.45	447.65	807.1	9.22	11.48	20.69
5	39	5@7 + 2x2	III I-beam	70	6	61.15	72.29	133.44	366.9	433.74	800.64	9.41	11.12	20.53
6	39	4@9 + 2x1.5	III I-beam	80	5	82.39	91.78	174.17	411.95	458.9	870.85	10.56	11.77	22.33
7	39	5@7 + 2x2	III I-beam	80	6	69.76	73.53	143.29	418.56	441.18	859.74	10.73	11.31	22.04
8	39	6@6 + 2x1.5	III I-beam	80	7	64.27	62.67	126.94	449.89	438.69	888.58	11.54	11.25	22.78
9	39	6@6 + 2x1.5	III I-beam	90	7	72.21	63.21	135.42	505.47	442.47	947.94	12.96	11.35	24.31
10	39	3@12 + 2x1.5	IV I-beam	90	4	123.68	113.49	237.17	494.72	453.96	948.68	12.69	11.64	24.33
11	39	4@9 + 2x1.5	IV I-beam	90	5	103.01	91.95	194.96	515.05	459.75	974.8	13.21	11.79	24.99
12	39	4@9 + 2x1.5	IV I-beam	100	5	114.29	92.33	206.62	571.45	461.65	1033.1	14.65	11.84	26.49
13	39	5@7 + 2x2	IV I-beam	100	6	99.01	74.44	173.45	594.06	446.64	1040.7	15.23	11.45	26.68
14	39	6@6 + 2x1.5	IV I-beam	100	7	92.15	63.46	155.61	645.05	444.22	1089.27	16.54	11.39	27.93
15	39	3@12 + 2x1.5	4.5 INBT	100	4	137.04	114.06	251.1	548.16	456.24	1004.4	14.06	11.70	25.75
16	39	3@12 + 2x1.5	5 INBT	100	4	142.27	114.06	256.33	569.08	456.24	1025.32	14.59	11.70	26.29

A plot of the results on the last three columns of Table B.1, indicate the linearity in both dead and live loads with varying span length (Figure B.1). Based on these results, and for the span lengths of interest, average load values were determined and used in the current study (Table B.2).

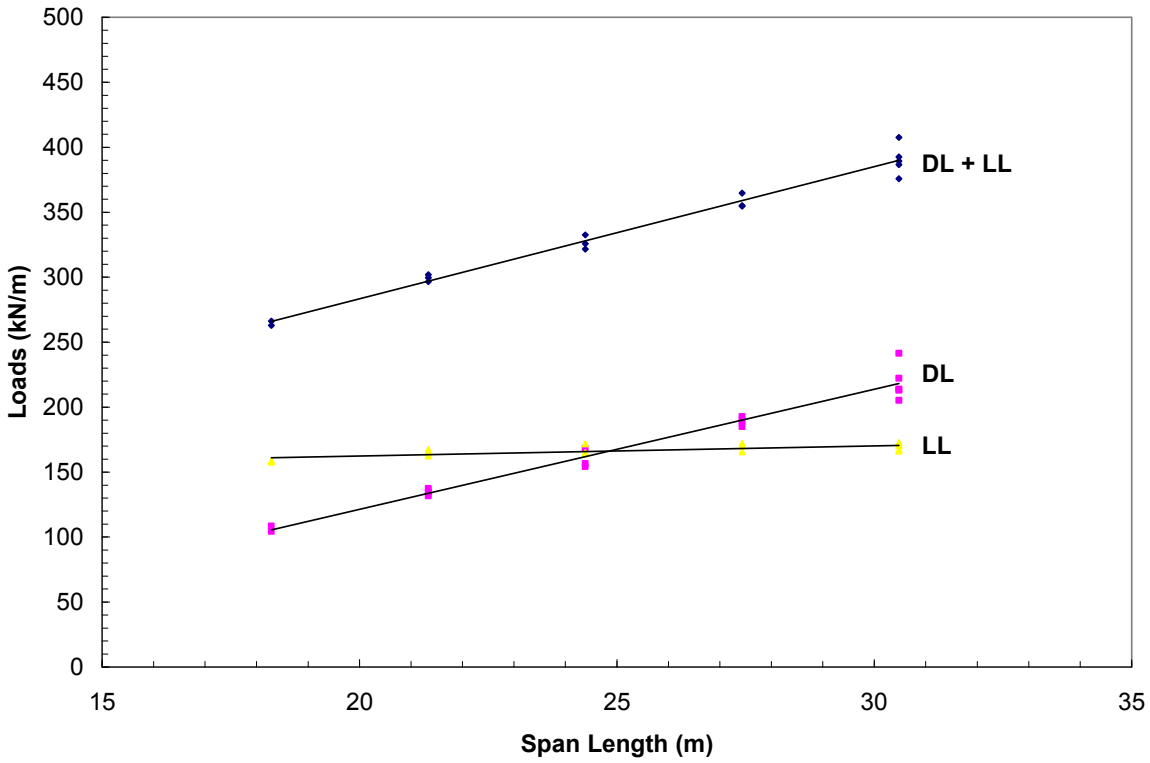

Figure B.1 Variation of bridge loads with span lengths

Table B.2 Average values of dead and live loads

Span Length (m)	DL (kN/m)	LL (kN/m)	DL+LL (kN/m)
18	105	160	265
24	160	165	325
30	215	170	385

Appendix C. Soils formation in Indiana

Indiana is located toward the eastern edge of the great interior plains of North America. These plains extend from the Appalachian Mountains to the east, to the Rocky Mountains to the west. This area has been glaciated to its biggest part and its terrain is mainly flat. Figure C.1 shows the distribution of glacial deposits in the north-central US; it can be seen that most of the Indiana terrain is a glaciated area and that the glacial boundary passes through southern Indiana.

So, glaciation and its effects have played a major role in the formation of the local soils, especially in the northern and central part (West, 1995). The other controlling factor in the formation of soils is the resistance to erosion of bedrock in southern Indiana. Overall, the State can be divided into three major landscape zones that trend into an east-west direction across the State: the “Wisconsin” zone, the “Illinoian” zone, and the “Driftless Area” (Figure C.1). Figure C.2 shows the distribution of the major soil formations across the State. The following comments can be made:

Northern and Central Indiana

The material that is found in these two zones is a glaciated deposit. The northern part of Indiana is a glacial deposit of the “Wisconsin” period. The central part is an extensive plain of deposits left by the glaciers of the “Illinoian” period. In both cases, the bedrock is buried beneath the glacial deposits. The difference between the two zones is that the northern one has some small parts with non-glacial sediments, such as dunes, and stream or lake deposits.

The soil formation that is most widely encountered in the northern and central Indiana is till, i.e. a sandy-clay silt material. The way that till is generally formed is the following: The debris transported by a glacier is eventually deposited after the ice has melted and it is then called drift. The deposition takes place either on site, in which case we refer to unstratified drift or after the debris is being carried away by the meltwater, in which case we refer to stratified drift. The unstratified drift consists of material known as till; till consists of a rather random mixture of materials ranging in size from clay to large boulders and it is composed mostly of

silt and clay with occasional pebbles. Till is deposited by the receding glacier to yield landforms collectively known as moraines. Much of the north-central Indiana is known as the Tipton till plain, and it consists of ground moraines and end moraines (West, 1995).

Southern Indiana

Southern Indiana is partially glaciated and partially non-glaciated. The non-glaciated area, located south-central and called the “Driftless Area”, forms a landform mainly resulting from the erosion of the bedrock. The bedrock is composed of sedimentary rocks, like shales, limestones, and siltstones. So, the terrain is composed primarily of residual soils (clayey material). Note that some cobble and boulder size fragments of igneous and metamorphic rocks can be found generally across the state since they were brought in the area by glaciers. In the area underlain by limestones, the residuum is a red silty clay (terra rossa). In most places there is also a thin (1 to 2 ft) cover of wind blown silt, or loess that was derived from the glacial deposits. Also, in the south-central area there are some stream (alluvial) deposits.

The southeastern Indiana is glaciated. The glacial deposits are thin, averaging perhaps 5 m (15 ft) to 8 m (25 ft) near the Ohio River, thickening northward to about 15 m (50 ft). A few thin stream deposits in the area average less than 3 m (10 ft). In places where the glacial deposits are thin or absent, or beneath the glacial deposits, there is a surficial deposit called residuum. This is a weathered residue of whatever bedrock is present. The thickness is a couple meters (few feet) at most.

Finally, residuum from various types of bedrock, or even the bedrock itself, is present in the far southwestern Indiana, which has not been glaciated. The rest has been glaciated and the thickness of the glacial deposits increases northward, exceeding 30 m (100 ft) in some areas near Terre Haute. In the rest of the glaciated southwestern Indiana, the glacial deposits are thin. Wind deposits, like sands forming dunes and silts forming loess, are also common in southwestern Indiana. Loess, which is the most extensive, can be found in thickness of 9 m (30

ft) to 12 m (40 ft) along the bluffs of the Wabash and Ohio Rivers, but this thickness decreases to less than a meter (2 to 3 ft) in a distance of 65 km to 80 km (40 to 50 miles) eastward.

Figure C.3 and Figure C.4 give a good overview of the main soil formations across the State.

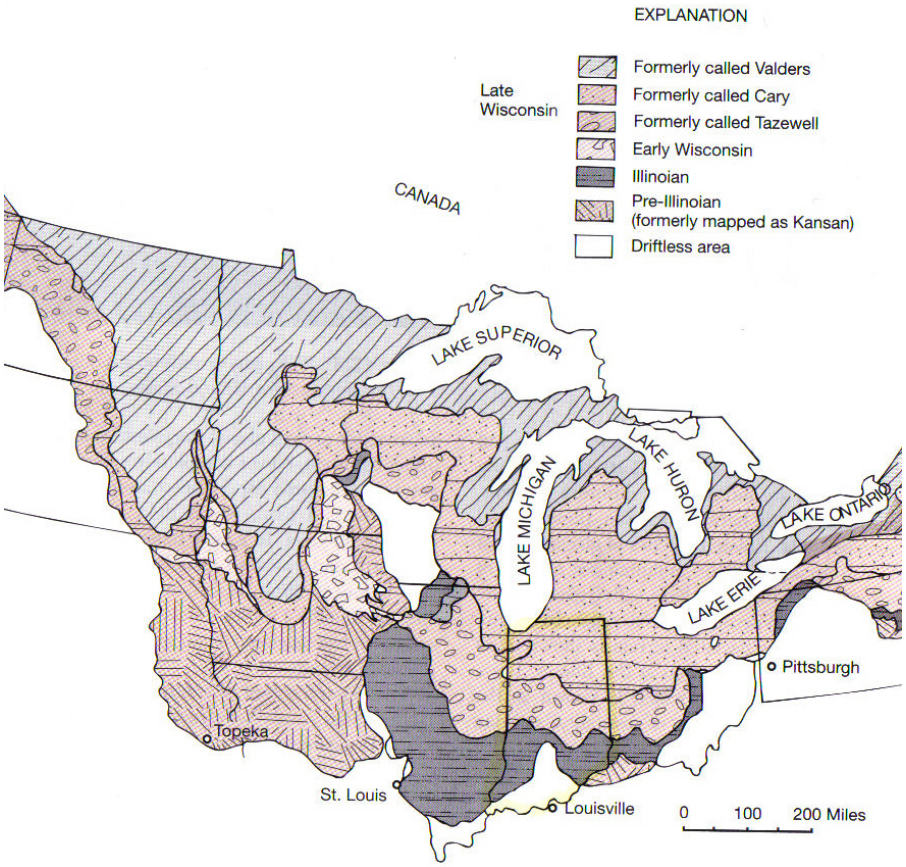

Figure C.1 Glacial deposits' distribution in the north-central US (West, 1995)

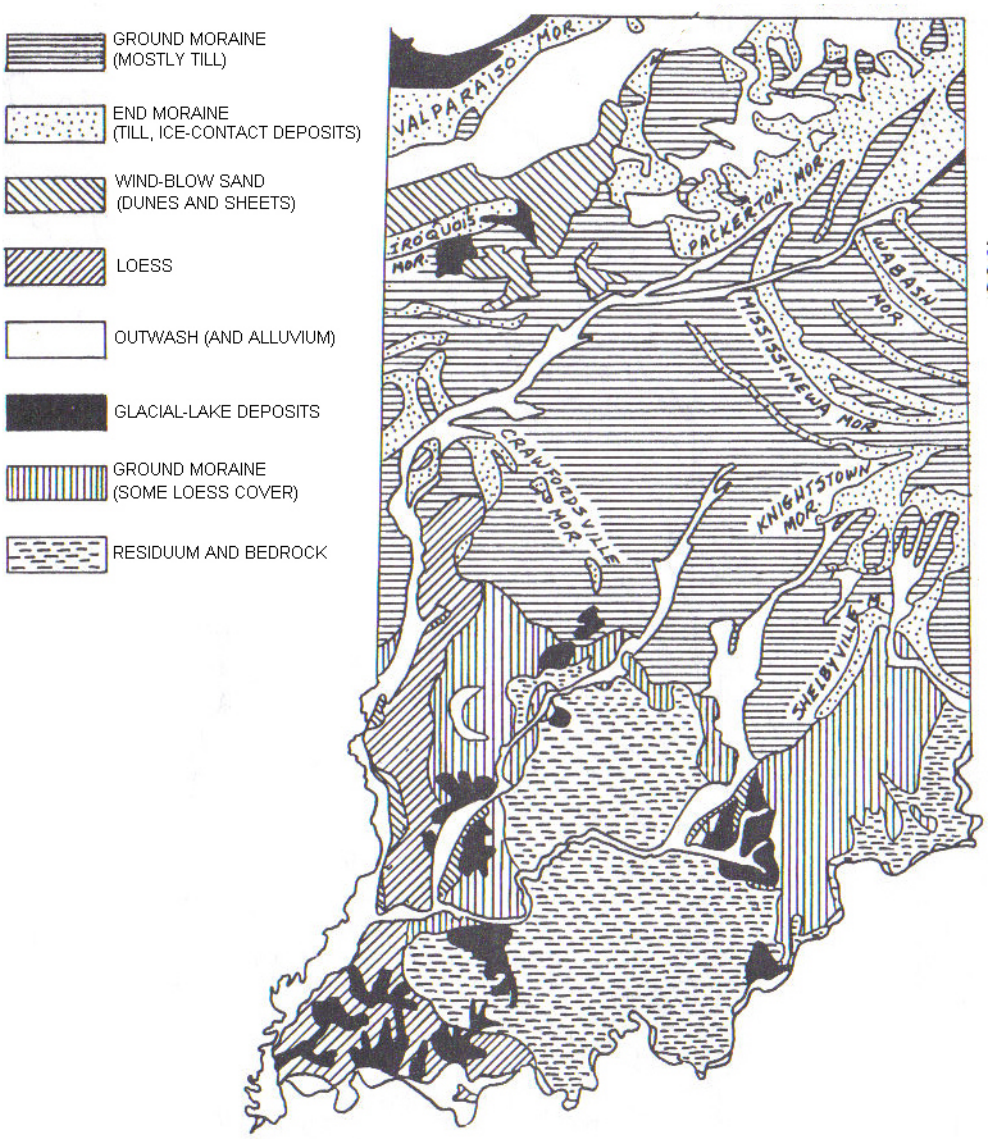

Figure C.2 Major soil formations in the State of Indiana (Hall, 1989)

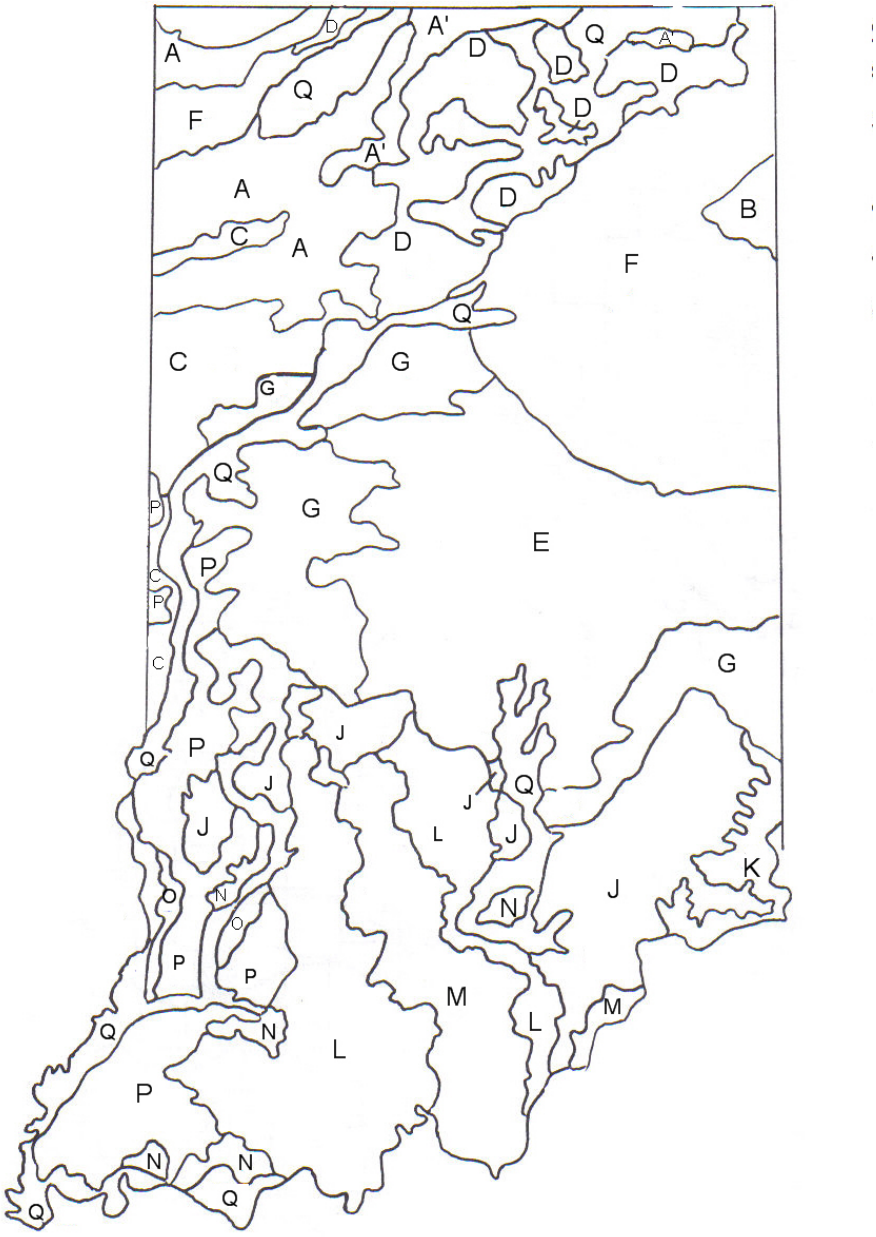

Figure C.3 Soils formation (Hall, 1989)

A: wind-blown sand and lake deposit, A': wind-blown sand, B: lake deposit, C: sandy glacial deposit, D: sandy glacial deposit, E: glacial deposit with thin silt cover, F: glacial deposit, G: glacial deposit with thick silt cover, J: older glacial deposit, K: limestone and shale, L: shale and siltstone, M: limestone, N: lake deposit, O: wind-blown sand, P: wind-blown silt, Q: stream deposit.

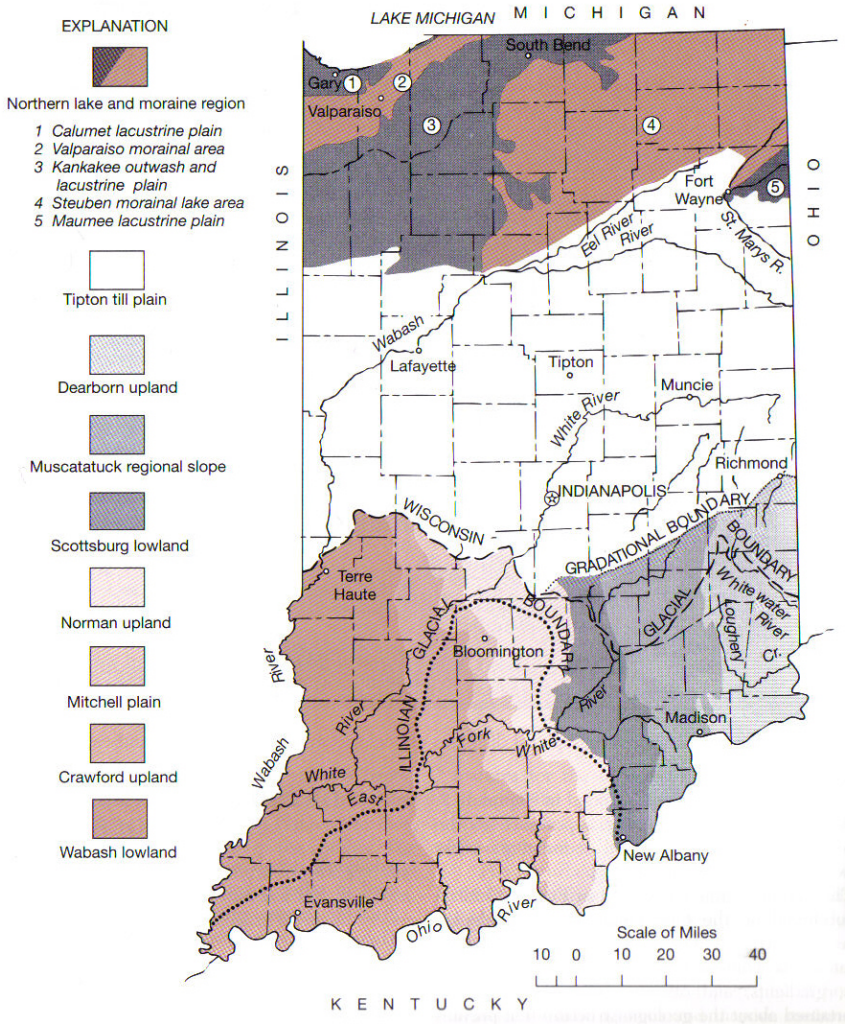

Figure C.4 Regional physiographic units of Indiana (West, 1995)

Calumet Lacustrine Plain: Lake sediments of glacial Lake Chicago. Series of beach ridges and sand dunes from former and present shorelines. Valparaiso Morainal Area: Wide terminal moraine of a substage of Wisconsin glaciation. Kankakee Outwash and Lacustrine Plain: Sandy glacial lake deposits developed on outwash from the Valparaiso moraine. Many low scattered sand dunes on the flat lake plain. Steuben Morainal Lake Area: Composed of recessional moraines from the ice lobe that entered the state from the northeast. Maumee Lacustrine Plain: Lake sediments, an extension into Indiana from an xtensive lake plain in Ohio. Tipton Till Plain: Flat Wisconsin age till sheet underlain by locally rugged bedrock topograph giving rise to a great range in thickness of glacial deposits. Wabash Lowland: Area of moderate to low relief developed in Pennsylvanian age shales and sandstones. Crawford Upland: Most rugged topography in Southern Indiana, results from erosion of alternating sandstones, shales, and limestones of Late Mississippian age. Mitchell Plain: Area of moderate to low relief developed by solution of Mississippian limestones, many caves. Norman Upland: Gently westward-sloping surface on resistant sandstones and siltstones of Early Mississippian age. Scottsburg Lowland: Narrow lowland area developed on Devonian and Early Mississippian age shales. Muscatatuck Regional Slope: A westward-sloping surface held up in the east by resistant cherty Silurian limestones along the border of the Dearborn upland. Dearborn Upland: Flat upland surface with deeply entrenched valleys developed on Upper Ordovician limestones.

Appendix D. Soil Hardening constitutive model parameters

In the absence of field or laboratory data, soil model properties for the compressible layer (clay layer) were derived based on values for Indiana soils found on the literature and on well known relationships.

Compression index, c_c

Values from the literature

- According to Ludlow (1997), compression indices in the state of Indiana typically range between 0.2 ~ 0.3 with an average about 0.246.
- Also, based on Holtz & Kovacs (1981), typical values for normally consolidated clays (of medium sensitivity) range between 0.2 ~ 0.5.
- The same authors indicate that Chicago silty clays have a compression index between 0.15 ~ 0.30.
- Last, again Holtz and Kovacs (1981) provide data from consolidation tests on Indiana glacial clay, which gives:

$$c_c = \frac{\Delta e}{\log \frac{\sigma_2'}{\sigma_1'}} = \frac{0.17}{\log \frac{1270}{302}} = 0.272$$

Relationships

Assuming LL = 40 and PI = 18 (Lee & Bourdeau, 2006):

- For remolded clays (Skempton, 1944):

  $c_c = 0.007(LL - 7) = 0.007(40 - 7) = 0.231$

- For undisturbed clays of low to medium plasticity (Terzaghi & Peck, 1967):

  $c_c = 0.009(LL - 10) = 0.009(40 - 10) = 0.270$

  The above correlation has a reliability range of about ± 30%.

- For clays with PI < 50, Nakase et al (1988), Bowles(1997):

- $c_c = 0.046 + 0.0104PI = 0.046 + 0.0104(18) = 0.2332$

Note that the correlations using the PI, may even be more reliable because they are actually using two index properties (remember PI = LL – PL).

Based on the above correlations and the resulting values for c_c, this study assumes that **c_c = 0.250**.

Recompression index (unloading/reloading) c_r or c_{ur}

Relationships

- Using the Plasticity Index PI:

  For clays with PI < 50, Nakase et al (1988), Bowles(1997):

  $c_r = c_{ur} = 0.00194(PI - 4.6) = 0.00194(18 - 4.6) = 0.025996$ **= 0.026**

In the absence of any information:

- Holtz & Kovacs (1981) and Bowles (1997) suggest:

  $5\%\ c_c \le c_r \le 10\%\ c_c \Rightarrow$ **0.0125 ≤ c_r ≤ 0.025**

- Typical values of c_r (Leonards, 1976): **0.015 ≤ c_r ≤ 0.035**

  In the above range, the lower values are for clays of lower plasticity and OCR. Values outside the range of 0.005 to 0.05 should be considered questionable.

Based on the above correlations and the resulting values for c_r, this study assumes that **c_r = 0.025**.

Initial void ratio e_o

- Terzaghi and Peck:

Glacial till, very mixed grained	0.25
Stiff glacial clay	0.60
Soft glacial clay	1.20

- Das

Glacial till	0.30
Stiff clay	0.60
Soft clay	0.90 – 1.20

- Holtz and Kovacs

Uniform inorganic silt	0.40 – 1.10

Based on the above, I could come up with the following ranges:

Stiff clays	0.60 – 0.70
Medium clays	0.80 – 0.90
Soft clays	0.90 – 1.20

- Ludlow (1997) **e_o = 0.700** (used the above value for all his cases).

- Using the compression index c_c:

For all clays (Nishida, 1956 from Bowles and Holtz & Kovacs):

$$c_c = 1.15\left(e_o - 0.35\right) \Rightarrow e_o = 0.35 + \frac{c_c}{1.15}$$

For c_c = 0.250 → ***e_o = 0.576***

For inorganic, cohesive soil; silt, some clay; silty clay; clay (Holtz & Kovacs):

$$c_c = 0.30\left(e_o - 0.27\right) \Rightarrow e_o = 0.27 + \frac{c_c}{0.30}$$

For c_c = 0.250 → ***e_o = 1.103***

- Using the compression ratio c_{ce} where $c_{ce} = \frac{c_c}{1+e_o}$:

For Chicago clays (Holtz and Kovacs):

$$c_{ce} = 0.208e_o + 0.0083 \Rightarrow \frac{c_c}{1+e_o} = 0.208e_o + 0.0083 \Rightarrow$$

$$c_c = 0.208e_o + 0.0083 + 0.208e_o^2 + 0.0083e_o \Rightarrow 0.208e_o^2 + 0.2163e_o + 0.0083 - c_c = 0$$

For c_c = 0.250 → ***e_o = 0.677***

Based on the above correlations and the resulting values for e, this study assumes that **e = 1.00**.

Coefficient of consolidation, c_v

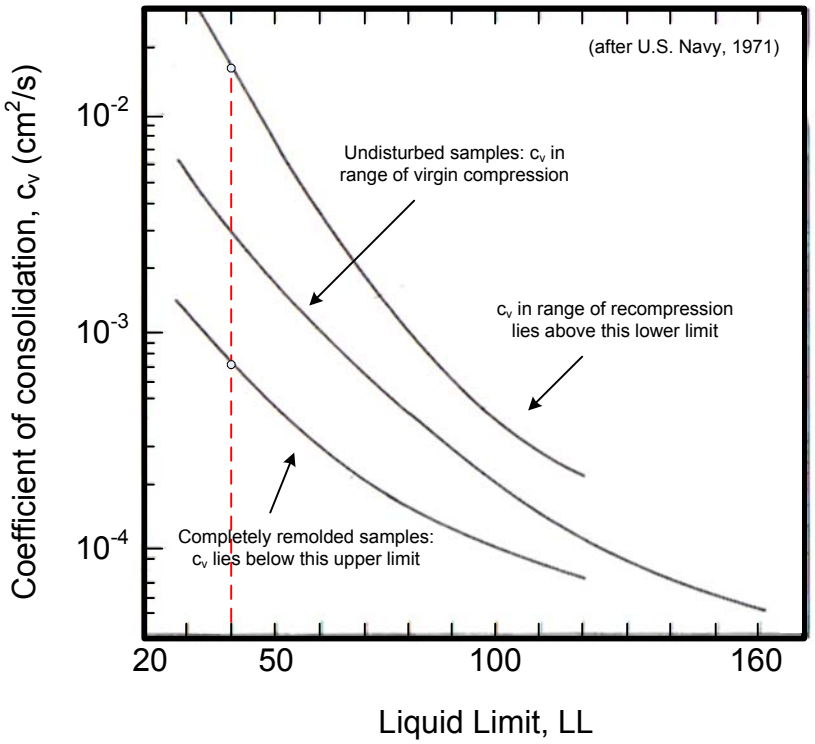

Figure D.1 Liquid Limits vs. Coefficients of Consolidation

For LL = 40 → 7 x 10^{-4} $cm^2/s \leq c_v \leq$ 1.5 x 10^{-2} cm^2/s

- Holtz and Kovacs
  Glacial lake clays (CL): 6.5 – 8.7 x 10^{-4} cm^2/s
  Chicago silty clay (CL): 8.5 x 10^{-4} cm^2/s

Based on the above, we assume **c_v = 12 × 10^{-4} cm^2/s**.

TECHNICAL REPORT STANDARD TITLE PAGE

1. Report No.	2. Government Accession No.	3. Recipient's Catalog No.
FHWA/IN/JTRP-2006/38		

4. Title and Subtitle	5. Report Date
Investigation of Coarse Aggregate Strength for Use in Stone Matrix Asphalt	April 2007
	6. Performing Organization Code

7. Author(s)	8. Performing Organization Report No.
Ioannis Zevgolis and Philippe Bourdeau	FHWA/IN/JTRP-2006/38

9. Performing Organization Name and Address	10. Work Unit No.
Joint Transportation Research Program School of Civil Engineering Purdue University West Lafayette, IN 47907-1284	
	11. Contract or Grant No. SPR-2855

12. Sponsoring Agency Name and Address	13. Type of Report and Period Covered
Indiana Department of Transportation State Office Building 100 North Senate Avenue Indianapolis, IN 46204	Final Report
	14. Sponsoring Agency Code

15. Supplementary Notes

Prepared in cooperation with the Indiana Department of Transportation and Federal Highway Administration.

16. Abstract

The research is an investigation on the possible use of MSE bridge abutments as direct support of bridges on Indiana highways. First, analysis was performed following conventional design methods, in order to assess the performance of MSE bridge abutments with respect to ultimate limit states, i.e. external and internal stability. In the second part of the study, finite element analysis was performed, in order to assess the performance of the structures with respect to serviceability limit states, i.e. immediate and consolidation settlements. In both parts, analysis was performed on case examples that reflect relatively typical situations. The main findings confirm that the currently available methods of design provide the necessary methodology in order to design MSE bridge abutments by satisfying external and internal stability criteria. In terms of deformations, the main findings of the finite element analysis indicate that the fraction of settlements that are caused due to the bridge loads is small compared to the fraction that is caused by the MSE self-weight. Overall, the implementation of the work reported herein, would require a detailed site investigation. Based on these findings and information already available from the literature, it was concluded that the use of MSE walls as direct bridge abutments would be reliable under certain conditions.

17. Key Words	18. Distribution Statement
Retaining walls, retaining structures, bridge abutments, bridge loads, Mechanically Stabilized Earth (MSE), reinforced soil, settlements, consolidation, limit equilibrium analysis, numerical analysis, finite element method, deformations	No restrictions. This document is available to the public through the National Technical Information Service, Springfield, VA 22161

19. Security Classif. (of this report)	20. Security Classif. (of this page)	21. No. of Pages	22. Price
Unclassified	Unclassified	146	

Form DOT F 1700.7 (8-69)